FOURIER TRANSFORM SPECTROSCOPY AND ITS APPLICATION TO ELECTRONS AND HOLES IN HIGH-PURITY GERMANIUM

M.J.H. VAN DE STEEG

FOURIER TRANSFORM SPECTROSCOPY AND ITS APPLICATION TO ELECTRONS AND HOLES IN HIGH-PURITY GERMANIUM

PROMOTOR:
PROF. DR. P. WYDER

FOURIER TRANSFORM SPECTROSCOPY AND ITS APPLICATION TO ELECTRONS AND HOLES IN HIGH-PURITY GERMANIUM

PROEFSCHRIFT

TER VERKRIJGING VAN DE GRAAD VAN DOCTOR IN DE
WISKUNDE EN NATUURWETENSCHAPPEN
AAN DE KATHOLIEKE UNIVERSITEIT TE NIJMEGEN, OP GEZAG VAN
DE RECTOR MAGNIFICUS PROF. DR. J.H.G.I. GIESBERS,
VOLGENS BESLUIT VAN HET COLLEGE VAN DEKANEN
IN HET OPENBAAR TE VERDEDIGEN
OP VRIJDAG 8 OKTOBER 1982
DES NAMIDDAGS TE 2.00 UUR PRECIES

door

MARTINUS JOHANNES HENRICUS VAN DE STEEG
geboren te Wanroij

1982
Druk: Krips Repro Meppel

In dit voorwoord wil ik een woord van dank uitbrengen aan een ieder die, voor een groot of klein gedeelte, heeft meegewerkt aan het tot stand komen van dit proefschrift. Voordat ik enkelen met name ga noemen en danken, wil ik eerst alle medewerkers van de afdeling experimentele natuurkunde IV bedanken voor de prettige tijd die ik samen met hen op het laboratorium heb doorgebracht.

Hans Stoelinga wil ik allereerst noemen, die mij steeds stimuleerde en belangstelling toonde tot aan zijn overlijden, en die op de inhoud van dit proefschrift een duidelijk stempel drukte.

Henk Jongbloets, met wie ik luidruchtig de mooiste fysische luchtkastelen bouwde en die bij mijn eigen luchtkastelen toch altijd het geniepig verborgen ventiel wist te vinden. Hij heeft mij al die jaren met raad en daad bijgestaan en is mij in de laatste fase van het schrijven van dit proefschrift nog vaak behulpzaam geweest.

Jan Gerritsen, voor het snel bouwen van de mooiste electronische schakelingen en het aan elkaar knopen van alle mogelijke computers, die de metingen met zichtbaar licht toch nog tot een succes maakten.

Jan Hermsen, voor het ontwerpen, bouwen en dichten van mijn meetsystemen, voor de moeite om de micrometer nog nauwkeuriger te maken en voor het maken van de illustraties.

Cees Beers, voor alle adviezen in al die jaren.

Rob van der Heijden, voor de prettige begeleiding tijdens de metingen met de laser.

Louis Jansen, voor zijn kritische lezing van het manuscript.

Riki Gommers, voor haar belangstelling in alles en haar adviezen om het typewerk echt mooi te maken.

Tjalling Jongma, die het pionierswerk deed bij het opbouwen van de PDP-11.

C.M.G. Jochem van het Philips Natuurkundig Laboratorium te Eindhoven, voor alle ultrazuivere germanium kristallen.

Johan Lummen, voor de verbeteringen in de engelse tekst.

Mijn schoonouders, bij wie ik in de laatste turbulente fase van het schrijven van het manuscript dagenlang mocht logeren.

Verder wil ik alle dienstverlenende afdelingen van de Faculteit der Wiskunde en Natuurwetenschappen bedanken, met name: Instrumentmakerij, Glasinstrumentmakerij, Electronica, Ontwerp, Reprografie, Illustratie en Fotografie.

Ik ben dankbaar dat mijn vader en mijn moeder, toen zij nog in leven was,

het klimaat schiepen door hun belangstelling en stimulans, zodat ik mede door hen met plezier mijn opleiding tot fysicus kon voltooien.

En dan tenslotte nog Marianne, die mijn klaagzangen over boosaardige apparatuur geduldig aanhoorde, van wie ik zonder mopperen vele uren op de faculteit mocht doorbrengen en die ook nog eens al het typewerk op zich nam.

Dit onderzoek werd uitgevoerd op de afdeling experimentele natuurkunde IV van het Research Instituut voor Materialen van de Katholieke Universiteit te Nijmegen, onder leiding van Prof.Dr. P. Wyder. Een gedeelte van dit onderzoek is gesteund door de Stichting voor Fundamenteel Onderzoek der Materie (F.O.M.) met financiele bijdragen van de Nederlandse Organisatie voor Zuiver Wetenschappelijk Onderzoek (Z.W.O.).

We acknowledge the permission to reprint a previously published paper obtained from the publisher of Infrared Physics.

Aan mijn ouders

Aan Marianne

Contents

VOORWOORD

CHAPTER 1 GENERAL INTRODUCTION 1

References 5

CHAPTER 2 GHOSTLINES IN FOURIER TRANSFORM SPECTROSCOPY 7

General introduction 7

References 8

2.I Basic principles of Fourier transform spectroscopy 9

The interferogram 9

Sampling, phase errors and phase correction 10

Spectral resolution and apodization 11

References 12

2.II Hardware of the Michelson interferometer 13

References 16

2.III Experimental investigation of ghostlines in Fourier spectroscopy in the far-infrared 17

Abstract 17

Introduction 17

Experimental 17

Relation between ghostline intensity and amplitude of periodic travel distortion 19

Discussion and conclusions 21

References 22

2.IV Reducing the effects of ghostlines in a step-record Fourier spectrometer 23

Abstract 23

Introduction 24

Theory 24

Experiment 27

Discussion 29

Conclusions 35
References 36

CHAPTER 3 SEARCH FOR FRACTIONAL CHARGE IMPURITIES IN SEMICONDUCTORS WITH PHOTOTHERMAL IONIZATION SPECTROSCOPY 37

Abstract 37
3.I Introduction 38
3.II The critical concentration β/α 41
A. Thermal ionization 43
B. Ionization by background radiation 45
3.III PTIS signal formation 50
3.IV Experimental search for FCI's with PTIS 53
3.V Minimal detectable concentration of FCI's by PTIS 55
3.VI Conclusions 58
Appendix: Determination of a numerical value for β 59
References 60

CHAPTER 4 FAR-INFRARED PHOTOTHERMAL IONIZATION SPECTROSCOPY IN THE PRESENCE OF INTRINSIC LIGHT 63

Abstract 63
4.I Introduction 64
4.II The distribution of electrons and holes over impurity states and energy bands in a semiconductor 68
4.III Experiment 76
4.IV Discussion and conclusions 86
References 90

APPENDIX: COMPUTER PROGRAM "FIR" 91

Description 91
General flowchart of the interactive program "FIR" 94

SUMMARY 99

SAMENVATTING 101

CURRICULUM VITAE 103

Since more than one decade ultra-pure germanium single crystals can be produced with electrically active impurity concentrations of about 10^{10} per cm^3 [1]. This means that only one atom is "wrong" in 10^{13} "right" Ge atoms (10^{13} is about 1000 times the total number of people living on earth). At this high purity the wavefunctions of shallow donors and acceptors are localized to an extremely high degree and do not overlap those of neighbouring impurities, hence the associated energy levels are very sharp. The impurities exhibit hydrogenlike energy level schemes. The binding energies are about a factor of 1000 smaller than those of isolated hydrogen atoms (13.6 eV), because of the dielectric constant of the semiconducting material and the effective mass of the charge carriers. For germanium this leads to binding energies of shallow donors and acceptors of the order of 10 meV, which corresponds to the far-infrared (FIR) region of the electromagnetic spectrum. An ultra-pure semiconductor with shallow impurities is a model system and plays a part in solid state physics as the Drosophila in biology. It enables us to study hydrogenlike structures with common solid-state-physics techniques. Problems in getting isolated hydrogen atoms, as in atomic physics, can be avoided and e.g. much lower magnetic field strengths are needed for Zeeman-effect studies.

Conventional absorption spectroscopy fails to detect impurities with concentrations below 10^{13} cm^{-3}. For the identification of impurities with concentrations down to 10^{8} cm^{-3}, Photothermal Ionization Spectroscopy (PTIS) is a unique tool. The PTIS technique, originally developed by Lifshits and Nad' in 1964[2,3], is applied at liquid helium temperatures. With PTIS one measures changes in electrical conductivity of a semiconducting sample, caused by changes in the number of free electrons (holes) in an energy band after ionization of a donor (acceptor). This ionization is achieved in a two-step process. In the first step of the process the electron (hole) is raised from the ground state of the donor (acceptor) to an excited state by the absorption of a photon. In the second step the electron (hole) is subsequently promoted into the energy band by interaction with thermal acoustic phonons. Fig. 1 gives an example of a set of photoconductivity spectra of a polycrystalline Ge sample, recorded at several temperatures. The sample was p-type material, containing B and Al acceptor impurities. The spectra show two series of sharp photoconductivity peaks, corresponding to ground state - excited state

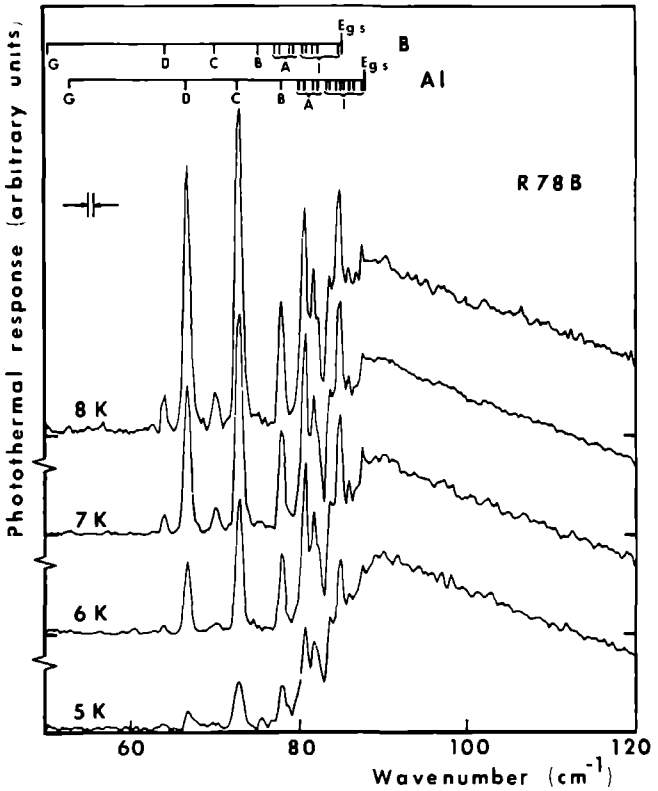

Fig. 1: Measured photoconductivity spectra at several temperatures of a polycrystalline Ge sample, containing aluminium and boron in a concentration of $\sim 10^{10} - 10^{11}$ cm^{-3}. *The expected positions and nomenclature of the transition lines are taken from ref. 11. The spectral resolution is indicated by arrows.*

transitions of the two acceptors. These series are situated on the low-energy side of a broad continuum originating from direct optical transitions of the holes to the valence band. The temperature dependence of the intensity of the photoconductivity peaks is determined by the second step in the photothermal process.

Because of the sharpness of the energy levels, the influence of e.g. a magnetic field[4,5] or uniaxial stress[6,7,8] on the energy level schemes of the impurities can be determined very accurately. By considering the tempera-

ture-dependence of the intensity of the photoconductivity peaks, the second step in the photothermal process can be investigated[9,10].

PTIS is a very sensitive tool for the detection of extremely low concentrations of electrically active impurities in semiconductors, showing a characteristic set of very sharp transition lines for each type of impurity. Therefore it seems a very straightforward idea to apply this technique to the detection of Fractional Charge Impurities (FCI's), possibly present in semiconductors. An example of an acceptor-like FCI is a quark-nucleon complex, consisting of one negative quark with fractional charge -1/3 e, bound to the nucleus of a semiconductor host atom. Analogous with normal shallow donors and acceptors, the donor- and acceptor-like FCI's bind an electron or hole respectively. The binding energies are those of normal donors and acceptors, reduced by a factor of $(1/3)^2$ or $(2/3)^2$, depending on the type of FCI's involved. Therefore we studied the expected PTIS signal strength by considering acceptor-like FCI's in germanium in detail. From the absence of a PTIS signal associated with acceptor-like FCI's in a measured photoconductivity spectrum of a p-type ultra-pure germanium sample, we could conclude that this sample contained less than 1.5×10^{11} acceptor-like FCI's per cm^3. The minimal detectable concentration of FCI's with PTIS, associated with a typical experimental arrangement for PTIS, was determined, yielding 1×10^7 FCI's per cm^3. Modifications to this arrangement are proposed which could lower this limit considerably.

At low temperatures and in the absence of intrinsic light - i.e. radiation able to transfer electrons directly from the valence band into the conduction band, thereby creating free electrons and free holes at the same time - all minority impurities are ionized because of compensation, a fraction of the majority impurities is in the ground state and the only type of free charge carriers present are majority carriers. In this situation PTIS can only detect majority impurities. By illuminating the semiconducting sample with intrinsic light, also free minority charge carriers are created and some of the minority impurities return in the ground state again. Now PTIS can detect minority as well as majority impurities in principle. Absorption of intrinsic light or ionization of impurities tends to increase the number of free carriers, whereas capture of free charge carriers in impurity states or electron-hole recombination tends to decrease it. One is able to study the response of the established equilibrium to a separate additional injection of minority and majority free charge carriers into the bands by photothermal ionization of minority and

majority impurities respectively.

In PTIS spectra of ultra-pure germanium samples, recorded under continuous illumination with intrinsic light, one usually observes in the literature that there is an increase in electrical conductivity associated with photothermal ionization of majority impurities and a decrease associated with minority impurities, a phenomenon not well understood[1]. In similar PTIS spectra obtained in our laboratory, the PTIS signal from the minority impurities sometimes revealed an increase in conductivity, sometimes a decrease, depending on the applied electronic detection technique. By a description of the equilibrium distribution of electrons and holes over impurity states and energy bands with a set of rate of change equations, we analyzed the response of the equilibrium system to photothermal ionization of majority and minority impurities. This analysis predicted the decrease in conductivity, usually observed in the literature in the photoresponse originating from minority impurities. We built an experimental arrangement suited to inverstigate the time-evolution of the PTIS signal after the start of the photothermal process. The measured response revealed fast (<0.5 msec) components in the PTIS signal, associated with both majority and minority impurities, and an additional slow component, associated with the minority impurities. The response time of the slow component (~ 5 msec) - attributed to the electron-hole recombination process in the bulk - has approximately the same magnitude as the applied chopping times of the far-infrared light. It is demonstrated that this slow response time, in conjunction with the applied phase-sensitive detection techniques with a lock-in amplifier, was responsible for the strange behaviour of the PTIS signal from the minority impurities.

For the recording of the PTIS spectra, a far-infrared Michelson interferometer - the most commonly used type of Fourier spectrometer - was used. In a Michelson interferometer radiation, originating from a broad-band source, is divided into two beams by a semitransparent mirror. After the beams have travelled along different paths they are recombined again by the same beamsplitter and directed towards a detector. The intensity of the light, reaching the detector, is recorded as a function of optical path difference between the two divided beams. The optical path difference, achieved by translating a movable mirror, is usually increased in equal length intervals. During the build-up of the Michelson interferometer we discovered that the pitch of the leading micrometer exhibited a periodic error. The resulting periodic non-linearity in the travel of the movable mirror causes ghostline structures to appear in the

spectra. We found that this ghostline structure for a given non-linearity and optical arrangement depends on the way the spectra are calculated. From this dependence, verified both experimentally and theoretically, a method was deduced, which enables the experimentalist to reduce the effect of ghostlines by a suited choice of optical arrangement and a suited way of calculating the spectra, without the necessity of constructing a complicated fringe-reference system.

This thesis is organized as follows. Chapter 2 deals with the principles of Fourier transform spectroscopy, the description of the hardware of a Michelson interferometer, constructed by the author, and the investigation of the ghostline structures. The search for fractional charge impurities in semiconductors with photothermal ionization spectroscopy is described in chapter 3. Chapter 4 deals with the study of high-purity semiconductors, continuously illuminated with intrinsic light, by application of photothermal ionization spectroscopy. In an appendix to this thesis the set of programs, developed to manipulate interferograms and spectra on a PDP-11 computer, is described.

References:

1. E.E. Haller, W.L. Hansen and F.S. Goulding, Adv. Phys. 30, 93 (1981) (Review).
2. T.M. Lifshits and F.Ya.Nad', Sov. Phys. Doklady 10, 532 (1965).
3. Sh.M. Kogan and T.M. Lifshits, Phys. Status Solidi (a) 39, 11 (1977) (Review).
4. J. Broeckx, P. Clauws, K. van den Steen and J. Vennik, J. Phys. C: Solid St. Phys. 12, 4061 (1979).
5. H.W.H.M. Jongbloets, M.J.H. van de Steeg, J.H.M. Stoelinga and P. Wyder, J. Phys. C: Solid St. Phys. 13, 4769 (1980).
6. E.E. Haller and L.M. Falicov, Phys. Rev. Lett. 41, 1192 (1978).
7. E.E. Haller, B. Joós and L.M. Falicov, Phys. Rev. B 21, 4729 (1980).
8. B. Joós, E.E. Haller and L.M. Falicov, Phys. Rev. B 22, 832 (1980).
9. H.W.H.M. Jongbloets, J.H.M. Stoelinga, M.J.H. van de Steeg and P. Wyder, Phys. Rev. B 20, 3328 (1979).
10. H.W.H.M. Jongbloets, M.J.H. van de Steeg, J.H.M. Stoelinga and P. Wyder, J. Phys. C: Solid St. Phys. 13, 2139 (1980).
11. E.E. Haller and W.L. Hansen, Solid State Commun. 15, 687 (1974).

General introduction

Fourier transform spectroscopy (FTS) is a method of recording optical spectra, using interference properties of light. Its main characteristic is that all spectral elements are measured simultaneously. In FTS the light, reaching the detector, is encoded according to intensity and wavelength of the radiation. Next the measured signal is decoded into a spectrum by means of a Fourier transformation.

Although at first sight the method seems needlessly intricate, it offers substantial advantages - which we will mention briefly - over conventional dispersive techniques, such as e.g. grating spectrometers.

1. A considerable improvement in the signal-to-noise ratio, since each spectral element is observed during the whole experiment, known as the multiplex- or Felgett advantage[1] (Only true if the noise is mainly detector noise, which is usually the case in the far-infrared region).
2. The high throughput of an interferometric system, often called the Jacquinot advantage[2] (As a guide, the relative throughput of respectively prism, grating and interferometric spectrometers is 1:7:2000[3]).
3. The relative insensitivity to stray light and overlapping diffraction orders.
4. The relatively simple mechanical construction.

Although the principles of FTS were already known in the beginning of this century, computational problems concerning the Fourier transform prevented general application. The availability of modern fast computers and in addition the development of the fast Fourier transform algorithm[4] made Fourier transform spectroscopy the widely applied technique, especially in the far infrared. For a review see for example Bell[5].

This chapter is organized as follows: Section 1 deals with the principles of Fourier transform spectroscopy and the associated theoretical and experimental problems. Section 2 describes the hardware of the Michelson interferometer, constructed by the author. In section 3 and 4 the ghostline structure is discussed, caused by non-linearities in the travel of the movable mirror in a Fourier spectrometer.

References:

1. P. Felgett, J. de Phys. C.2 28, 165 (1967).
2. P. Jacquinot, J. Opt. Soc. Am. 44, 761 (1954).
3. J. Fleming, Chem. in Britain 13, 328 (1977).
4. J.W. Cooley and J.W. Tukey, Math. Comput. 19, 297 (1965).
5. R.J. Bell, "Introductory Fourier Transform Spectroscopy", Academic Press, New York (1972).

The interferogram

In a two-beam interferometer radiation, originating from a light source, is divided into two beams. These beams are given an optical path difference and are recombined. Since the combined beams are mutually coherent, they will interfere during their travel towards the detector. In a Michelson interferometer the original wavefront is split into two wavefronts by a beamsplitter. In a lamellar grating interferometer the wavefront itself is physically separated into two components. For a detailed description of several types of interferometers see e.g. Chantry[1].

Let the spectral intensity of the light source as a function of the wavenumber σ be denoted by $S(\sigma)$ ($\sigma=1/\lambda$, λ wavelength of the radiation). Then the intensity of the radiation $I'(x)$, reaching the detector, is given by[2,3]

$$I'(x) = \int_0^\infty T(\sigma) \cdot S(\sigma) \cdot (1 + \cos 4\pi\sigma x) \cdot d\sigma \qquad (1)$$

for an optical path difference $2x$. Here $T(\sigma)$ represents the properties of the optical components between source and detector, e.g. beamsplitter, filters and sample.

The x-dependent part in equation (1) is called the interferogram $I(x)$, yielding

$$I(x) = \int_0^\infty T(\sigma) \cdot S(\sigma) \cdot \cos 4\pi\sigma x \cdot d\sigma \quad . \qquad (2)$$

Making an extension to negative wavenumbers by stating that $T(-\sigma)=T(\sigma)$ and $S(-\sigma)=S(\sigma)$, equation (2) can be rewritten as

$$I(x) = \tfrac{1}{2} \int_{-\infty}^\infty T(\sigma) \cdot S(\sigma) \cdot \cos 4\pi\sigma x \cdot d\sigma \quad . \qquad (3)$$

From this equation one can infer that the spectral function $S(\sigma) \cdot T(\sigma)$ can be recovered from the measured interferogram by a cosine Fourier transform.

In order to use phase-sensitive detection techniques the radiation has to be modulated. This can be achieved by chopping the light from the source, called Amplitude Modulation. In a Michelson interferometer one can also modulate the path difference between the beams by a vibration of one of the two mirrors, called Phase Modulation. Each kind of modulation gives rise to a characteristic change in the form of the interferogram I(x). Since this does not affect the principles of the theory, described in this section, we will ignore this and refer the interested reader to the literature[1].

Sampling, phase errors and phase correction

Since the Fourier transform has to be calculated with a digital computer, the interferogram has to be sampled at discrete points over a finite length. Henceforth we will assume that the sampling occurs at regular intervals Δx.

According to a basic sampling theorem each spectral element has to be sampled at least twice within its corresponding wavelength. This is the case because an infinite number of waves with higher wavenumbers will also fit through the points of observation, a phenomenon called "aliasing". The use of a finite sampling interval defines an upper limit $\sigma_{max}=1/(2.\Delta x)$ to the range of wavenumbers, above which no intensity may pass the interferometer. For this purpose low-pass cut-off optical filters are used in practice.

So far it was assumed that the point x=0 was chosen as being the symmetry point, where all cosine Fourier components have zero phase. In practice, however, wavenumber dependent phase shifts $\phi(\sigma)$ can occur, e.g. when none of the points of the sampling comb coincides with the symmetry point. In that case the interferogram $I_a(x)$ is an asymmetric function of x, given by

$$I_a(x) = \int_0^\infty T(\sigma) \cdot S(\sigma) \cdot \cos[4\pi\sigma x + \phi(\sigma)] \cdot d\sigma \quad . \tag{4}$$

Application of a cosine Fourier transform would now result in a distorted spectrum[4]. Two methods of eliminating the effect of phase errors are currently used.

The first method, described in all textbooks on FTS [1,2], involves the use of the complex Fourier transform of $I_a(x)$. Subsequently calculating the modulus of this complex spectrum, yields a spectrum P(σ) given by

$$P(\sigma) = \tfrac{1}{2} . | T(\sigma) . S(\sigma) | \quad . \tag{5}$$

In practice this implies the recording of two-sided interferograms, i.e. interferograms resulting from scans with x-values ranging from -L to +L. If no phase errors had been present, all spectral information could have been recovered from a one-sided interferogram, recorded in scans from 0 to +L. Thus this method has the disadvantage that it takes twice as much time to measure a two-sided interferogram, and the resulting datapoints take a larger amount of computer memory. In addition it degrades the signal-to-noise ratio, since noise is transformed non-linearly, as shown by Loewenstein[5].

The second, more intricate method, called the convolution method, removes all disadvantages of the two-sided interferogram[6]. Assuming one knows $\phi(\sigma)$, this method recovers the ideal, symmetrized interferogram, corresponding to the absence of a phase error, from the measured interferogram $I_a(x)$. This enables us to use a simple cosine Fourier transform again, resulting in a spectrum $P'(\sigma)$, given by

$$P'(\sigma) = \tfrac{1}{2} . T(\sigma) . S(\sigma) \quad . \tag{6}$$

In practice one does not scan a one-sided interferogram from 0 to +L, but from $-\Delta L$ to L ($\Delta L \ll L$). From the short two-sided interferogram (range $-\Delta L$ to $+\Delta L$) a complex spectrum is calculated by a complex Fourier transform. From this spectrum $\phi(\sigma)$ can be determined. Of course the method only holds if $\phi(\sigma)$ is a slowly varying function of σ. The convolution method, however, does not completely eliminate the effects of phase errors from the calculated spectra, as distinct from the modulus spectra, obtained with the first method. In our computerprogram (described in an appendix to this thesis) the errors amount to 1%, determined by the number of points in the short two-sided interferogram, being 32 points. The convolution method has the additional disadvantage of requiring extra computer time in order to calculate the symmetrized interferogram.

Spectral resolution and apodization

The recording of the interferogram over a finite range of x-values, also confines the spectral resolution. The resolution is determined by the maximum distance L of the movable mirror with respect to the centre of the interfero-

gram. (It should be noted that the corresponding maximum optical path difference is twice as long, i.e. 2L). Consider the set of wavenumbers, for which an integer multiple of $\lambda/2$ just fits the maximum optical path difference. The interval, separating these wavenumbers, which are given by $\sigma_n = n/(4L)$, n=1, 2, ..., corresponds to the optical resolution. Therefore, if one scans a two-sided interferogram from -L to +L, or a one-sided interferogram from 0 to L, the resolution is equal to 1/(4L). Thus in principle a better resolution can be obtained with FTS simply by extending the scanning range.

The truncation of the interferogram also gives rise to unwanted spectral features: the spectrum of a monochromatic line with wave number σ_o, after a Fourier transform of the truncated interferogram, shows a broadened line at wave number σ_o with a halfwidth of about 1/(4L), symmetrically surrounded by large ans slowly decaying sidelobes. These sidelobes can be suppressed considerably by multiplying the interferogram with suited functions. These functions, called apodization functions, degrade the spectral resolution at the same time. The apodization functions $\cos[x\pi/(2L)]$ and $\cos^2[x\pi/(2L)]$, which can be chosen optionally in our computer program, degrade the spectral resolution by a factor of 1.3 and 1.5 respectively. For more details about resolution and apodization, the interested reader is again referred to the textbooks[1,2].

References:

1. G.W. Chantry, "Submillimetre Spectroscopy", Academic Press, New York (1971).
2. R.J. Bell, "Introductory Fourier Transform Spectroscopy", Academic Press, New York (1972).
3. H.W.H.M. Jongbloets, Catholic University, Nijmegen, thesis (unpublished).
4. J. Connes, Revue Opt. théor. instrum. 40, 45 (1961).
5. E.V. Loewenstein, Aspen International Conference on Fourier Spectroscopy, 1970, edited by G.A. Vanasse, A.T. Stair, Jr., and D.J. Baker, Air Force Office Report No. AFCRL-71-0019, page 3 ff.
6. H. Sakai, G.A. Vanasse and M.L. Forman, J. Opt. Soc. Am. 58, 84 (1968).

2.II. *Hardware of the Michelson interferometer*

For the majority of the experiments described in this thesis a Michelson interferometer was used. This type of Fourier spectrometer was constructed by the author during his stay at the laboratory. It is the second Michelson interferometer in the lab, and will be referred to in the text as MI2. A very detailed description of the first Michelson interferometer has already been given by Jongbloets[1]. Therefore only a rough sketch of the MI2 will be given, emphasizing the differences between the MI1 and MI2.

Both the MI1 and MI2 are modular instruments, manufactured by Grubb Parsons Company[2] and modified in our workshop. A detailed survey of the hardware of the MI2 is shown in Fig. 1. Light, emerging from a broad-band source (5), is collimated by a combination of two mirrors (1). The resulting parallel beam is divided by the beamsplitter (13) into two beams. These beams are given an optical path difference by a translation of a mirror (14), driven by a stepping motor (16) in combination with a micrometer screw (15). After reflection on mirrors (12) and (14), the beams recombine at the beamsplitter, and interfere during their travel towards the detector. A TPX lens (11) focuses the beam onto the entrance of a lightpipe (9). The combination of TPX material of the lens (11) and a black polyethylene window (8) removes all radiation above 380 cm^{-1}. The spectral domain can be further confined by a suitable set of low-pass transmission filters (7). Modulation of the radiation can be achieved by a mechanical chopper (4) (Amplitude Modulation) or a vibration of mirror (12) (Phase Modulation).

There are three differences between the MI1 and the MI2.

1. The collimator mirrors (1) in the MI1 consist of a combination of a concave and a convex mirror. In the MI2 this is a combination of a concave and a flat mirror, resulting in a better collimating performance, but a somewhat smaller light-throughput.
2. For both the MI1 and the MI2 a set of mylar beamsplitters is available with thickness 6, 12.5, 25, 50 and 100 μm. The MI2 also has a 250 μm beamsplitter, providing the opportunity of recording spectra down to 2.5 cm^{-1}.
3. The micrometer in the MI1 allows a translation of the moving mirror over a maximum distance of 2 cm. In the MI2 this range is extended to 5 cm by a micrometer, manufactured by the L.S. Starrett Company[3], enabling us to record spectra with a higher resolution. With the MI2 the highest resolution is 0.05 cm^{-1}, if one records a one-sided interferogram and if one does not

F.I.R. MICHELSON INTERFEROMETER 2

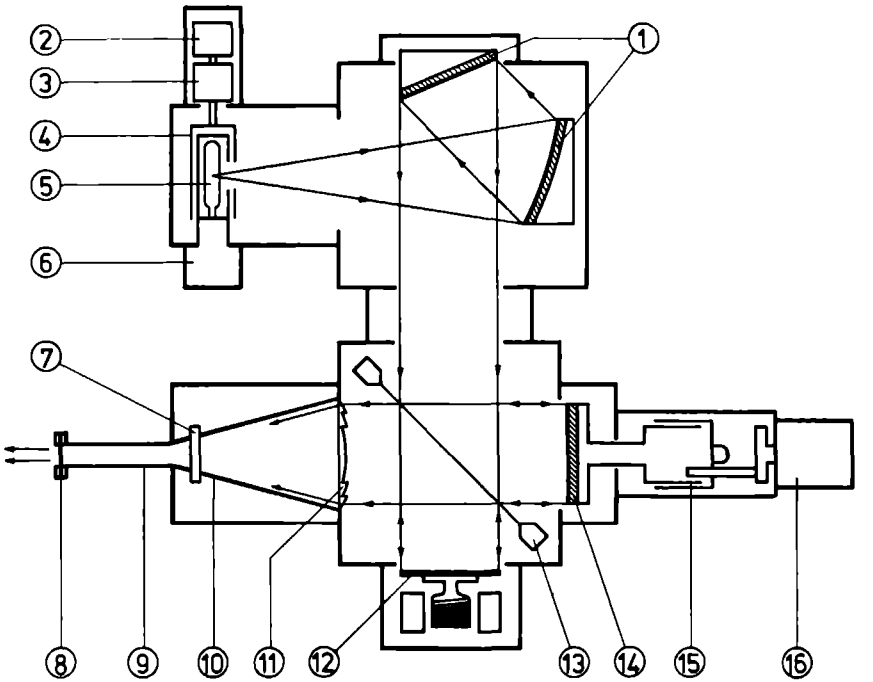

①	Collimator mirrors	⑨	Lightpipe (polished brass)
②	Reference signal generator	⑩	Brass cone
③	Chopper motor	⑪	TPX Fresnel lens
④	Chopper	⑫	Vibrating mirror
⑤	Medium pressure mercury lamp	⑬	Beamsplitter (mylar film)
⑥	Water-cooled lamp mount	⑭	Moving mirror
⑦	Transmission filter	⑮	Micrometer
⑧	Black polyethylene window	⑯	Stepping motor

Fig. 1

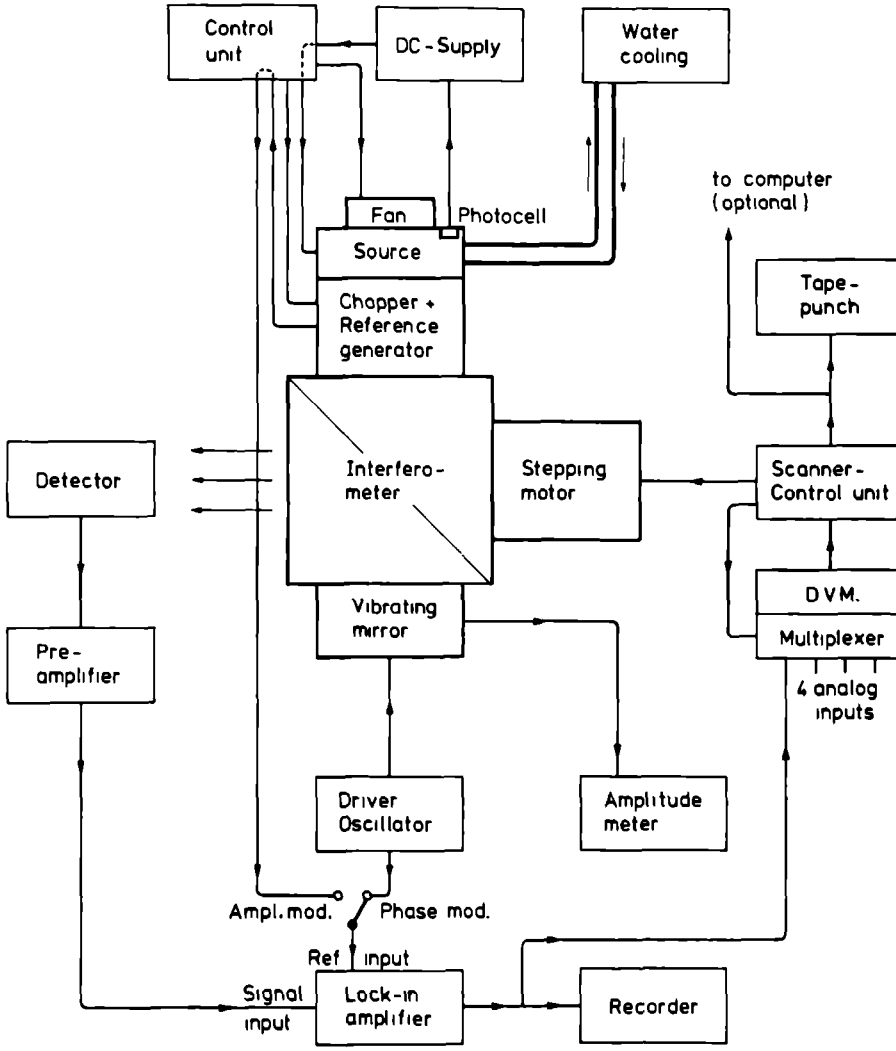

SCHEMATIC DIAGRAM OF FOURIER SPECTROMETER

Fig. 2

use an apodization function.

The electronic system of the Michelson interferometer, designed to record interferograms in the step-and-integrate mode, is shown in Fig. 2. For details the interested reader is again referred to the thesis of Jongbloets[1]. The resulting data-output of this system can optionally be punched on papertape or sent on-line to a PDP-11 computer. The configuration of the PDP-11 computer system and the sets of programs developed to manipulate interferograms and spectra are described in an appendix to this thesis.

References:

1. H.W.H.M. Jongbloets, Catholic University, Nijmegen, thesis (unpublished).
2. Sir Howard Grubb Parsons and Company Limited, Walkergate, Newcastle upon Tyne NE62YB, England.
3. The L.S. Starrett Co., Athol, Massachusetts, U.S.A., type no. 465 M.

Infrared Physics Vol 20 pp 121 to 126

2. III.

EXPERIMENTAL INVESTIGATION OF GHOSTLINES IN FOURIER SPECTROSCOPY IN THE FAR-INFRARED

M. J. H. VAN DE STEEG, H. W. H M. JONGBLOETS, J. H. M STOFLINGA, R. W VAN DER HEIJDEN, R. J. M. VAN VUCHT and P. WYDER
Research Institute for Materials, University of Nijmegen, Toernooiveld, Nijmegen, The Netherlands

(*Received* 19 *September* 1979)

Abstract In this work we have investigated the intensity of ghostlines which occur in the spectrum obtained with a two-beam Fourier interferometer when the travel of its moving mirror is periodically distorted This intensity has been compared quantitatively with the amplitude of the periodic travel distortion as measured directly with a dilatometer, enabling the determination of travel distortions as small as 0 2 μm It is concluded that the amplitude of the periodic distortion as calculated from the measured intensity of the ghostlines is in fair agreement with the distortion as obtained from a direct measurement

INTRODUCTION

The movable mirror used to vary the optical path difference in a two-beam Fourier spectrometer is either stepped between sampling points, or driven, ideally at constant speed. The influence of drive non-linearities has been treated theoretically by several authors for the case of drive speed variations in a continuous drive Michelson interferometer (e.g. by Connes[1] and Zachor[2]). From this it is well known that periodic non-linearities give rise to ghostlines in line spectra.

This provides a serious problem in spectra with a distinct peak behaviour. To illustrate this, in Fig. 1 part of a photoconductivity spectrum is shown for a germanium-sample, containing boron as the major and aluminum as the minor impurity (Jongbloets *et al*[3,4]). These spectra were recorded with an interferometer using two different micrometers (Fig. 1a,b). The two pairs of peaks at wave numbers 64.0 and 70.1 cm^{-1}, and at 66.7 and 72.8 cm^{-1}, correspond to the *D*- and *C*-transition lines of the B and Al impurities respectively. The measurements described below revealed that the extra peaks in Fig. 1b are ghostlines, originating from both a pitch error in the micrometer screw and a play in its assembly.

To investigate the occurrence of ghostlines in more detail, the spectra of some monochromatic far-infrared sources were measured with the interferometer combined with the two different micrometer units mentioned above. In the case of a monochromatic source, periodic non-linearities give rise to ghostlines, which are symmetrically spread around the central monochromatic line. This phenomenon has been demonstrated qualitatively by Gebbie,[5] using a laser line at 336.6 μm (29.71 cm^{-1}). In this work, this phenomenon is analysed quantitatively. The distortion amplitude determined from the intensity of the first ghostline is compared with the direct measurement of the periodic distortion using a contact dilatometer.

EXPERIMENTAL

The interferometer used was a Grubb Parsons Cube Interferometer, as described by Chantry *et al.*[6] Its moving mirror was connected directly to the spindle of a micrometer, the thimble of which is rotated by a Slo-Syn stepping motor, type SS25. This motor carries out 200 steps in one revolution yielding a 0.5 mm mirror travel. Backlash is minimized by a spring.

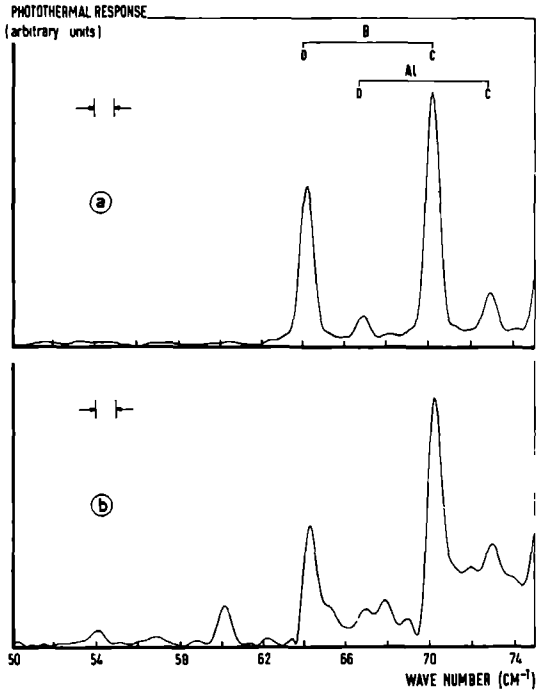

Fig 1 Photoconductivity spectra for a Ge sample, showing the *D*- and *C*-transition lines of B and Al impurities The spectra were obtained with a Michelson interferometer, using two different micrometer units (a) MM20 and (b) MM50-B. In (b) extra peaks due to ghostlines are shown The spectral resolution is indicated by arrows

Two different micrometers are used: a micrometer of 20 mm range, manufactured by GKN Shadlow Metrology, Sheffield, England, referred to in the text as MM20, and one of 50 mm range, manufactured by the L. S. Starret Co., Athol, Mass., U.S.A., type-no. 465 M. This 50 mm range micrometer is referred to as MM50-A in its original state and as MM50-B after a home made improvement.

The monochromatic sources were an optically pumped FIR laser, operating at a wavelength of 118.8 μm (84.2 cm^{-1}), and a simple far-infrared grating monochromator as described by Dorigo *et al.*[5] A pyro-electric detector was used in conjunction with the laser, while a He-cooled Ge-bolometer system from Infrared Laboratories was exploited when working with the monochromator. The output data of the interferograms were sent on-line to a PDP-11 laboratory computer, and handled there by a program with various facilities for manipulating interferograms and spectra.

For the direct determination of the periodic distortion in the travel of the micrometer, use was made of a contact displacement meter, type Tesatronic, manufactured by TESA S.A., Switzerland. The data from the analogue output of the dilatometer were also sent on-line to the computer. This made it possible to determine deviations from a linear movement with an accuracy of 0.2 μm.

In Fig. 2a and b the spectrum of a monochromatic line is shown for the MM50-A unit, using the 118.8 μm (84.2 cm^{-1}) laser line and a line of the grating monochromator at 126.4 cm^{-1} respectively. In Fig. 2c and d the corresponding spectra are shown for the MM20 and MM50-B units respectively. When the laser was used, the widths of the monochromatic lines in these figures were determined by the maximal optical path

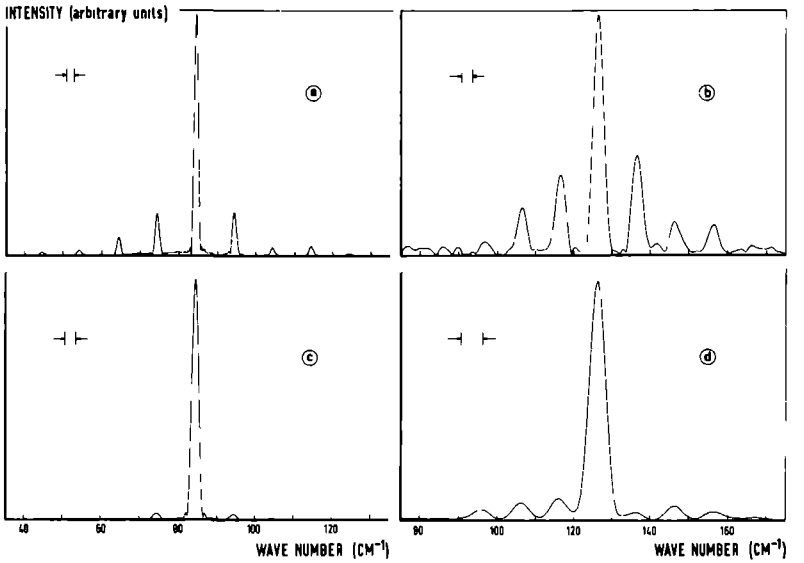

Fig 2 Central lines from a monochromatic source accompanied by ghostlines in spectra obtained with a Michelson interferometer As source of monochromatic radiation and as micrometer units use was made of respectively (a) laser MM50-A (b) grating monochromator MM50-A (c) laser MM20 and (d) grating monochromator MM50 B The spectral resolution is indicated by arrows

difference used in scanning the interferogram When the monochromator was used, the widths were determined mainly by the shape of the line itself

In Fig 3a, b and c the deviations from a linear movement of the mirror have been plotted for the MM50-A, MM20 and the MM50-B units respectively, as measured with the displacement meter equipment The runs were taken over 3 consecutive revolutions of the micrometers The little jumps in the figures are caused by the resolution of the *A–D* converter used in conjunction with the dilatometer Because of the play in the assembly, the direct measurements of the deviations for the MM50-A unit did not reproduce, therefore Fig 3a has to be considered as a typical result

All spectra in Fig 2a–d show ghostlines spread around the wave number of the monochromatic source lines The separation between the ghostlines is precisely $10\,cm^{-1}$, corresponding to a travel of 0 5 mm in one revolution of the micrometers The intensities of the ghostlines in Fig 2a and b, both obtained with the MM50-A unit, increase with increasing wavenumber The intensities are obviously larger the larger the deviations are from a linear movement, as is clearly seen by comparing Fig 2a–d with Fig 3a–c

In the following section the relation between the intensities of the ghostlines and the magnitude of a periodic travel distortion will be derived as a function of wavenumber

RELATION BETWEEN GHOSTLINE INTENSITY AND AMPLITUDE OF PERIODIC TRAVEL DISTORTION

Consider the case of a moving mirror driven in discrete steps of length Δx by a micrometer which travels a length L in one revolution Assume a sinusoidal distortion with period L and amplitude ϵ of the micrometer Since in a Michelson interferometer, the optical path difference is twice the travel difference of the moving mirror, the optical

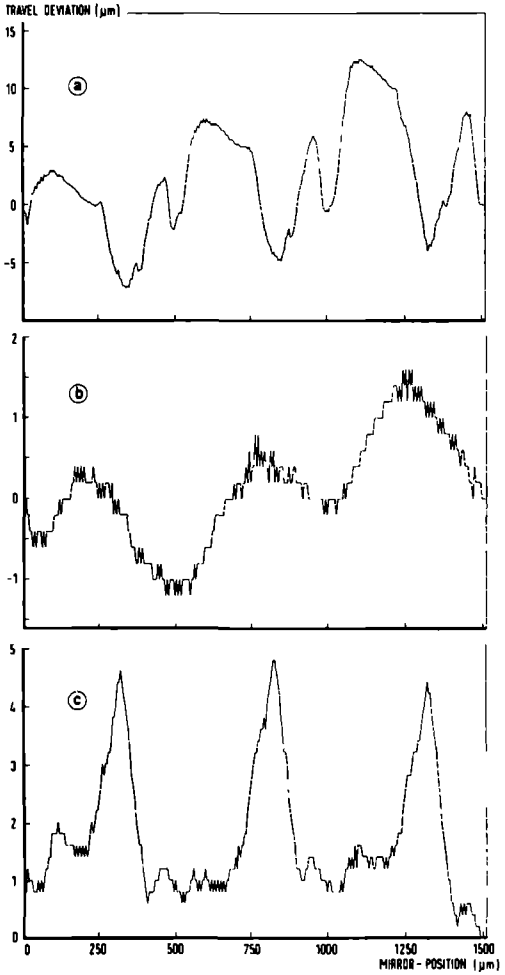

Fig. 3 Measured deviation from a linear movement of the travel of the moving mirror of the Michelson interferometer, using different micrometer units (a) MM50-A, (b) MM20 and (c) MM50-B. The jumps of 0.2 μm were caused by the limited resolution of the *A–D* converter, used in conjunction with the dilatometer

path difference x after N steps is given by:

$$x = 2N\Delta x + 2\epsilon \sin\left(\frac{2\pi N\Delta x}{L} - \varphi\right) \tag{1}$$

where φ is a phase-angle, determined by the choice of the $x = 0$ position. This angle can be chosen as $\varphi = 0$ without affecting the results.

In case of a monochromatic line with wave number σ_0 and intensity $S(\sigma_0)$, the interferogram $I(x)$ is given by:[8]

$$I(x) = S(\sigma_0) \cdot \cos\left\{4\pi\sigma_0\left[N\Delta x + \epsilon \sin\left(\frac{2\pi N\Delta x}{L}\right)\right]\right\} \tag{2}$$

This formula can be rewritten as [9]

$$I(x) = S(\sigma_0) \sum_{n=-\infty}^{\infty} J_n(4\pi\sigma_0\epsilon)\cos\left[4\pi\left(\sigma_0 + \frac{n}{2L}\right)N\Delta x\right] \tag{3}$$

where J_n are Bessel functions After a Fourier transform of the interferogram, the resulting spectrum $S(\sigma)$ is a discrete line-spectrum with

$$S(\sigma_n) = S(\sigma_0)J_n(4\pi\sigma_0\epsilon)$$

for

$$\sigma_n = \sigma_0 + \frac{n}{2L}, n = 0, \pm 1, \pm 2,$$

and

$$S(\sigma) = 0 \text{ elsewhere} \tag{4}$$

Defining H as the ratio between the intensities of the first ghostline at $\sigma = \sigma_0 \pm 1/(2L)$ and the central monochromatic line, equation (4) yields

$$H = \frac{J_1(4\pi\sigma_0\epsilon)}{J_0(4\pi\sigma_0\epsilon)} \tag{5}$$

If there is a non-sinusoidal distortion of period L, this distortion can be expanded in terms of a Fourier series In analogy with the derivation given above, each Fourier component gives rise to a set of ghostlines around the central monochromatic line The mth Fourier component will have its first ghostlines at $\sigma = \sigma_0 \pm m/(2L)$. Thus the ghostlines at $\sigma = \sigma_0 \pm 1/(2L)$ are only originating from the first Fourier component of the distortion with the fundamental period L Using the same definition for H as given above, ϵ in equation (5) represents the amplitude connected with the first Fourier component

DISCUSSION AND CONCLUSIONS

If in a Michelson interferometer the moving mirror is directly driven by a micrometer with a periodic distortion in its linear movement, then every line in a line-spectrum is accompanied by a set of ghostlines This was shown most clearly in the photoconductivity spectra and the monochromatic line spectra of Fig 1a, b and Fig 2a–d respectively By comparing Fig 2a with Fig 2b it can be seen that the intensities of the ghostlines, relative to that of the central monochromatic line, increase with increasing wavenumber For the left and right first ghostline this is in agreement with equation (5) By comparing Fig 3a–c with Fig 2a–d, it is seen that a larger distortion amplitude yields intenser ghostlines, which is also in agreement with equation (5) for the first ghostlines From the values of H in Fig 2a–d values for ϵ have been calculated, using equation (5) These are given in Table 1

The ratio H is only determined by that component of the distortion which has the same period as the revolution period of the micrometer The amplitude of this com-

Table 1 Values for ϵ determined from the ghostlines and from direct measurements for the micrometer units MM50-A, MM20 and MM50-B

Micrometer unit	σ_0(cm^{-1})	$\epsilon(\mu m)$ From direct measurements	$\epsilon(\mu m)$ From ghostlines
MM50-A	84 2	—	3 3 ± 0 2
	126 4	—	4 4 ± 0 6
MM20	84 2	0 6	0 42 ± 0 03
MM50-B	126 4	1 4	0 8 ± 0 4

ponent is determined from the curves in Fig 3 by approximating these curves by a sine and equalizing the area under the curves In Table 1 the results are given for Fig 3b,c

The values for ϵ calculated from the direct measurements are slightly higher than those obtained from the ghostlines The method described above for obtaining a value for ϵ from the direct measurements cannot distinguish contributions to the deviation curves from distortions with period $3L$, $5L$, $7L$, , while the values for ϵ from the first ghostline are only caused by the distortion component with period L Taking this into account, the agreement between the obtained values for ϵ for the MM20 and MM50-B micrometer units is satisfactory

It can be concluded that it is possible to get a reliable value for the travel distortion amplitude of the moving mirror of a Fourier spectrometer from the measured intensities of the ghostlines alone

Acknowledgements—Part of this work has been supported by the 'Stichting voor Fundamenteel Onderzoek der Materie" (FOM) with financial support of the ' Nederlandse Organisatie voor Zuiver Wetenschappelijk Onderzoek" (ZWO)

REFERENCES

1 CONNES J , *Revue Opt theor instrum* **40,** 45 (1961)
2 ZACHOR A S , *Appl Opt* **16,** 1412 (1977)
3 JONGBLOETS H W H M , J H M STOELINGA, M J H VAN DE STEEG & P WYDER, *Proc Int Conf Magneto Optics Physica* **89B,** 18 (1977)
4 JONGBLOETS H W H, M J H M STOELINGA M J H VAN DE STEEG & P WYDER, *Phys Rev* **B 20,** 3328 (1979)
5 GEBBIE H A , *Pure appl Chem* **11,** 577 (1965)
6 CHANTRY G W , H M EVANS, J CHAMBERLAIN & H A GEBBIE, *Infrared Phys* **9,** 85 (1969).
7 DORIGO M V , J H M STOELINGA & P WYDER, *Z angew Math Phys* **20,** 565 (1969)
8 CHANTRY G W (Editor), *Submillimetre Spectroscopy*, Chapter 3 Academic Press, New York (1971)
9 CONNES J , *Revue Opt theor instrum* **40,** 76 (1961)

2.IV. *Reducing the effects of ghostlines in a step-record Fourier spectrometer*

Abstract

Presented is an analysis of the intensity of ghostlines, caused by a periodic non-linearity in the travel of the movable mirror in a two-beam Fourier spectrometer, used in the step-record mode. The ghostlines are studied for two cases: 1. For a modulus spectrum, calculated after a complex Fourier transform. 2. For a spectrum, calculated by a cosine Fourier transform after symmetrizing the measured interferogram. In the latter case the intensity of the ghostlines is also dependent on the position of the centre of the interferogram. This dependence has been examined theoretically and verified experimentally, for the case of a monochromatic source. It is shown that an appropriate choice of the position of the centre of the interferogram and the application of a cosine Fourier transform can reduce the intensity of the ghostlines drastically in practice.

Introduction

In a two-beam Fourier spectrometer one of the mirrors is movable to be able to vary the optical path difference between the two interfering beams. The movable mirror is either translated in equal length intervals - the step record mode -, or driven with constant speed. Deviations in the length of the intervals or non-linearities in the drive speed give rise to ghostline structures in the spectra[1,2,3].

For a continuous drive Michelson interferometer, provided with a fringe-reference sampling system, the intensity of ghostlines can be reduced by delaying the reference fringes[4,5,6]. A fringe-reference system in a Fourier spectrometer, used in the step-record mode, provides perfect sampling of the interferogram. In this article a new method of reducing the intensity of ghostlines, without the necessity of constructing a fringe-reference system is presented. This method can be applied to spectra, calculated by using a cosine Fourier transform after symmetrizing the measured interferogram. For such spectra the intensity of the ghostlines is a periodic cosinelike function of the position of the centre of the interferogram (PCI). Thus the intensity of the ghostlines can be reduced by an appropriate choice of PCI.

In the next section the theory behind this method is developed for the case of a monochromatic source. The following sections describe an experimental verification of this theory with a laser source and give an experimental example of the possibility of reducing the intensities of ghostlines with this method for a broad spectrum with a distinct peak behaviour.

Theory

Let the position readout of the driving system of the movable mirror be denoted by x and let x' be the actual position of this mirror. Assuming a sinusoidal deviation from the desired position with amplitude ε and period L, x' and x are related by

$$x' = x + \varepsilon \cdot \sin [2\pi(x-x_o)/L] \quad . \tag{1}$$

Here x_o defines the position of the comb of points with zero deviation. Let for the case of no deviation, x_c denote the position of the centre of the interferogram (PCI), i.e. the unique position of the movable mirror, where the two beams interfere constructively for all wavelengths.

Assume a monochromatic source with wave number σ_o and intensity S. Remembering that the optical path difference is twice the travel distance of the moving mirror, the interferogram I(x) is given by

$$I(x) = S \cdot \cos\left\{4\pi\sigma_o \left[(x-x_c) + \epsilon \cdot \sin[2\pi(x-x_o)/L]\right]\right\} \qquad (2)$$

Using the expansions of $\cos(z\sin\theta)$ and $\sin(z\sin\theta)$ into Bessel functions $J_n(z)$ and using basic goniometric relations, a straightforward calculation yields

$$I(x) = S \cdot \sum_{n=-\infty}^{\infty} J_n(4\pi\sigma_o\epsilon) \cdot \cos[2\pi n(x_o-x_c)/L] \cdot \cos[4\pi(\sigma_o+\frac{n}{2L}) \cdot (x-x_c)]$$

$$+ S \cdot \sum_{n=-\infty}^{\infty} J_n(4\pi\sigma_o\epsilon) \cdot \sin[2\pi n(x_o-x_c)/L] \cdot \sin[4\pi(\sigma_o+\frac{n}{2L}) \cdot (x-x_c)] \quad .(3)$$

If no deviation was present, the interferogram would have been a symmetric function of $(x-x_c)$. As can be inferred from equation (3), the sinusoidal deviation gives rise to both symmetric and antisymmetric terms in the interferogram. From interferograms, recorded around PCI, spectra can be obtained in two different ways. First a modulus spectrum $P(\sigma)$ can be calculated after a complex Fourier transform of the interferogram. Secondly, - after symmetrizing the interferogram, if necessary -, a spectrum $S(\sigma)$ can be calculated by application of a cosine Fourier transform. Hereafter the spectra $P(\sigma)$ and $S(\sigma)$ will be referred to as modulus and real spectrum respectively.

The modulus spectrum of interferogram I(x) is given by

$$P(\sigma_n) = S \cdot |J_n(4\pi\sigma_o\epsilon)|$$

$$\text{for} \quad \sigma_n = \sigma_o + n/(2L) \quad , \quad n = 0, \pm1, \pm2, \ldots. \qquad (4)$$

and $P(\sigma) = 0$ elsewhere.

The intensity of the central monochromatic line is reduced by a factor $J_o(4\pi\sigma_o\epsilon)$ and additionally accompanied by a set of ghostlines, at symmetric positions around the central line. The intensity of the ghostline structure is only a function of the amplitude of the distortion and the wave number of the monochromatic line.

The real spectrum $S(\sigma)$ is given by

$$S(\sigma_n) = S \cdot J_n(4\pi\sigma_o\varepsilon) \cdot \cos[2\pi n(x_o - x_c)/L]$$

$$\text{for } \sigma_n = \sigma_o + n/(2L) \quad , \quad n = 0, \pm 1, \pm 2, \ldots . \tag{5}$$

and $S(\sigma) = 0$ elsewhere.

Here the intensity of the ghostlines at positions $\sigma_o + n/(2L)$ is a cosinelike function of $(x_o - x_c)$ with period L/n. Corresponding ghostlines at wavenumbers $n/(2L)$ above and below σ_o are opposite in sign, if n is odd and equal in sign for even n. The amplitude of the cosine in equation (5) is equal to the intensity of the corresponding ghostlines in equation (4). The intensity of the central monochromatic line for n=0 does not depend on the method of Fourier transform. Thus application of a cosine Fourier transform and a suitable experimental choice of x_c provides a method of reducing the intensity of the ghostlines.

If the periodic deviation with period L is not simply sinusoidal, the deviation x'-x can be expanded in terms of a Fourier series, given by

$$x' - x = \sum_{m=1}^{\infty} \varepsilon_m \cdot \sin[2\pi m(x - x_{o,m})/L] \quad . \tag{6}$$

Analogous with the theory developed before each Fourier component gives rise to an additional ghostline structure. For example in a modulus spectrum after a complex Fourier transform the contribution to the intensity of the ghostlines nearest to the central monochromatic line and associated with the m-th Fourier component, is given by

$$P(\sigma_{m,1}) = S \cdot |J_1(4\pi\sigma_o\varepsilon_m)| \quad , \tag{7}$$

with $\sigma_{m,1} = \sigma_o \pm m/(2L)$. The corresponding contribution in a spectrum, obtained with a cosine Fourier transform is given by

$$S(\sigma_{m,1}) = S \cdot J_1(4\pi\sigma_o\varepsilon_m) \cdot \cos[2\pi m(x_{o,m} - x_c)/L] \quad . \tag{8}$$

The Fourier spectrometer used was a Grubb Parsons Cube Michelson interferometer as described by Chantry et al.[7]. Its movable mirror was connected directly to the spindle of a micrometer of 50 mm range and a pitch of 0.5 mm, manufactured by the L.S. Starrett Co., Athol, Massachusetts, U.S.A., type 465 M. A 200 steps/rev. SLO-SYN stepping motor, type SS25, rotated the thimble of the micrometer. An additional spring was used to reduce backlash.

The deviation from a linear translation as a function of the position of the movable mirror is shown in Fig. 1 by a continuous curve. The periodic deviation was recorded over two consecutive periods, coupled to the pitch of the micrometer. The position was measured directly by a contact displacement meter, type Tesatronic, manufactured by TESA S.A., Switzerland. The data from the analogue output of the dilatometer were processed by a PDP-11 computer. This configuration enabled us to determine deviations with an accuracy of about 0.2 μm.

In order to check the theory, developed in the preceding section, the standard broad-band source of the interferometer was replaced by a monochromatic, optically pumped FIR laser, operating at a wavelength λ of 118.8 μm (84.2 cm^{-1}). In conjunction with the laser a pyro-electric detector was used. From the output data of the measured two-sided interferograms a real and a modulus spectrum were calculated on the computer. Before calculating the real spectrum by a cosine Fourier transform, the interferogram was symmetrized by phase-correction, using the convolution method of Sakai, Vanasse and Forman[8].

The combination of the very sharp laser line and the nearly perfect optical alignment of the interferometer made the interferogram invariant for shifts of $\lambda/2$ in the position of the movable mirror. This enabled us to vary the PCI in a combination of two ways. First by shifting the position of the fixed mirror by means of adjustment screws. Secondly, after recording the interferogram around the adjusted PCI, by a simulated shift in PCI in integer multiples of $\lambda/2$ afterwards. This is achieved by calculating symmetrized interferograms around new positions in the array of interferogram datapoints, corresponding with such shifts.

Figure 2 shows a modulus spectrum, recorded at PCI=0 μm. A ghostline structure is clearly visible, symmetrically spread around the central monochromatic line at 84.2 cm^{-1} with spacings of precisely 10 cm^{-1}. In this figure one can see that ghostlines R_1, R_2 and R_3 have the same intensity as L_1, L_2

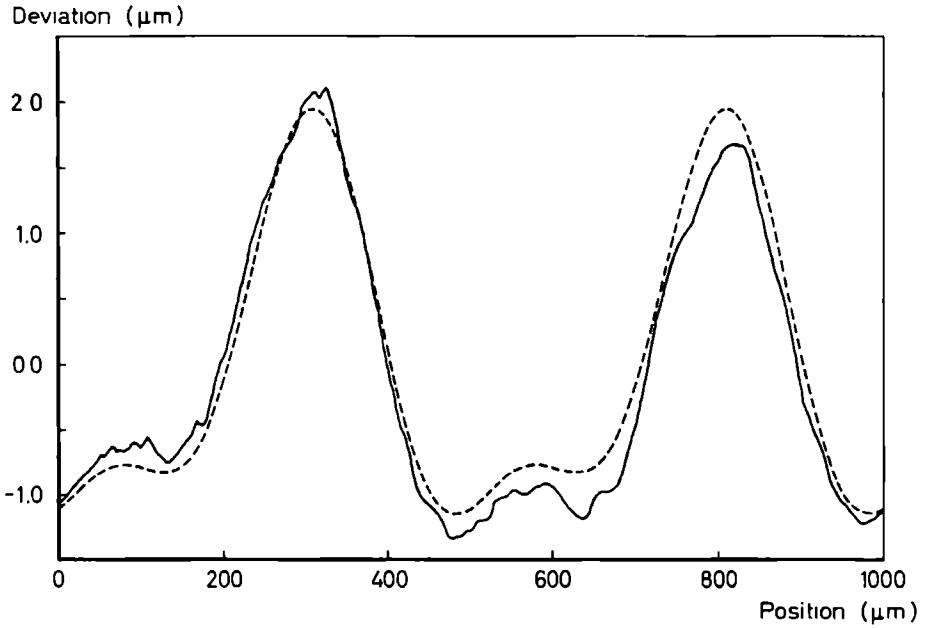

Fig. 1: Deviation from a linear translation as a function of the position of the movable mirror. Continuous curve: measured deviation. Dashed curve: description of the measured deviation by the first two terms of a Fourier analysis.

and L_3 respectively. Modulus spectra, recorded at other PCI's, were identical to the spectrum shown in figure 2.

A set of real spectra, recorded for PCI's within one revolution period of the micrometer at regular intervals of 50 μm, is shown in Fig. 3. As can be inferred from this figure, ghostlines R_1, R_2 and R_3 have the same amplitude as L_1, L_2 and L_3 respectively, but are opposite in sign. The intensity of the central monochromatic line did not show any dependence on PCI.

The intensity of ghostlines R_1, R_2 and R_3, normalized to the intensity of the central monochromatic line is shown in Fig. 4, as a function of the PCI for two consecutive revolutions of the micrometer. Corresponding values of the positions in Figures 1 and 4 refer to the same settings of the micrometer. It is clearly visible in Fig. 4 that the period of change in intensity of R_2 and R_3 is one half and one third of the corresponding period of R_1 respectively. The solid curves represent fits to the datapoints, using the expression

$$y_{o,n} \cdot \cos[2\pi n(x-x_{o,n})/L] \quad ,$$

where n=1, 2, 3 for lines R_1, R_2 and R_3 respectively and L=500 μm.

Discussion

We have seen before that the deviation of the position of the movable mirror is a periodic function, coupled to the revolution period of the micrometer. Therefore the deviation x'-x can be expanded in terms of a Fourier series, given by equation (6) with L=500 μm. The results of a Fourier analysis of the deviation curve of Fig. 1 are given in table 1 for the first three harmonic terms.

The dashed curve in Fig. 1, being the sum of the first two terms, shows that the deviation can be described very well by the first two harmonic terms. Considering Fig. 1 it should be noted that the exact form of the deviation curve changed, whenever the driving system of the movable mirror had to be remounted. Although the area under the deviation curve did not change appreciably, the individual contribution of each harmonic term did.

As mentioned before, the intensity of the ghostlines in the real spectra, as shown in Fig. 3, exhibited a cosinelike dependence on the PCI. In the corresponding modulus spectra, as illustrated in Fig. 2, the intensity of the ghostlines appeared to be independent of the PCI. For the magnitude of the

Table 1: Values for the parameters (defined in equation (6)) of the first three terms of the Fourier expansion of the periodic non-linearity in the travel of the movable mirror. These values are obtained from direct measurement of the deviation and from an analysis based on the intensity of the ghostlines in the spectra. L = 500 μm.

	From direct measurement		From ghostlines in real spectra		From ghostlines in modulus spectra
m	ε_m (μm)	$x_{o,m}$ (μm)	ε_m (μm)	$x_{o,m}$ (μm)	ε_m (μm)
1	1.38	175	1.10 ± 0.05	269	1.12 ± 0.05
2	0.58	249	0.81 ± 0.05	136	0.76 ± 0.05
3	0.02	-	0.29 ± 0.05	118	0.28 ± 0.05

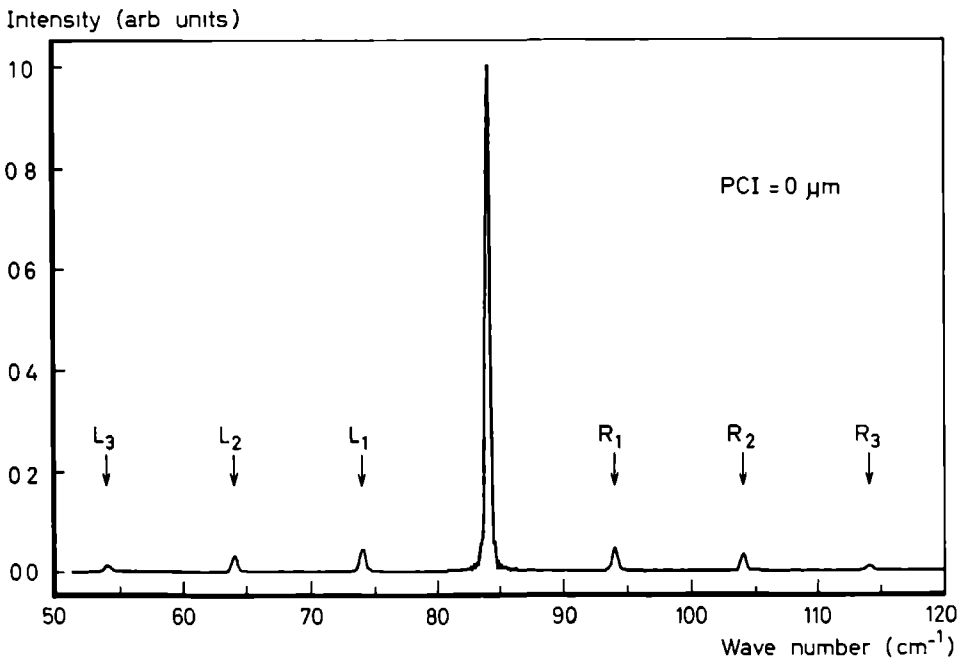

Fig. 2: Measured modulus spectrum at PCI = 0 μm, using a monochromatic source.

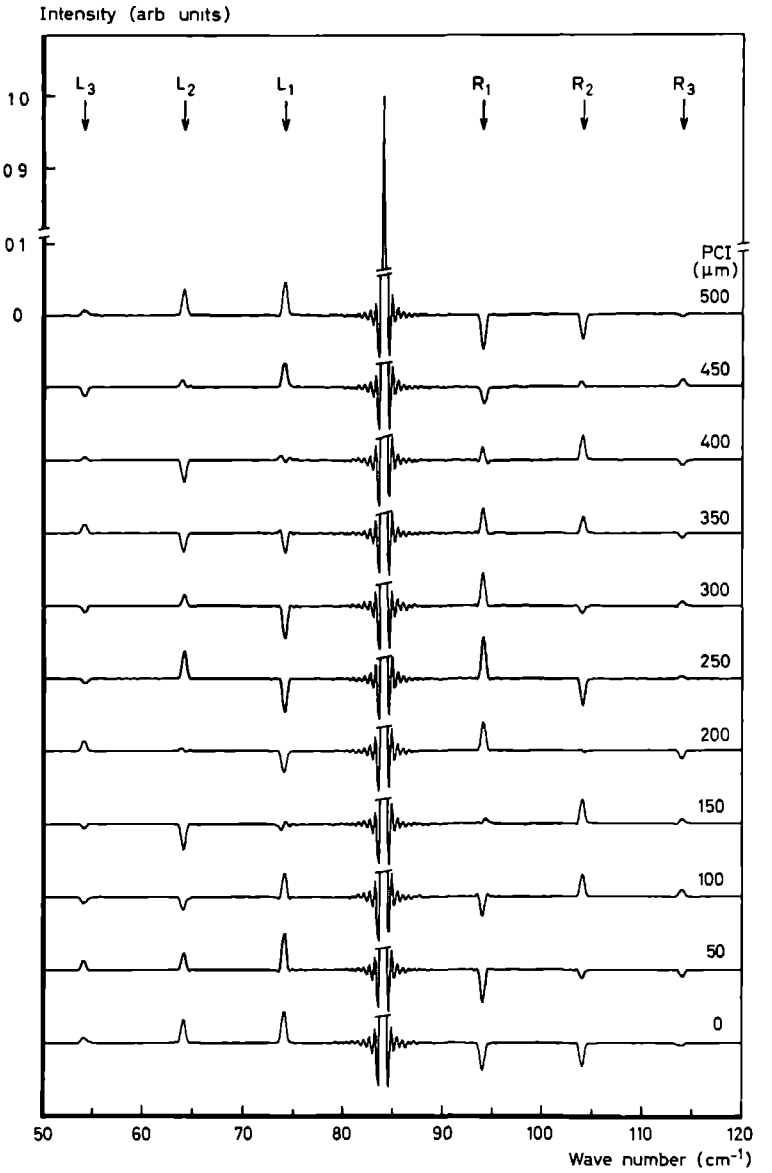

Fig. 3: Measured real spectra for different PCI's within one revolution period of the micrometer, using a monochromatic source.

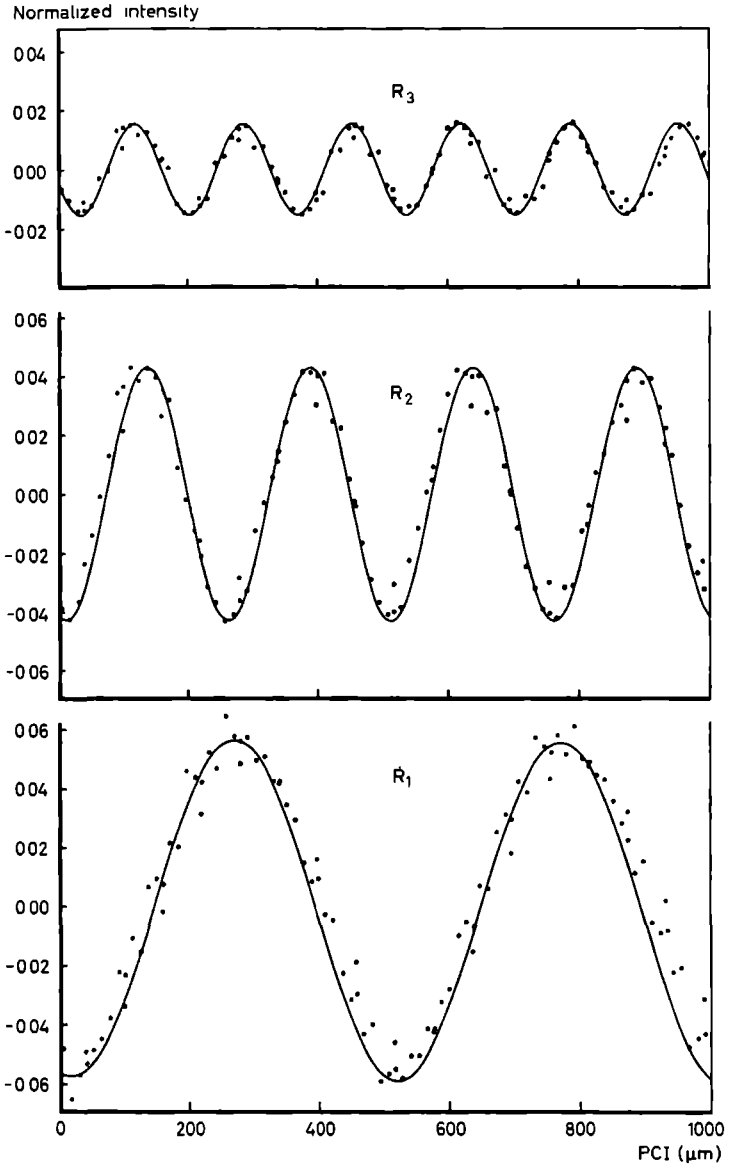

Fig. 4: Intensities of ghostlines R_1, R_2 and R_3 as a function of the PCI, taken from the real spectra and normalized to the intensity of the monochromatic line.

deviation of interest here and for σ_o=84.2 cm^{-1}, the values of the higher order Bessel functions J_2, J_3, ... can be neglected with respect to those of J_1. Furthermore the reduction in intensity of the central monochromatic line, caused by the value of the J_o multiplication factor, can also be neglected.

A pure sinusoidal deviation in the travel of the movable mirror with period L=500 μm would explain the periodicity of the observed cosinelike intensity of the ghostlines in the real spectra. Such sinusoidal deviation would predict, however, that ghostlines R_2 and L_2 point in the same direction, as distinct from the observed behaviour in Fig. 3. Moreover, it cannot account for the observed magnitude of ghostlines L_2, L_3, R_2 and R_3 in the modulus spectra.

Therefore we consider the description of the periodic deviation in terms of a Fourier series again. According to the theory developed before each Fourier component adds its individual ghostline structure to the spectra. We associate the intensities of ghostlines L_1 and R_1, L_2 and R_2, and L_3 and R_3, shown in Figures 2, 3 and 4, with the J_1 Bessel functions of the 1^{st}, 2^{nd} and 3^{rd} Fourier component of a periodic deviation with period L=500 μm respectively. The observed periods in the intensity of the ghostline-pairs in the real spectra, as shown in Fig. 4, are consistent with this assumption, as can be seen in equation (8). Using this equation, values for ϵ_m and $x_{o,m}$ have been determined for the first three harmonic terms from the fitted curves in Fig. 4. The results are given in table 1. Under the same assumption table 1 contains values for ϵ_m, determined from the modulus spectra by means of equation (7).

The values for ϵ_m in table 1, obtained from the ghostline intensity in the real spectra and the modulus spectra are consistent with each other. This is in accordance with the theoretical analysis, which predicts that the amplitude of the cosine of the ghostline intensity in the real spectra is equal to the intensity of the corresponding ghostlines in the modulus spectra (see equations (7) and (8)). In table 1 corresponding values of ϵ_m and $x_{o,m}$, obtained from direct measurement of the deviation from a linear translation of the moving mirror and from the intensity of the ghostlines, are slightly different. This difference can be accounted for by the fact that between the direct measurement of the deviation and the recording of the spectra, the driving system of the movable mirror had to be remounted. We have already mentioned before that the direct measured deviation curves never reproduced well after a new build-up of the driving system.

We have seen before that the intensity of the ghostlines in a real spectrum is a cosinelike function of the PCI. The amplitude of these cosine

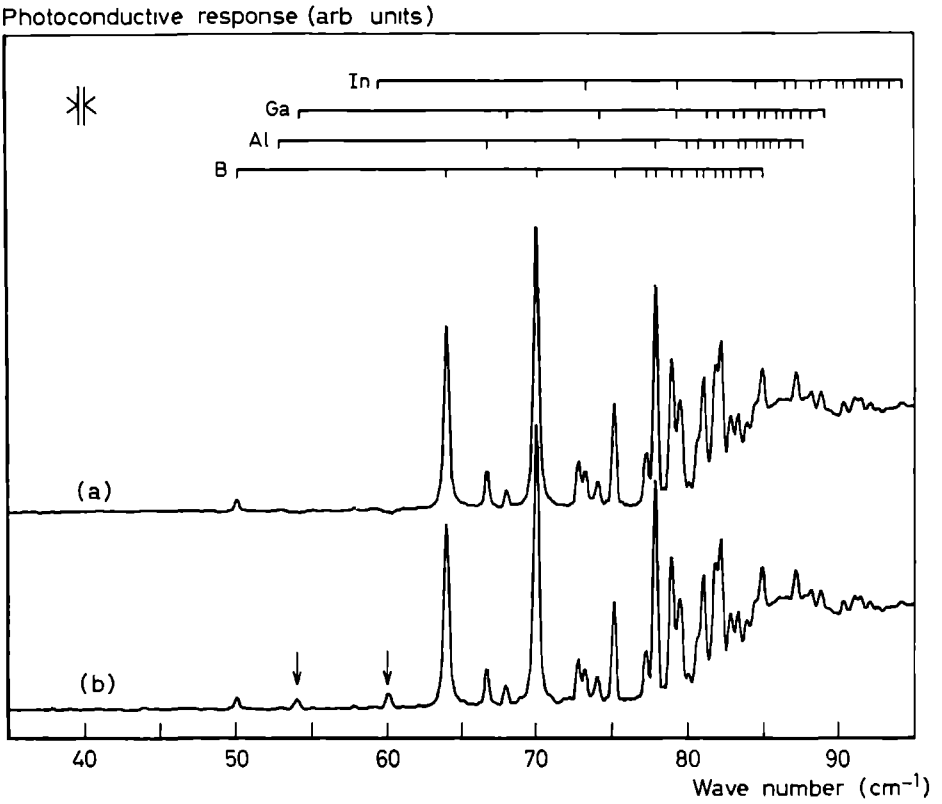

Fig. 5: Photoconductivity spectra for a high purity germanium sample, originating from one interferogram, (a): real spectrum, (b): modulus spectrum. The expected line positions for the boron, aluminium, gallium and indium shallow acceptor impurities and the spectral resolution are indicated in the upper part of this figure. The structure indicated by the arrows is ascribed to ghostlines.

functions is equal to the intensity of the corresponding ghostline in the modulus spectrum. The cosinelike dependence of the ghostline intensity in real spectra offers the experimentalist a method to reduce this intensity. This can be obtained merely by calculating real spectra after a suitable choice of the PCI.

For the situation shown in Figures 3 and 4 there is no unique position of the PCI, for which the intensities of all ghostlines are minimal at the same time. This is caused by the fact that there is no phase relation between the different harmonic components of the periodic deviation. Such a unique position would exist, if the deviation was nearly sinusoidal. Fortunately such an ideal situation was approached after a new build-up of the driving system. This enabled us to prove the practical applicability of the method.

For this purpose Fig. 5 shows photoconductivity spectra with a distinct peak behaviour. The spectra were recorded with the Photothermal Ionization Spectroscopy method[9] on a p-type high purity germanium sample, containing B, Al, Ga and In as dominating shallow impurities. The experimental set-up was the same as described in ref. 10. For a carefully chosen PCI a real spectrum is shown in Fig. 5a and a modulus spectrum in Fig. 5b, both spectra originating from the same interferogram. Indicated by arrows in the modulus spectrum, two ghostlines are clearly visible at wavenumbers 54 and 60 cm^{-1}, associated with the strong lines at 64 and 70 cm^{-1} respectively. These ghostlines are nearly completely absent in the real spectrum.

Conclusions

If in a two-beam Fourier spectrometer, operated in the step-record mode, the travel of the movable mirror is subject to a periodic nonlinearity, every spectral element in a spectrum is accompanied by a set of ghostlines. In a modulus spectrum, calculated after a complex Fourier transform of the interferogram, the intensity of the ghostlines is only dependent on the amplitude of the nonlinearity and the wavenumber of the spectral element. In a spectrum obtained by applying a cosine Fourier transform after symmetrizing the interferogram this intensity is also dependent on the position of the centre of the interferogram. This dependence has been examined theoretically and verified experimentally. It has been shown that an appropriate choice of the position of the centre of the interferogram, together with the use of a cosine Fourier transform for symmetrized interferograms, offers a method of reducing the intensity of the ghostlines considerably in practice.

References:

1. J. Connes, Revue Opt. théor. instrum. 40, 45 (1961).
2. A.S. Zachor, Appl. Opt. 16, 1412 (1977).
3. M.J.H. van de Steeg, H.W.H.M. Jongbloets, J.H.M. Stoelinga, R.W. van der Heijden, R.J.M. van Vucht and P. Wyder, Infrared Phys. 20, 121 (1980).
4. T. Nishiyama, T. Yamauchi, M. Ohno, M. Morii, N. Ura and K. Masutani, Jpn. J. Appl. Phys. 14, Suppl. 14-1, 67 (1975).
5. A.S. Zachor and S.M. Aaronson, Appl. Opt. 18, 68 (1979).
6. A.S. Zachor, I. Coleman and W.G. Mankin, "Spectrometric techniques, vol II", Academic Press, New York (1981), chapter 3.
7. G.W. Chantry, H.M. Evans, J. Chamberlain and H.A. Gebbie, Infrared Phys. 9, 85 (1969).
8. H. Sakai, G.A. Vanasse and M.L. Forman, J. Opt. Soc. Am. 58, 84 (1968).
9. For a review see: Sh.M. Kogan and T.M. Lifshits, Phys. Status Solidi (a) 39, 11 (1977).
10. H.W.H.M. Jongbloets, J.H.M. Stoelinga, M.J.H. van de Steeg and P. Wyder, Phys. Rev. B 20, 3328 (1979).

Abstract

This article deals with the detection of possible Fractional Charge Impurities (FCI's) in semiconductors with Photothermal Ionization Spectroscopy (PTIS) at low temperatures. Analytical formulas are given for the PTIS signal strength and the minimal concentration of impurities, detectable with PTIS, both for majority FCI's and normal shallow majority impurities. Account has been taken of semiconductor material constants, as well as temperature, background radiation and degree of compensation. The experimental set-up used for a search for FCI's with PTIS on a p-type germanium sample is described. From the absence of a PTIS signal, originating from FCI's, it is concluded that this sample contains less than 1.5×10^{11} acceptor-like FCI's per cm^3 (corresponding to a free quark density of 5×10^{-14} quarks per nucleon). It is shown that, with the experimental configuration used, down to 10^7 FCI's per cm^3, if present, can be detected. Modifications to the experiment are proposed which lower this limit with a factor of at least 100.

3.I. *Introduction*

In 1964 Gell-Mann[1] and Zweig[2] independently suggested that particles with fractional charges might be the basic constituents of nucleons. These particles were christened "quarks" by Gell-Mann. Since then numerous searches for quarks have been reported. For a review see for example Kim[3], Jones[4] and Marinelli and Morpurgo[5].

In 1977 LaRue, Fairbank and Hebard[6] reported the first successful observation of third-integral charges. The technique applied was a modification of the original Millikan oil-drop experiment[7]. A superconducting niobium ball was suspended magnetically between two horizontal capacitor plates at liquid helium temperature. The position of the ball was sensed with a SQUID magnetometer and the charge of the ball could be changed at will by movable β^+ and β^- emitters. The electric charge of a ball could be deduced by measuring its position response to an alternating electric field between the capacitor plates. After their publication suggestions in the literature about possible systematical errors were ruled out by additional measurements, confirming their original results[8]. But up to now they are the only group that claims to have observed fractional charge. Therefore it may be desirable to check their results in a different environment.

It is well known that an isolated atom, consisting of an electron and a nucleus with charge Ze (-e is the charge of an electron) exhibits a hydrogen-like energy level scheme with an ionization energy $E_{o,Z}$ given by

$$E_{o,Z} = Z^2 \cdot \frac{m}{2} \cdot \left(\frac{e^2}{4\pi\varepsilon_o \hbar} \right)^2 , \qquad (1)$$

where m is the rest mass of an electron, ε_o the permittivity of free space and $\hbar$ is Planck's constant, divided by 2π. A similar situation arises in a semiconductor, when an electron (or hole) is bound in the Coulomb field of a localized donor (or acceptor) impurity. According to the Effective Mass Theory, originally developed by Kittel and Mitchell[9] and Kohn and Luttinger[10], one can attribute a hydrogenlike energy level scheme to this situation with an ionization energy $E_{i,Z}$ given by

$$E_{i,Z} = \frac{m^*}{m} \cdot \frac{1}{\varepsilon^2} \cdot E_{o,Z} , \qquad (2)$$

since one has to take into account an effective mass m* and a relative dielectric constant ε. The associated Bohr radius is enlarged by a factor $\frac{m}{m^*}\cdot\varepsilon$ with respect to that of a hydrogenlike atom. In this context Z denotes the difference in valence of the donor (acceptor) impurity and the atoms of the host material. In germanium for instance this leads to an ionization energy of about 10 meV for shallow (i.e. Z=1) donors and acceptors, a value more than a thousand times smaller than the ionization energy of a hydrogen atom (13.6 eV).

In 1980 Chaudhuri, Coon and Derkits[11] suggested the possible existence of Fractional Charge Impurities (FCI's) in semiconductors. An example of an acceptor-like Z=1/3 or 2/3 FCI is a quark-nucleon complex, consisting of one or two negative quarks bound to the nucleus of a semiconductor host atom. One or two negative quarks, bound to the nucleus of a shallow donor, give rise to a Z=2/3 or 1/3 donor-like FCI respectively. Analogous with normal shallow donors and acceptors, the donor- and acceptor-like FCI's bind an electron or hole respectively. These FCI's exhibit donor- or acceptor-like energy level schemes, with binding energies reduced by a factor Z^2 (and the splitting of ground-state levels reduced by a factor Z^4), with Z=1/3 or 2/3. As an illustration, Fig. 1 shows the energy level schemes for acceptor-like FCI's and the shallow boron acceptor in germanium. The binding energies of the FCI's are deduced from those of the boron acceptor by means of equation (2). The notation for the energy levels has been taken from the corresponding spectral transition lines, as given by Haller and Hansen[12].

Chaudhuri, Coon and Derkits[11] also discussed the possible existence of substitutional or interstitial FCI's in germanium. According to them, substitutional FCI's may be formed during crystal growth from the melt or zone refining, assuming these FCI's also show up segregation. In view of the high rates of diffusion of H, He and Li^+ in common semiconductors, small interstitial FCI's could be introduced from FCI-rich contiguous matter by standard doping and drifting techniques.

Photothermal ionization spectroscopy (PTIS) has proved to be a very sensitive technique to detect extremely low concentrations of shallow donors and acceptors. This technique, also called photoelectric spectroscopy, was originally developed by Lifshits and Nad' in 1965[13]. Extensive reviews of this technique and its application to ultra-pure germanium have been given by Kogan and Lifshits[14], and Haller, Hansen and Goulding[15]. Whereas conventional absorption spectroscopy fails to detect impurity concentrations below 10^{13} cm^{-3}, PTIS has demonstrated its usefulness even for impurity concentrations down

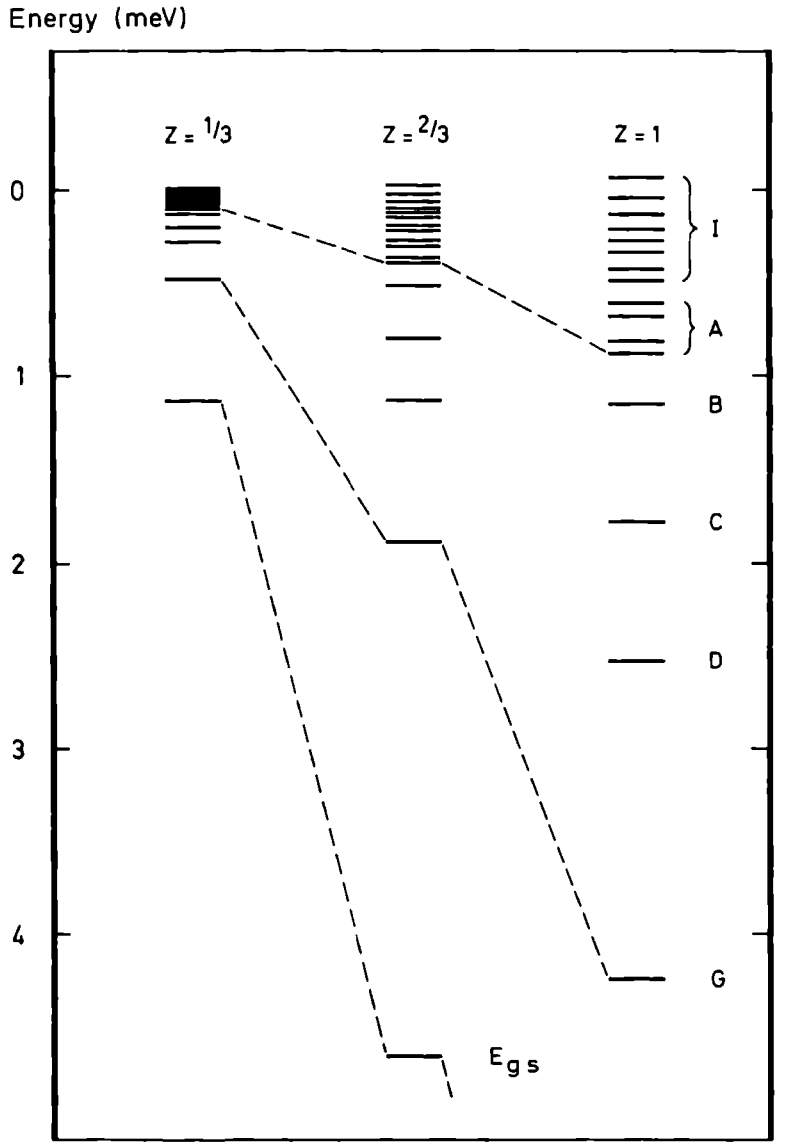

Fig. 1: Energy level schemes for two acceptor-like FCI's and a normal shallow acceptor in germanium. The nomenclature has been taken from ref. 12.

to 10^8 cm^{-3}.

For that reason it seems a very straightforward idea to start a search for FCI's with PTIS. PTIS has the advantage that it can also give a value for the concentration of FCI's, if present. A Millikan-like experiment, however, can only prove the existence of quarks. In section II and III we present the theory behind PTIS and discuss the modifications needed for its application to the detection of FCI's. In section IV we show the experimental arrangement necessary for PTIS and give the results of a search for FCI's in one particular sample. In section V we shall calculate the lower limit on the concentration of detectable FCI's with this particular experimental set-up. In addition we shall discuss the modifications of the experimental arrangement, which will enable us to detect FCI's with the same sensitivity as quarks were detected in the successful experiment of LaRue, Fairbank and Hebard.

3.II. The critical concentration β/α

PTIS is a spectroscopic technique which measures the change in electrical conductivity of a semiconducting sample, caused by a change in number of free electrons (holes) in an energy band due to ionization of a donor (acceptor) in a two-step process. The bound electron (hole) is raised from the ground state to an excited state by the absorption of a photon and is subsequently thermally promoted into the conduction (valence) band. The PTIS spectrum of an impurity consists of a series of photoconductivity peaks, situated on the low-energy side of a broad continuum. This continuum originates from direct optical ionization of a donor (acceptor).

Detailed understanding of the PTIS signal formation first of all requires knowledge of the occupation of the ground state of impurities. Moreover, the number of equilibrium free carriers in the band should be known, as well as the time response of this system of free carriers after the injection of additional free carriers. The relevant processes depend on temperature, background radiation and degree of compensation.

Consider a semiconductor with free carrier concentration n and one type of majority impurity with concentration N. Let N^o and N^1 denote the concentration of neutral and ionized majority impurities respectively and KN the concentration of compensating minority impurities, where K is the degree of compensation, then this system is described by the set of rate of change equations :

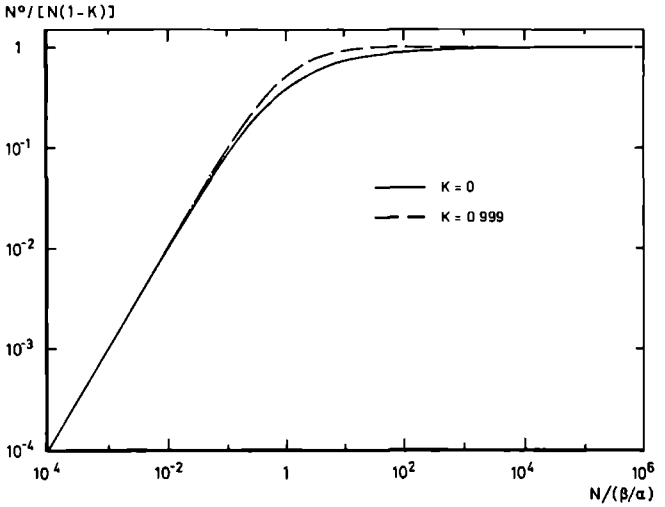

Fig. 2: Normalized occupation of the ground state of a majority impurity as a function of N/(β/α) for the situation of one type of majority impurity for the two limiting cases of compensation.

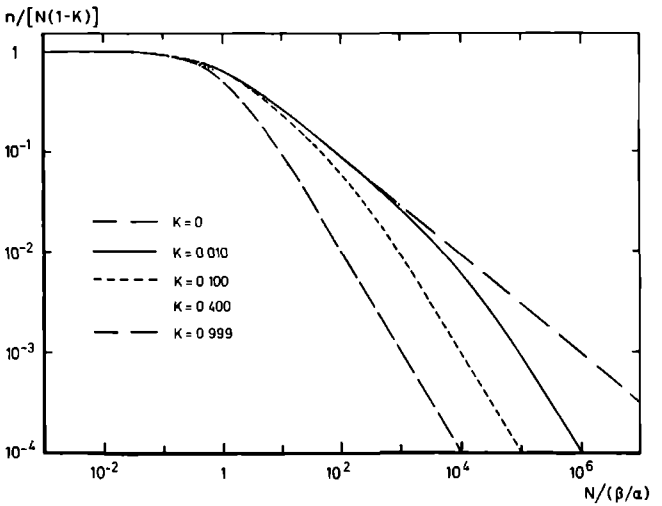

Fig. 3: Normalized concentration of free majority carriers as a function of N/(β/α) for the situation of one type of majority impurity for several degrees of compensation.

$$\frac{dn}{dt} = \beta \cdot N^{o} - \alpha \cdot n \cdot N^{1}$$

$$\frac{dn}{dt} = -\frac{dN^{o}}{dt} = \frac{dN^{1}}{dt} \quad . \tag{3}$$

Here β is the coefficient of impurity ionization by thermal phonons and by background radiation, expressed in units sec^{-1} and α is the trapping rate coefficient in units $cm^{3}sec^{-1}$. In equilibrium expressions can be derived for N^{o}, N^{1} and n, containing terms K, N and β/α only. This can be done by using the obvious relation $N = N^{o} + N^{1}$, the condition of electrical neutrality $N^{1} = n + KN$ and $\frac{dn}{dt} = 0$ because of the equilibrium situation. The resulting normalized concentrations $N^{o}/[N(1-K)]$ and $n/[N(1-K)]$ are shown in Figures 2 and 3 respectively as a function of the dimensionless constant $N/(\beta/\alpha)$ for several values of K. These figures show that the quantity β/α, having dimensions cm^{-3}, acts as a critical impurity concentration: For impurity concentrations N much higher than β/α almost all majority impurities are in the ground state (except those which are ionized because of the presence of compensating minority impurities) and hence the concentration of free carriers is very low. For impurity concentrations well below this critical concentration β/α nearly all majority impurities are ionized and n approaches its maximum value N(1-K).

The quantity β/α also acts as a critical concentration for the strength of the PTIS signal; therefore we will study β/α in detail. Subsection A deals with the case that the influence of the background radiation on the degree of ionization of the majority impurities is negligible and β/α is only determined by thermal ionization. Subsection B deals with the opposite.

A. Thermal ionization

In this section the influence of background radiation on the ionization of the majority impurities is assumed to be negligible with respect to thermal ionization at temperature T. Although for this case β and α can be evaluated separately [16,17], there also exists one simple expression for β/α [18]:

$$\left(\frac{\beta}{\alpha}\right)_{Z}(T) = \frac{2}{g} \cdot \left(\frac{2\pi m^{*} kT}{h^{2}}\right)^{3/2} e^{-E_{1,Z}/kT} \quad . \tag{4}$$

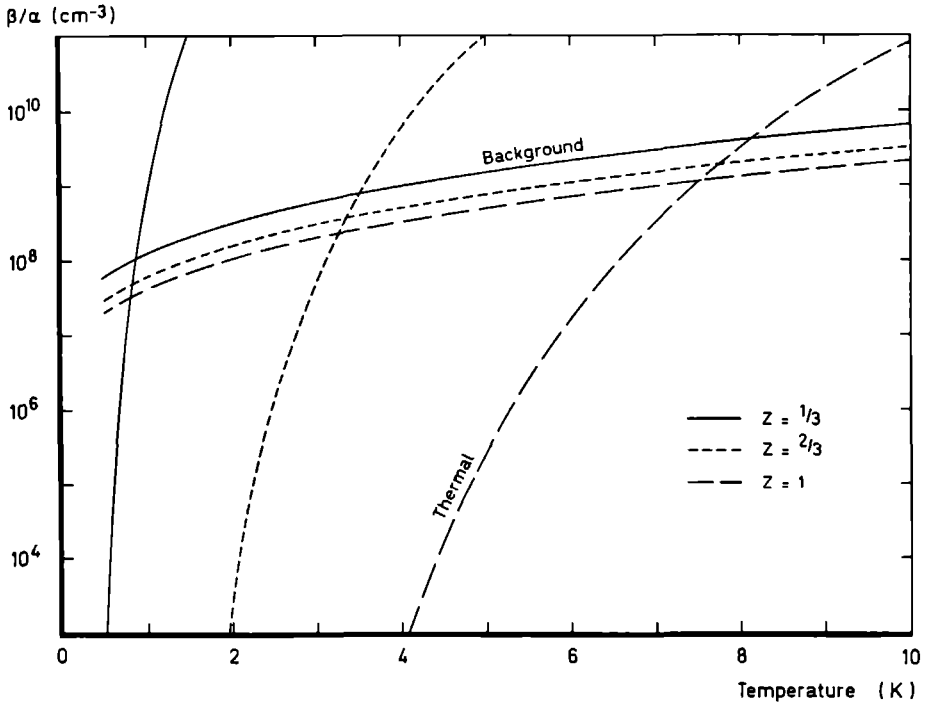

Fig. 4: Temperature dependence of the critical concentration for the situation of one type of Z=1/3, 2/3 and 1 acceptor-like majority impurity in germanium for the limiting cases of thermal ionization and ionization by background radiation.

Here g denotes the degeneracy of the ground state of the majority impurity and k is the Boltzmann constant.

The temperature dependence of β/α in case of thermal ionization is shown in Fig. 4 for two acceptor-like FCI's and one shallow acceptor in germanium. The curves are calculated by taking g=4, m*/m =0.38 and $E_{i,1}$=10 meV, and using eq. (2). The temperature range is chosen between 0.5 and 10 K and the values of β/α between 10^3 cm^{-3} and 10^{11} cm^{-3}, since this is the interesting range of values, as will appear later on.

B. *Ionization by background radiation*

This section deals with the situation where thermal ionization of the majority impurities is negligible with respect to the ionization by background radiation. For this situation no simple expression for $(\beta/\alpha)_Z$ exists. Therefore it is necessary to consider β and α separately. We will confine ourselves to the case of acceptor-like impurities in germanium. First β will be evaluated and subsequently α.

The quantity β is totally determined by the broad-band background radiation, and is independent of temperature. In practice, when applying the PTIS technique, always low-pass optical filters are used, thus limiting the range of energies of the radiation, reaching the semiconducting sample below a maximum energy $E_{max,Z}$. The additional subscript Z indicates the possibility that one chooses the filtering according to the type of impurity - characterized by Z - one searches for.

The quantity β is given by the expression

$$\beta_Z = \int_{E_{i,Z}}^{E_{max,Z}} \frac{\sigma_{i,Z}(E)}{A} \cdot F(E) \cdot dE \quad . \tag{5}$$

Here A is the area of the illuminated surface of the sample and F(E) . dE the number of photons per second with energies between E and E + dE, reaching the sample. The symbol $\sigma_{i,Z}(E)$ denotes the cross section for optical ionization of a carrier from the ground state of an impurity, characterized by Z, for light with energy E.

To find an expression for $\sigma_{i,Z}(E)$ in equation (5), we first look at the solution of the problem for an isolated one electron atom with a nucleus with

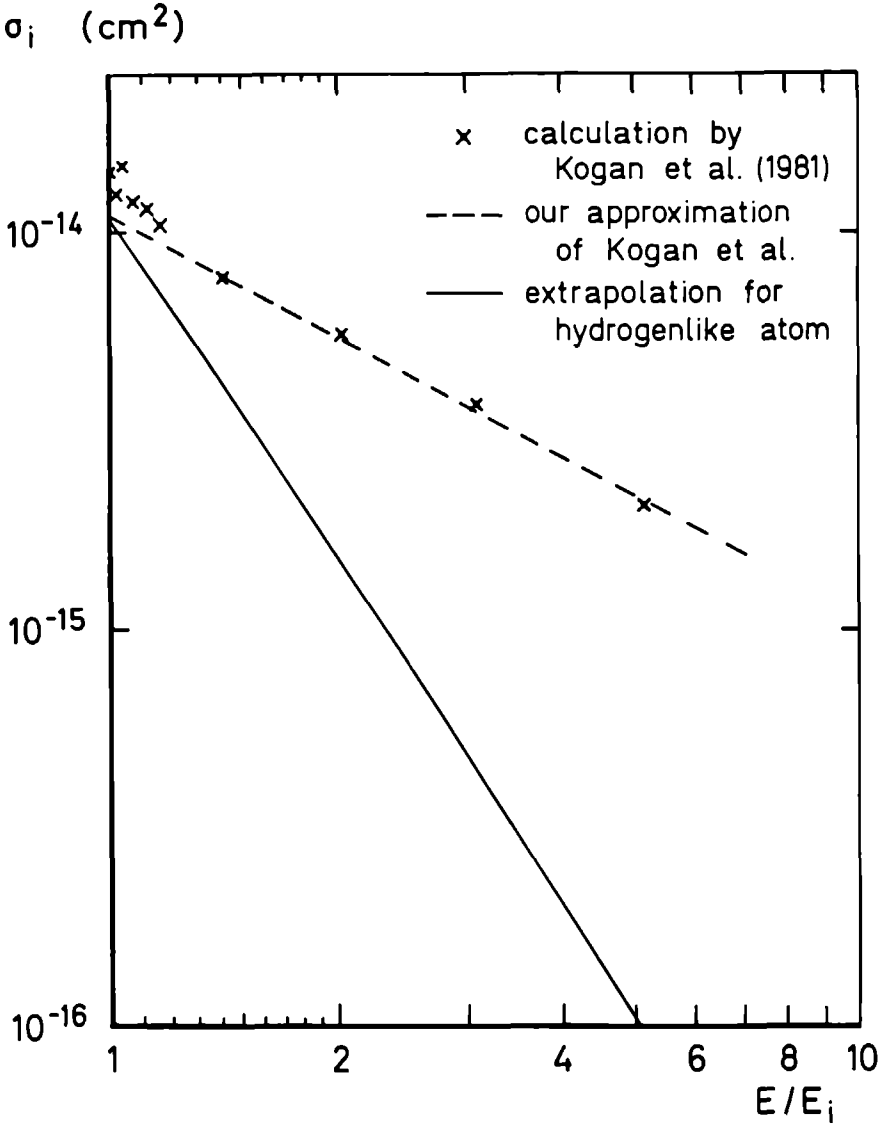

Fig. 5: Theoretical values for the cross section for optical ionization of a shallow acceptor impurity in germanium as a function of E/E_i (for details, see text).

charge Ze. For such an atom the cross section is an explicit analytic formula, expressed in units of a_o^2, a_o being the Bohr radius of the ground state of the hydrogen atom (see e.g. Sobel'man [19]). This expression exhibits the property[19]

$$\sigma_{i,Z}(E_{i,Z}) = \frac{1}{Z^2} \cdot \sigma_{i,1}(E_{i,1}) \quad . \tag{6}$$

Extrapolating Sobel'man's solution for the one electron atom to the case of acceptors in germanium, one has to correct for the different Bohr radius of the ground state of an acceptor as well as for the fact that one deals with a dielectric. In Fig. 5 the solid curve represents this extrapolation as a function of E/E_i. As noticed by Kogan and Polupanov[20], experiments revealed a quite different $E/E_{i,1}$-dependence for $\sigma_{i,1}$, but a correct value for $E=E_{i,1}$. They recalculated the cross section, using the detailed forms of the wave-functions of the acceptors and of the light and heavy hole valence band. The results of their calculations for the shallow boron acceptor in germanium are also shown in Fig. 5, indicated by crosses. Fortuitously Kogan and Polupanov's calculations can be described with an $(E/E_i)^{-1}$-dependence, when ignoring the detailed structure below $E/E_i=1.2$, as illustrated in Fig. 5 by the dashed line. Hence we obtain

$$\sigma_{i,Z}(E) = \frac{f}{Z^2} \cdot \frac{E_{i,Z}}{E} \tag{7}$$

for the energy dependent cross section of acceptors in germanium in a very good approximation, the factor f being about $1.\times10^{-14}$ cm^2.

Assuming the background radiation consists of (room temperature) black-body radiation, $F(E) \cdot dE$ is given by

$$F(E) \cdot dE = C \cdot \frac{E^2}{e^{E/kT_e} - 1} \quad , \tag{8}$$

where C is a quantity in units of $Joule^{-3}sec^{-1}$, depending on the experimental arrangement, and T_e the temperature of the blackbody. For the range of energies of interest here, we can approximate the denominator in equation (8) by E/kT_e, and $F(E) \cdot dE$ is simply proportional to E. With this approximation equations (5) to (8) finally lead to the relation

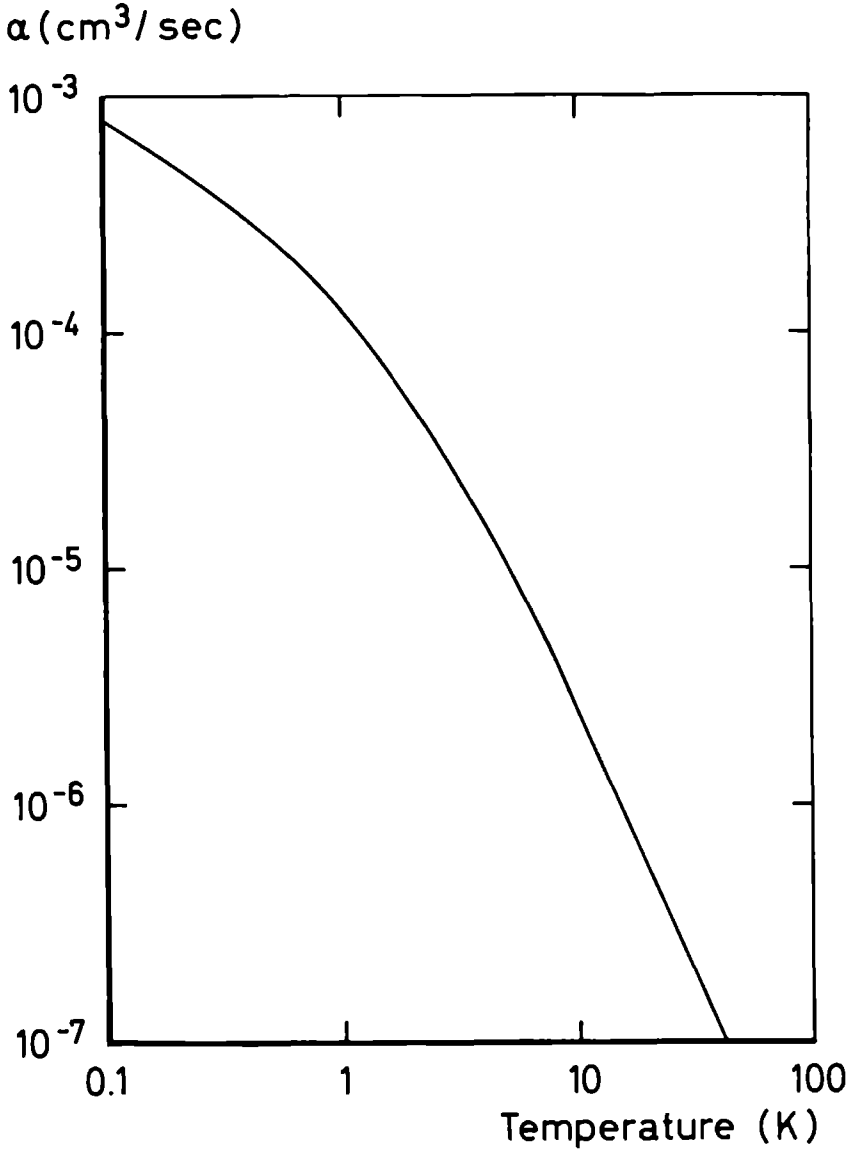

Fig. 6: Temperature dependence of the theoretical values for the capture cross section of holes for shallow acceptors in germanium.

$$\beta_Z = \left(\frac{E_{max,Z} - E_{i,Z}}{E_{max,1} - E_{i,1}} \right) . \beta_1 \quad . \tag{9}$$

Our next step is to consider the trapping rate coefficient α. We will use the results of Abakumov, Perel' and Yassievich[17], who used an improved version of the original cascade theory of Lax[21]. In this cascade model the capture of a carrier occurs through a continuous fall of the carrier in energy space from band-state levels with positive energy into higher impurity states with negative energies. It is assumed that the energy relaxation of the carrier during its fall is entirely due to interaction with acoustic phonons. A carrier is considered to be practically bound if it has descended into an impurity state with a binding energy greater than kT. This model also takes into account that a carrier cannot lose all its kinetic energy in the emission of a single acoustic phonon because of the laws of conservation of energy and momentum.

The expression for the temperature dependence of α[17] contains several parameters, depending on the semiconductor material and type of charge carriers, such as ε, m* and, because acoustic phonons are involved, the velocity of sound, and the mean free path of the carrier. It shows the property

$$\alpha_Z = Z^3 . \alpha_1 \quad . \tag{10}$$

The temperature dependence of α_1 for shallow acceptors in germanium is shown in Fig. 6, where we used parameter values given in reference 17. This temperature behaviour is also confirmed by experiment[17].

Several factors, however, can influence this T-dependence for α_1. Such factors are the overlap of impurity states at high impurity concentrations, the freezing out of recombination centres by the formation of donor-acceptor dipole pairs and the capture of carriers in potential wells because of potential fluctuations. Nevertheless, in ultra-pure germanium these factors are unimportant at temperatures above 0.5 K[17], just as the possible influence of optical phonons[22]. The most serious factor is the application of an electric field, necessary for recording PTIS spectra. An electric field distorts higher levels of impurity states and causes extra heating of carriers, but in ultra-pure germanium these effects are small for electric field strengths lower than 100 mV/cm at temperatures above 0.5 K[23].

Having considered β and α separately, we can write down the important relation from equations (9) and (10):

$$\left(\frac{\beta}{\alpha}\right)_Z = \frac{1}{Z^3} \cdot \frac{E_{max,Z} - E_{i,Z}}{E_{max,1} - E_{i,1}} \cdot \left(\frac{\beta}{\alpha}\right)_1 \quad . \tag{11}$$

Thus knowing $(\beta/\alpha)_1$ for ionization purely by background radiation for shallow acceptors, β/α for acceptor-like FCI's simply follows from this equation. As will appear in the next section, a low value for $(\beta/\alpha)_Z$ enhances the PTIS signal strength. Because of equation (2), the optimal cut-off energy, when searching for FCI's, is much lower than when searching for shallow acceptors. Regarding the optical cross section, shown in Fig. 5, the optimal choice is when $E_{max,Z}$ is about $2E_{i,Z}$.

Figure 4 shows the temperature dependence of $(\beta/\alpha)_Z$ in case of ionization by background radiation for different values of Z. For the determination of the $(\beta/\alpha)_1$ curve we used $\beta=5\times10^{3}$ sec^{-1} (see appendix at the end of this article) and α according to Fig. 6. The curves for Z=1/3 and 2/3 were calculated by assuming that optical filtering was used with $E_{max,Z}=2E_{i,Z}$.

3.III. PTIS signal formation

With PTIS one essentially measures the change in concentration of free carriers in the band, Δn, with regard to the equilibrium concentration of free carriers, n, as a function of the energy of the light irradiated onto the semiconducting sample. In practice this can be done in two fundamentally different ways: measuring the changes in voltage across the sample, using a constant current source, or measuring the changes in current, using a constant voltage. An elementary analysis demonstrates that both methods basically measure the quantity Δn/n. By considering this quantity, the PTIS signal will be analyzed for a semiconductor with one type and with two types of majority impurities respectively. In addition an explicit expression will be given for the minimal concentration of impurities, which can be detected with PTIS for a semiconductor with one type of majority impurity.

Consider a semiconductor with one type of majority impurity. If the number of impurities is very low, the flux of photons can be regarded as constant throughout the sample and mutual shielding of impurities can be neglected. Assuming monochromatic radiation (apart from broad-band background radiation,

if present) is incident on the sample with energy E and with intensity I(E), then $\Delta n/n$ is given by [14,24]

$$\frac{\Delta n}{n} = \frac{I(E) \cdot \sigma_i(E)}{A} \cdot \frac{N^o \tau}{n} \quad , \tag{12}$$

where τ is the lifetime of the non-equilibrium carrier.

This equation indicates that the dependence on temperature and on background radiation of $\Delta n/n$ occurs via the quantity $(N^o\tau)/n$. To illustrate this we will evaluate the dependence of the dimensionless quantity $(\beta N^o\tau)/n$ - being proportional to $\Delta n/n$ - on β/α. The quantities N^o and n in $(\beta N^o\tau)/n$ have already been considered before. The non-equilibrium lifetime τ is defined as the time response of the system of free carriers, after the equilibrium is disturbed by an additional number of free carriers. By means of equation (3), an expression for τ can easily be obtained by using a linear relaxation-time approximation. Figure 7 shows the resulting dependence of $(\beta N^o\tau)/n$ on the dimensionless quantity $N/(\beta/\alpha)$. This figure demonstrates the remarkable properties and strength of PTIS. The different behaviour of the curves for $N/(\beta/\alpha) > 0.1$ basically originates from the strong dependence of n and τ on the degree of compensation K in this region. If $N \gg \beta/\alpha$, the signal strength $(\beta N^o\tau)/n$ becomes independent of $N/(\beta/\alpha)$ and the degree of compensation K. For $K \neq 0$, the PTIS signal strength is even twice as large as the corresponding PTIS signal for K=0. With conventional absorption spectroscopy, however, the signal exhibits a linear dependence on impurity concentration.

Now consider a semiconductor with two types of majority impurities, denoted by 1 and 2 respectively. For this situation we want to be able to deduce the relative concentration N_1/N_2 from the measured PTIS spectrum. Therefore assume that the semiconducting sample, apart from possible background radiation, is irradiated with monochromatic light with energy E_1 and intensity $I(E_1)$, which ionizes impurity 1 and which causes a signal $\Delta n_1/n$. Assume the same for impurity 2. Under the condition that the system is only slightly distorted by this additional radiation, we can write down the following formula for the relative signal strength [14]

$$\frac{\Delta n_1}{\Delta n_2} = \frac{N_1}{N_2} \cdot \frac{\alpha_{Z_2}}{\alpha_{Z_1}} \cdot \frac{I(E_1)}{I(E_2)} \cdot \frac{\sigma_{i,Z_1}(E_1)}{\sigma_{i,Z_2}(E_2)} \cdot \left(\frac{N_1^o/N_1}{N_2^o/N_2} \right)^2 \quad . \tag{13}$$

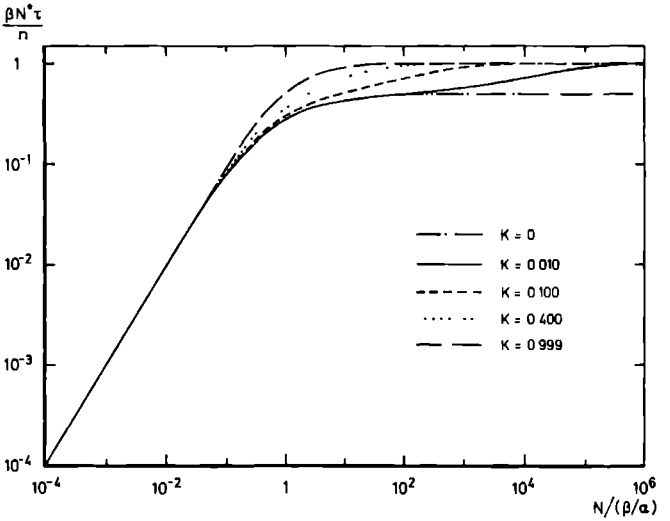

Fig. 7: Normalized strength of the PTIS signal for the situation of one type of majority impurity as a function of N/(β/α) for several degrees of compensation.

If minority impurities are present with concentration N_c, they are preferably compensated by carriers originating from the majority impurities with the lowest ionization energy. If e.g. impurity 1 and 2 denote an FCI and a normal shallow impurity respectively and if $N_1 < N_c$, the consequence is that $N_1^o = 0$ and hence these FCI's cannot be detected by PTIS at all.

We will now determine the minimal detectable concentration of impurities N_{min} for a semiconductor with one type of majority impurity. We assume an impurity can be detected by PTIS, if its corresponding signal-to-noise ratio exceeds 1. At low impurity concentration the Johnson noise is dominated by the generation-recombination noise[24]. Assuming we are in the low concentration area where N^o is proportional to $N/(\beta/\alpha)$ (see Fig. 2), N_{min}, corresponding to a SNR=1, is given by[24]

$$N_{min}(Z) = \left(\frac{\beta}{\alpha} \right)_Z \cdot \frac{2A}{I(E) \cdot \sigma_{i,Z}(E)} \cdot \left(\frac{\alpha_Z \, \Delta f}{V(1-K)} \right)^{1/2} . \qquad (14)$$

Here V is the volume of the sample and Δf denotes the frequency bandwidth of the amplifier.

3.IV. *Experimental search for FCI's with PTIS*

In this section we will describe an experimental search for FCI's on an ultra-pure germanium sample with PTIS. For that purpose we used the experimental set-up, shown in Fig. 8. The FIR light, produced by a Grubb Parsons Michelson interferometer, enters the lightpipe via a black polyethylene window, which blocks out all visible and near-infrared radiation. From there it passes through a cooled crystalline quartz filter with cut-off energy 220 cm^{-1} into a semispherical, integrating cavity. The sample is clamped onto the base of the cavity and its temperature can be raised above the temperature of the surrounding helium bath by means of a heater. Using the electric circuit, shown in Fig. 8, photoconductivity interferograms are recorded with phase-sensitive detection techniques and subsequently fourier-transformed and a PDP-11 computer.

The investigated sample was p-type material with net impurity concentration $N_A - N_D = 2 \times 10^{11}$ cm^{-3} and with a degree of compensation of about 0.4, containing boron as the dominating majority impurity. In order to avoid thermal ionization of possible FCI's and hence a reduction in the PTIS signal

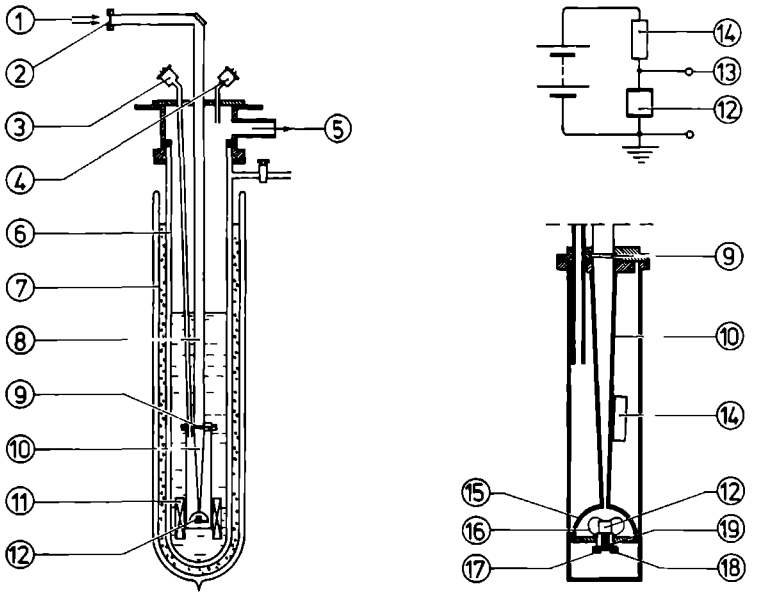

① Incident radiation
② Polyethylene window
③ Electrical connections for Ge-sample
④ Electrical connections for s.c magnet
⑤ To helium pump
⑥ Liquid helium dewar
⑦ Liquid nitrogen dewar
⑧ Light pipe (stainless steel)
⑨ Crystalline quartz filter
⑩ Cone (gold plated copper)
⑪ Superconducting magnet
⑫ Germanium sample
⑬ To amplifier
⑭ Load resistor
⑮ Cavity (gold plated copper)
⑯ Clamp
⑰ Thermometer
⑱ Heater
⑲ Tufnol insulation

Fig. 8

(see sections II and III), the spectra were recorded at low temperature, 1.2 K being the lowest temperature which can be achieved with the given experimental arrangement.

Figure 9 shows two PTIS spectra of this sample, measured at temperatures 1.2 K and 2.0 K respectively. Also indicated are the transitions belonging to the shallow Z=1 boron acceptor and the expected positions of the transition lines of the Z=1/3 and 2/3 acceptor-like FCI's, using the energy level schemes of Fig. 1. There is no evidence for a photoconductivity signal, originating from Z=1/3 or 2/3 acceptor-like FCI's, above the noise level. Using this negative result, we want to derive an upper limit on the concentration of Z=1/3 or 2/3 acceptor-like impurities in this particular sample.

In the preceding section it was demonstrated that an FCI concentration lower than the concentration of compensating impurities would explain the absence of a PTIS signal, originating from FCI's. For this sample this would yield an upper limit for FCI's of 1.3×10^{11} cm^{-3}. In principle it is possible, however, that the concentration of FCI's exceeds the concentration of compensating impurities, but that the corresponding PTIS signal is below the noise level visible in Fig. 9. This possibility can be numerically analyzed by means of equation (13), by assuming that e.g. impurities 1 and 2 denote acceptor-like FCI's and shallow Z=1 impurities respectively. This yields new upper limits of 1.5×10^{11} cm^{-3} and 1.6×10^{11} cm^{-3} for Z=1/3 and 2/3 acceptor-like impurities respectively. Together with equations (7) and (10), we used the form of the spectral intensity distribution of the radiation from the interferometer, as determined by Van der Werf[26], and we assumed that nearly all shallow impurities are in the ground state.

3.V. *Minimal detectable concentration of FCI's by PTIS*

In this section we want to discuss the limits of the detectable concentration of FCI's by PTIS. First this will be done for the typical experimental arrangement as described in the preceding section. At the end of this section we will discuss possibilities to lower this limit.

If we want the FCI's to be detectable by PTIS at all, the concentration of majority FCI's should exceed the concentration of compensating impurities. If this condition is fulfilled, the minimal detectable concentration N_{min} is determined by the generation-recombination noise, originating from transitions of carriers from and towards the majority FCI. The extra presence of shallow

Table 1: Minimal detectable concentrations of normal acceptors and FCI's with $Z = \frac{1}{3}, \frac{2}{3}$ in p-type germanium for several temperatures under experimental conditions, described in section 3.IV.

T (Kelvin)	$N_{min}(Z=1)$ (cm^{-3})	$N_{min}(Z=2/3)$ (cm^{-3})	$N_{min}(Z=1/3)$ (cm^{-3})
0.5	4×10^6	6×10^6	3×10^7
1.0	6×10^6	9×10^6	3×10^8
2.0	1×10^7	1×10^7	3×10^{11}

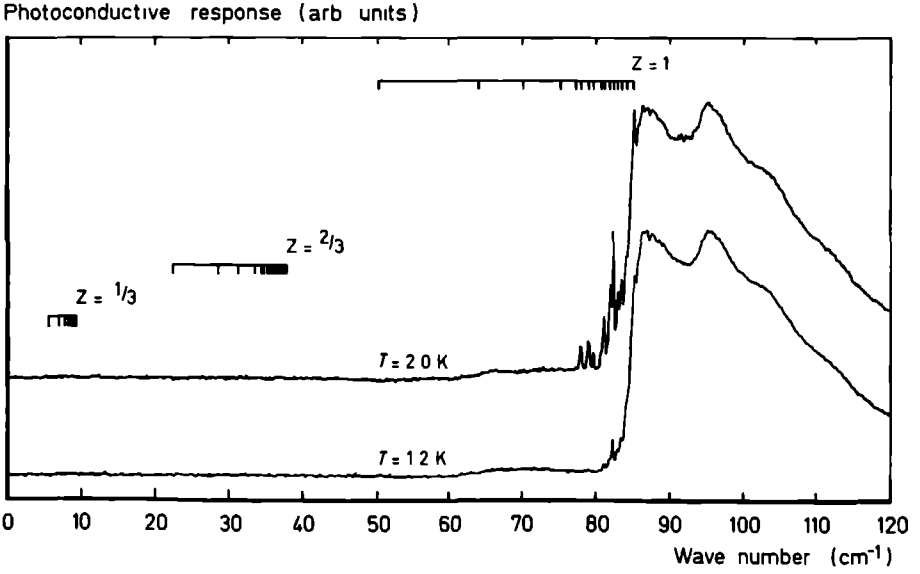

Fig. 9: Measured photoconductivity spectrum of a monocrystalline germanium sample ($N_A - N_D = 2 \times 10^{11}$ cm^{-3}, $K = 0.4$) at 1.2 and 2.0 Kelvin.

Z=1 majority impurities leads to additional generation-recombination noise. The application of an absorption filter with a cut-off energy E_{max} well below $E_{1,1}$ will reduce this additional noise to a large extent. If, moreover, the temperature is chosen low enough, all shallow majority impurities can be considered to be in their ground state. Under these conditions the problem of finding N_{min} is reduced to that for a semiconductor with one type of majority impurity, which was dealt with in section III.

For this situation N_{min} for Z=1/3, 2/3 and 1 acceptor-like impurities is calculated for three different temperatures, the result of which is given in Table 1. Here, in equation (14), we used the typical set of parameters A=1 cm^2, V=1 cm^3, K=0.5 and Δf=0.1 Hz. For each value of Z the additional monochromatic light was assumed to have an energy $E=E_{1,Z}$ and an associated photon flux I at that energy, typical for our spectrometer within a bandwidth of 1 cm^{-1} [25]. The values for $\sigma_{1,Z}$ and α_Z were taken from Figures 5 and 6, taking into account their particular Z-dependence. From Fig. 4 the highest of two possible values for β/α was chosen, corresponding to the dominating ionization mechanism, thermal or by background radiation, for a certain value of Z and T.

The values for N_{min}, given in Table 1, have to be considered as to give only an order of magnitude, in view of the approximations made. For Z=2/3 and 1 N_{min} is determined by ionization by background radiation. For Z=1/3 and temperatures above 1 K, however, N_{min} is determined by the process of thermal ionization. For the situation where background radiation is the dominating cause of ionization all values of N_{min} have the same order of magnitude, which is surprising in view of the different Z-dependence of the components of equation (14). We can conclude that at temperatures that are low enough - under the conditions outlined above - one should be able to detect about 10^7 acceptor-like majority FCI's per cm^3 in germanium with PTIS, using a conventional Michelson interferometer. In view of the similar behaviour of shallow donor impurities this should also apply to majority donor FCI's.

If one believes that the successful observation of third integral charge in little niobium balls at helium temperatures by LaRue, Fairbank and Hebard was caused by one free quark only, this corresponds to a free quark density of about 2×10^{-20} quarks per nucleon. Assuming the same quark density in Ge, this would correspond to 6×10^4 FCI's per cm^3. Therefore it would be preferable to lower the limit of 1×10^7 detectable FCI's with PTIS.

Ultra-pure germanium, probably the purest substance produced by man, can easily be produced nowadays with shallow impurity concentrations down to

10^{10} cm^{-3}, but going to lower concentrations one meets technical problems[15]. In view of this it would be preferable to relax the condition that the concentration of majority FCI's should exceed the concentration of minority impurities if one wants to be able to detect the FCI's with PTIS. This can be achieved by illuminating the semiconductor sample continuously with additional intrinsic light, i.e. radiation containing energies greater than the gap energy of the semiconductor. A fraction of the minority impurities will return to the ground state again. This means that the minority impurities, and thus also minority FCI's, if present, can also be detected by PTIS! Moreover, a fraction of the formerly ionized majority FCI's becomes detectable by PTIS. Application of intrinsic light, however, gives rise to additional noise, due to electron-hole recombination and also influences the free carrier lifetime, making a new estimate for N_{min} too complicated.

At very low temperatures the values of N_{min} are determined by the intensity of the background radiation. The application of a broad-band optical filter, which attenuates the intensity of the background radiation for energies around $E_{i,Z}$, reduces the value of β/α, associated with background radiation. This, however, does not alter N_{min}, since also I(E) reduces proportionally. Additional application of a FIR laser or e.g. a harmonic generator[26], which results in much higher photon fluxes I(E), can lead to detectable concentrations of FCI's of 10^5 cm^{-3} or lower.

3.VI. Conclusions

We can conclude that the Photothermal Ionization Spectroscopy (PTIS) technique is a very useful tool for the detection of possible Fractional Charge Impurities (FCI's) in semiconductors. From the absence of a PTIS signal, originating from FCI's in a p-type germanium sample, we conclude that this sample contained less than 1.5×10^{11} acceptor-like FCI's per cm^3. If the number of compensating impurities is smaller than the number of FCI's, PTIS can detect down to 10^7 FCI's per cm^3 - if present - with the experimental arrangement used, including a FIR Michelson interferometer. The application of intrinsic light, which releases the condition concerning compensating impurities, and the use of a FIR laser source can lower the concentration of detectable FCI's with a factor of at least 100.

Appendix: Determination of a numerical value for β

In germanium the concentration of ionized impurities N^i at temperatures below 10 K is in principle determined by three factors: the concentration of compensating impurities KN, thermal ionization and ionization by background radiation. In this appendix a numerical value for β will be derived for the situation that N^i, apart from its dependence on KN, is mainly determined by the intensity of the background radiation. This will be done for the experimental arrangement, described in section IV and a p-type sample with N= 3.3×10^{11} cm^{-3} and K=0.4.

For this purpose we determine the free carrier concentration n at 4.2 K, by measuring the resistance R_s of the sample and using the relation $n = G/(e\mu R_s)$, where μ is the mobility for holes and G a geometrical factor. From G=0.95 cm^{-1} for this sample, R_s=640 Ω and $\mu=1.1\times10^5$ $cm^2V^{-1}sec^{-1}$ [27] at 4.2 K, one obtains $n=4.4\times10^8$ cm^{-3}. From Fig. 4 one can see that this corresponds to $\beta/\alpha=5\times10^8$ cm^{-3}. Using the value for α at 4.2 K, obtained from Fig. 6 this finally leads to $\beta=7.5\times10^3$ sec^{-1}.

In our experimental arrangement we used a crystalline quartz filter with a cut-off energy E_{max}=27 meV. For this experimental situation $E_{max,1}=2.6\ E_{i,1}$, using the ionization energy 10.5 meV for the boron impurity. Therefore $\beta=5\times10^3$ sec^{-1} for $E_{max,1}=2E_{i,1}$ (see equation (9)). Regarding the approximations we feel this value to be right within a factor of 2.

References:

1. M. Gell-Mann, Phys. Lett. 8, 214 (1964).
2. G. Zweig, CERN Report No. 8182/TH, 401 (1964) (unpublished).
3. Y.S.Kim, Contemp. Phys. 14, 289 (1973).
4. L.W. Jones, Rev. Mod. Phys. 49, 717 (1977).
5. M. Marinelli and G. Morpurgo, Phys. Reports 85, 161 (1982).
6. G.S. LaRue, W.M. Fairbank and A.F. Hebard, Phys. Rev. Lett. 38, 1011 (1977).
7. R.A. Millikan, Phil. Mag. 19, 209 (1910).
8. G.S. LaRue, W.M. Fairbank and J.D. Phillips, Phys. Rev. Lett. 42, 142, 1019(E) (1979); G.S. LaRue, J.D.Phillips and W.M. Fairbank, Phys. Rev. Lett. 46, 967 (1981).
9. C. Kittel and A.H. Mitchell, Phys. Rev. 96, 1488 (1954).
10. W. Kohn and J.M. Luttinger, Phys. Rev. 98, 915 (1955).
11. S. Chaudhuri, D.D. Coon and G.E. Derkits, Jr., Phys. Rev. Lett. 45, 1374 (1980).
12. E.E. Haller and W.L. Hansen, Solid State Commun. 15, 687 (1974).
13. T.M. Lifshits and F.Ya.Nad', Dokl. Akad. Nauk SSSR 162, 801 (1965) [Sov. Phys. Dokl. 10, 532 (1965)].
14. Sh.M. Kogan and T.M. Lifshits, Phys. Stat. Solidi (a) 39, 11 (1977).
15. E.E. Haller, W.L. Hansen and F.S. Goulding, Adv. Phys. 30, 93 (1981).
16. V.N. Abakumov, L.N. Kreshchuk and I.N. Yassievich, Zh. Eksp. Teor. Fiz. 74, 1019 (1978) [Sov. Phys. JETP 47, 535 (1978)].
17. V.N. Abakumov, V.I. Perel' and I.N. Yassievich, Fiz. Tekh. Poluprov. 12, 3 (1978) [Sov. Phys. Semicond. 12, 1 (1978)] (Review article).
18. See e.g. E.H. Putley, Proc. Phys. Soc. 72, 917 (1958).
19. I.I. Sobel'man , "Introduction to the theory of atomic spectra", ed. Pergamon Press, 1972, New York.
20. Sh.M. Kogan and A.F. Polupanov, Zh. Eksp. Teor. Fiz. 80, 394 (1981) [Sov. Phys. JETP 53, 201 (1981)].
21. M. Lax, Phys. Rev. 119, 1502 (1960).
22. V.N. Abakumov, Fiz. Tekh. Poluprov. 13, 59 (1979) [Sov. Phys. Semicond. 13, 34 (1979)].
23. V.N. Abakumov, L.N. Kreshchuk and I.N. Yassievich, Fiz. Tekh. Poluprov. 12, 264 (1978) [Sov. Phys. Semicond. 12, 152 (1978).
24. Sh.M. Kogan, Fiz. Tekh. Poluprov. 7, 1231 (1973) [Sov. Phys. Semicond. 7, 828 (1973)].

25. E.J.C.M. van der Werf, students dissertation (1977) (unpublished).
26. M.J. Huyben, C.G.C.M. de Kort, J.H.M. Stoelinga and P. Wyder, Infrared Phys. 19, 257 (1979).
27. N.I. Golosai and V.I. Sidorov, Fiz. Tekh. Poluprov. 6, 2354 (1972) [Sov. Phys. Semicond. 6, 1976 (1973)].

Abstract

The equilibrium distribution of electrons and holes over shallow impurity states and energy bands of an ultra-pure semiconductor is studied for the situation where the semiconductor is continuously illuminated with intrinsic light (i.e. radiation with energies of the order of the gap-energy of the semiconductor). The response to additional injection of free minority or majority charge carriers into the energy bands - caused by photothermal ionization of minority or majority impurities respectively - is separately investigated. The equilibrium and the response have theoretically been analyzed by means of a description with a set of rate of change equations. This analysis explains the usually observed behaviour that photothermal ionization of minority impurities in ultra-pure germanium under continuous illumination with intrinsic light gives rise to a decrease in electrical conductivity. The measured time-evolution of the change in conductivity of an ultra-pure germanium sample after the start of the photothermal process revealed a slow ($\sim$ 5 msec) change, connected with minority impurities only, as well as a fast ($<$ 0.5 msec) change. The slow response time has been associated with the electron-hole recombination time, yielding a value 5×10^{-12} $cm^3 sec^{-1}$ for the electron-hole recombination constant. It is demonstrated that in photothermal ionization spectroscopy, when using phase-sensitive detection techniques by means of a lock-in amplifier, such a simultaneous presence of a fast and a slow (i.e. of the order of magnitude of the chopping times applied) change in conductivity can cause artefacts in the spectra.

4.I. *Introduction*

In the early seventies ultra-pure semiconductor single crystals became available with net electrically active impurity concentrations of about 10^{10} per cm^3. At this high purity the wavefunctions of shallow donors and acceptors are localized to an extremely high degree and do not overlap those of neighbouring impurities, hence the associated energy levels are very sharp. Shallow impurities in these ultra-low concentrations can only be identified with Photothermal Ionization Spectroscopy (PTIS)[1,2], since conventional absorption spectroscopy fails to detect impurities with concentrations below 10^{13} cm^{-3}.

The PTIS technique is used to measure changes in electrical conductivity of a semiconducting sample, caused by changes in the number of free electrons (holes) in an energy band, due to ionization of a donor (acceptor) in a two-step process. The bound electron (hole) is raised from the ground state to an excited state by the absorption of a photon and is subsequently thermally promoted into the conduction (valence) band. The PTIS spectrum of a particular impurity consists of a series of sharp photoconductivity peaks, situated on the low-energy side of a broad continuum. This continuum originates from direct optical ionization of a donor (acceptor). The radiation involved in the ionization of the impurities is hereafter referred to as extrinsic light. With PTIS the positions of the energy levels of the excited electronic states in a high-purity sample can be determined very accurately because of the sharpness of the associated photoconductivity peaks. Therefore PTIS is a very sensitive technique for the study of the influence of e.g. uniaxial stress[3,4,5] or a magnetic field[6,7] on the energy level schemes. One can also investigate the second step of the photothermal process itself from the temperature dependence of the intensity of the photoconductivity peaks[8,9].

At low temperatures and in the absence of intrinsic light - i.e. radiation which excites electrons directly from the valence band into the conduction band, also called band-edge light - all minority impurities are ionized because of compensation, a fraction of the majority impurities is in the ground state and only free majority charge carriers are present. When intrinsic light is applied, creating free electrons and free holes at the same time, also free minority charge carriers are present and a fraction of the minority impurities returns in the ground state due to the capture of the generated minority charge carriers. A new equilibrium situation is achieved in the distribution of electrons and holes over the impurity states and energy bands, governed by four

competing processes:

1. The release of free majority (minority) charge carriers from the ground states of majority (minority) impurities into the associated energy bands by thermal ionization or ionization caused by extrinsic background radiation.
2. The capture of free majority (minority) carriers into the ground state of majority (minority) impurities by the cascade mechanism.
3. The simultaneous generation of free electrons and free holes by absorption of the intrinsic light.
4. The reduction in the number of free holes and free electrons because of the electron-hole recombination process.

Since a fraction of both types of impurities is in the ground state, both minority and majority impurities can be ionized by the photothermal process. Therefore PTIS can be used to investigate this equilibrium distribution by separately studying its response to small injections of free minority or free majority charge carriers into the energy bands.

In PTIS spectra obtained with an ultra-pure germanium sample under continuous illumination with intrinsic light the photoresponse from majority impurities always corresponds to an increase in electrical conductivity, whereas the photoresponse from minority impurities usually reveals a decrease in conductivity (see e.g. references 10-13). Spectra recorded in our laboratory, however, exhibited a quite strange behaviour. This is illustrated by Figures 1 and 2, showing the photoconductive response of both donor and acceptor impurities in a germanium sample. The spectra were recorded by means of a far-infrared Michelson interferometer, a source of extrinsic as well as intrinsic radiation. The spectra in Figures 1 and 2 are obtained by means of a lock-in amplifier using amplitude modulation at 16 2/3 Hz and phase modulation at 90 Hz respectively under otherwise - apart from temperature - equal experimental conditions. In Fig. 1 the spectrum recorded at 8.5 K shows the usually observed behaviour where the acceptor and donor impurities contribute to the electrical conductivity with opposite sign. In the spectrum recorded at 6 K and in the spectra shown in Fig. 2 the photoresponse of both acceptors and donors reveals an increase in conductivity. Since at the high purity involved processes such as the electron-hole recombination can become rather slow, of the order of magnitude of the chopping times used, we suspected the electronic detection technique itself to be responsible for these effects. In the literature the negative photoresponse is presumed to be due to the reduction of the total

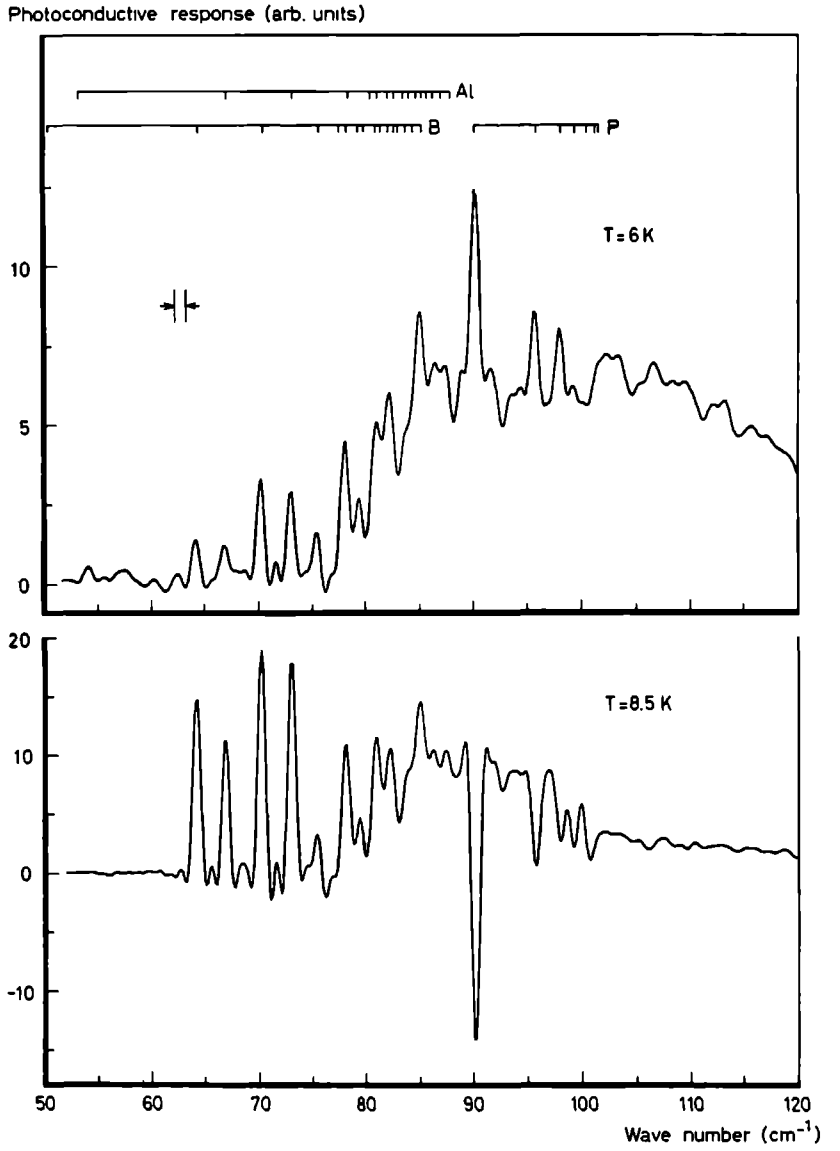

Fig. 1: Photoconductivity spectra of a germanium sample, recorded at 6 and 8.5 K. The corresponding interferograms are obtained with a Michelson interferometer operating with amplitude modulation at 16 2/3 Hz, using a lock-in amplifier. The spectral resolution is indicated by arrows and the line-positions of the phosphorus donor and of the boron and aluminium acceptors are taken from reference 12 and 13 respectively.

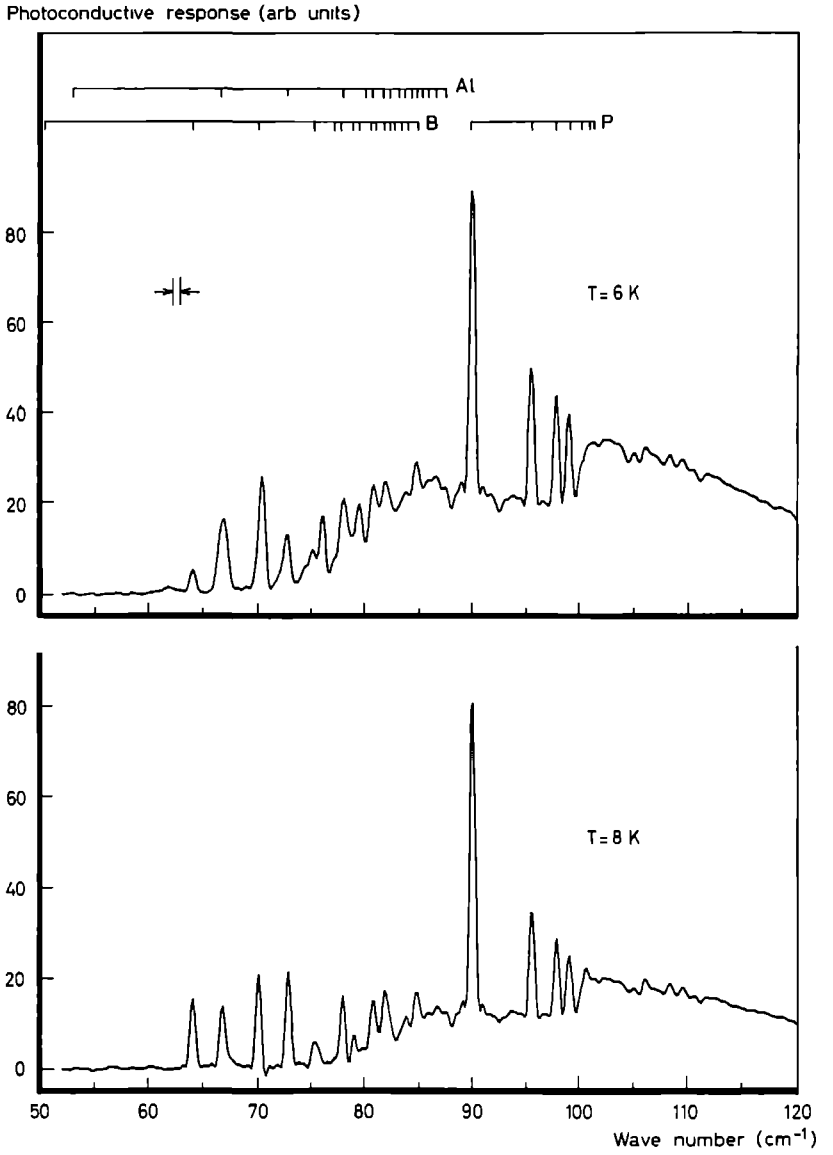

Fig. 2: Same as Fig. 1, but now recorded at 6 and 8 K and with the interferometer operating with phase modulation at 90 Hz.

charge carrier concentration by rapid recombination, but this phenomenon is not well understood up to now[1,13].

Therefore we decided to investigate the equilibrium distribution of electrons and holes over impurity states and energy bands under continuous illumination with intrinsic light in more detail by means of the PTIS technique. We examined the magnitude and time-response of the PTIS signal, originating from majority and minority impurities in ultra-pure germanium, under various experimental conditions. Section II gives a theoretical analysis of the equilibrium distribution and its response to photothermal ionization of impurities. Section III describes the experimental set-up for time-resolved far-infrared PTIS in the msec-region and gives the results, which will be discussed in section IV.

4.II. *The distribution of electrons and holes over impurity states and energy bands in a semiconductor*

In this section the distribution of electrons and holes over impurity states and energy bands in a semiconductor will be studied, when the semiconducting sample is subject to illumination with both intrinsic and extrinsic light. First we will sketch a model for an n-type semiconductor, from which one gains insight more easily than from an analysis for p-type material. The extension for a p-type semiconductor is straightforward. In practice the extrinsic light is mainly composed of room-temperature background radiation. When applying PTIS on a semiconducting sample, the additional extrinsic light from the spectrometer is usually only a fraction of the room-temperature background radiation. Therefore the influence of this spectrometer can be considered as a small disturbance on the total intensity of the extrinsic light. We will deal with the resulting photothermal ionization of majority and minority impurities in the last part of this section.

Consider an n-type semiconductor containing one type of majority impurity with concentration N and one type of minority impurity with concentration P. Let N^o and N^1 (P^o and P^1) denote the concentration of majority donor (minority acceptor) impurities, which are in the ground state or ionized respectively. Obviously

$$N^o + N^1 = N$$
$$P^o + P^1 = P \quad . \tag{1}$$

Finally let n and p be the concentration of free majority and minority charge carriers in the energy bands respectively.

The model shown in Fig. 3 describes the dependence of the distribution of electrons and holes over impurity states and energy bands on intrinsic light, extrinsic light and temperature. The rate of change in the population of the ground state is given by

$$-\frac{dN^o}{dt} = \frac{dN^1}{dt} = \beta_1 . N^o - \alpha_1 . n . N^1 \qquad (2)$$

for the majority impurities and

$$-\frac{dP^o}{dt} = \frac{dP^1}{dt} = \beta_2 . P^o - \alpha_2 . p . P^1 \qquad (3)$$

for the minority impurities. Here β_1 (β_2) is the coefficient of majority (minority) impurity ionization by thermal phonons and by extrinsic light, expressed in units sec^{-1} and α_1 (α_2) is the trapping rate coefficient for free majority (minority) charge carriers in units $cm^3 sec^{-1}$.

The influence of the intrinsic radiation is described by the quantities G and R. Here G is the number of free electrons and free holes per unit volume and unit time interval, created in the semiconductor by absorption of the intrinsic light and is proportional to the intensity G_{rel} of the intrinsic light. The quantity R denotes the recombination coefficient of free electrons and free holes in units $cm^{-6} sec^{-1}$ and, being a material constant, is independent of G_{rel}. Hence the rate of change of majority and minority carriers is given by

$$\frac{dn}{dt} = \beta_1 . N^o - \alpha_1 . n . N^1 + G - R . n . p \qquad (4)$$

and

$$\frac{dp}{dt} = \beta_2 . P^o - \alpha_2 . p . P^1 + G - R . n . p \quad . \qquad (5)$$

In equilibrium the left-hand side of equations (2)-(5) is zero. Using the condition of charge neutrality

$$n + P^1 - N^1 - p = 0 \quad , \qquad (6)$$

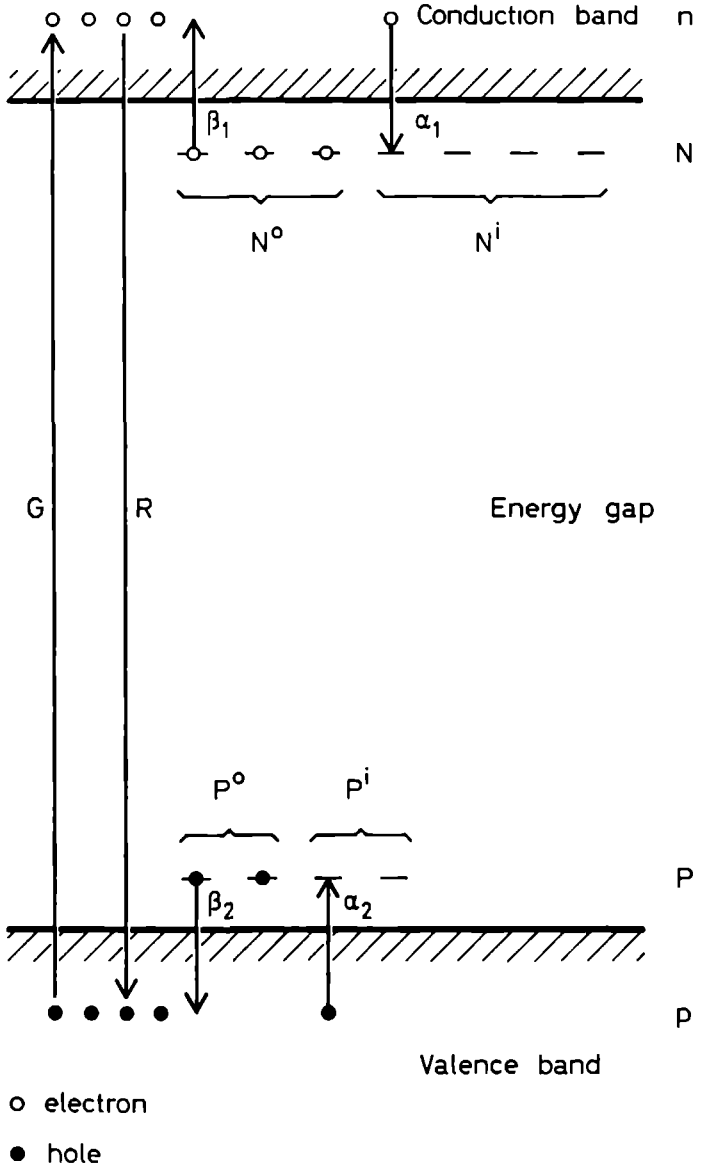

Fig. 3: Diagram of the theoretical model, describing the relevant processes for the distribution of electrons and holes over impurity states and energy bands, taking into account the influence of temperature and of extrinsic and intrinsic light.

the quantities n, p, N^o, N^i etc. can be determined in principle. Since one has to solve equations of degree four, the solutions can only be obtained numerically in general. For low intensities of extrinsic and intrinsic light and low temperature, equations (2)-(5) can be simplified considerably by substituting N-P for N^o and P for P^i. This means that N^o and P^i are totally determined by the process of compensation. With this simplification n and p for the equilibrium situation can be determined from quadratic equations, yielding

$$n = \frac{2V}{P + W} \tag{7}$$

and

$$p = \frac{1}{2} \cdot \frac{G}{R} \cdot \frac{(P + W)}{V} \quad , \tag{8}$$

where we used the definitions

$$V = \frac{\beta_1}{\alpha_1} \cdot (N - P) + \frac{G}{R} \cdot (1 + \frac{\alpha_2}{\beta_2} \cdot P) \tag{9a}$$

and

$$W = (P^2 + 4V)^{\frac{1}{2}} \tag{9b}$$

The distribution of electrons and holes over the impurity states and the energy bands does not depend on the quantities β_1, β_2, α_1, α_2, G and R separately, but only on the quotients β_1/α_1, β_2/α_2 and G/R. The trapping rate coefficients α_1 and α_2 are a function of temperature, but are independent of extrinsic light[14]. The coefficients β_1 and β_2 are the sum of contributions from ionization by thermal phonons and ionization by extrinsic light. Therefore the quotients (β_i/α_i) are the sum of a part $(\beta_i/\alpha_i)_{th}$, only determined by thermal ionization and a part $(\beta_i/\alpha_i)_{ex}$, describing the ionization by extrinsic light.

In the usual experimental arrangement for PTIS $(\beta_i/\alpha_i)_{ex}$ is predominantly determined by extrinsic room-temperature background radiation, and $(\beta_i/\alpha_i)_{th}$ is negligible with respect to $(\beta_i/\alpha_i)_{ex}$ up to a characteristic temperature. This enables us to calculate $(\beta_i/\alpha_i)_{ex}$ by experimentally determining n at low enough temperatures and by solving equations (4) and (5) for the equilibrium

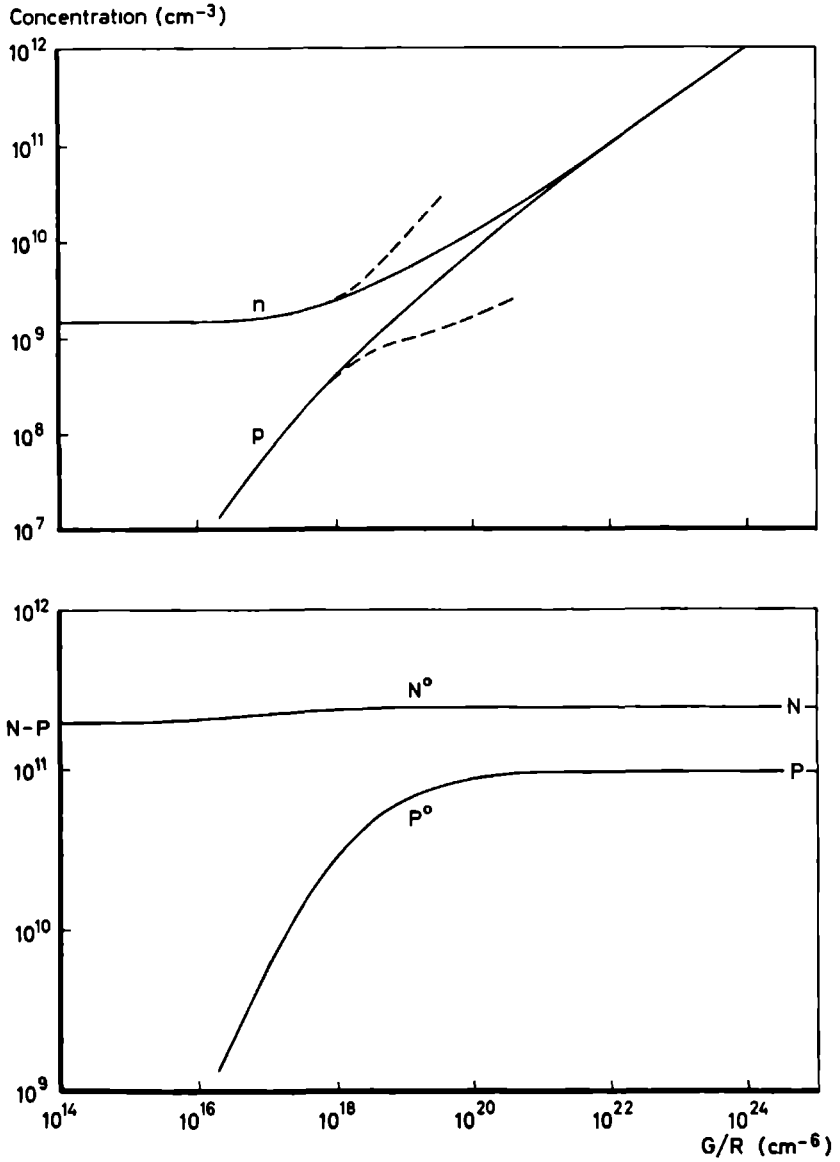

Fig. 4: The theoretical G/R-dependence of n, p, N^o and P^o from an exact numerical calculation (solid curves) and from approximate formulas (dashed curves) for $\beta_1/\alpha_1 = \beta_2/\alpha_2 = 1\text{x}10^9$ cm^{-3}, $N = 2.5\text{x}10^{11}$ cm^{-3} and $P = 1\text{x}10^{11}$ cm^{-3}.

situation in the absence of intrinsic light. The quantity n can be obtained by measuring the resistance of a semiconducting sample. For the p-type ultra-pure germanium sample on which the PTIS measurements were carried out (see next section), we determined the resistance at 4.2 K, yielding $(\beta_1/\alpha_1)_{ex}=5\times10^8$ cm^{-3} for the majority carriers. Here we used the value for the mobility of holes taken from reference 15.

For $(\beta_i/\alpha_i)_{th}$ there is an analytical expression, given by[16]

$$\left(\frac{\beta_i}{\alpha_i}\right)_{th} = \frac{2}{g_i}.\left(\frac{2\pi m_i^* kT}{h^2}\right)^{3/2} . e^{-E_{ion,i}/kT} \quad , \; i=1,2. \tag{10}$$

Here k and h denote Boltzmann's and Planck's constant respectively, m_1^* (m_2^*) the effective mass associated with majority (minority) free carriers, and g_1 (g_2) and $E_{ion,1}$ ($E_{ion,2}$) the degeneracy and binding energy of the ground state of majority (minority) impurities respectively. Equation (10) shows that $(\beta_i/\alpha_i)_{th}$ is a rapidly increasing function of temperature. For germanium $(\beta_i/\alpha_i)_{th}$ reaches the value of 5×10^8 cm^{-3} for a temperature of about 7 K for both i=1 and i=2 using $g_1=2$, $g_2=4$, $m_1^*/m=0.12$, $m_2^*/m=0.38$ and $E_{ion,1}=E_{ion,2}=10$ meV (m is the rest mass of the electron).

When applying PTIS on germanium samples one usually chooses temperatures between 6 and 8 K. This choice is determined by the demand that the temperature is low enough to have a substantial occupation of the ground state of the investigated impurity, but also high enough for the excited carrier to reach the energy band in the second step of the photothermal process. Thus the values of β_1/α_1 and β_2/α_2 at 7 K can be considered as typical values for PTIS in a germanium sample. Finally the assumption that also $(\beta_2/\alpha_2)_{ex} \approx (\beta_1/\alpha_1)_{ex}$ yields 1×10^9 cm^{-3} for both β_1/α_1 and β_2/α_2 at 7 K.

Figure 4 shows n, p, N^o and P^o as a function of G/R for a typical germanium sample ($N=2.5\times10^{11}$ cm^{-3}, $P=1.0\times10^{11}$ cm^{-3}) and for a typical experimental situation ($\beta_1/\alpha_1=\beta_2/\alpha_2=1\times10^9$ cm^{-3}). The solid curves represent the results of an exact numerical calculation, whereas the dashed curves for n and p represent results according to equations (7) and (8). The solid and the dashed curves coincide for G/R values up to 10^{18} cm^{-6}, and deviate for higher values of G/R. This deviation is caused by the violation of the assumption $N^o=N-P$ and $P^i=P$, as can be seen from the curves for $P^o(=P-P^i)$ and N^o. For low values of G/R, p rapidly goes to zero, but n approaches a constant, determined by the equilibrium distribution of the majority charge carriers over the ground state of

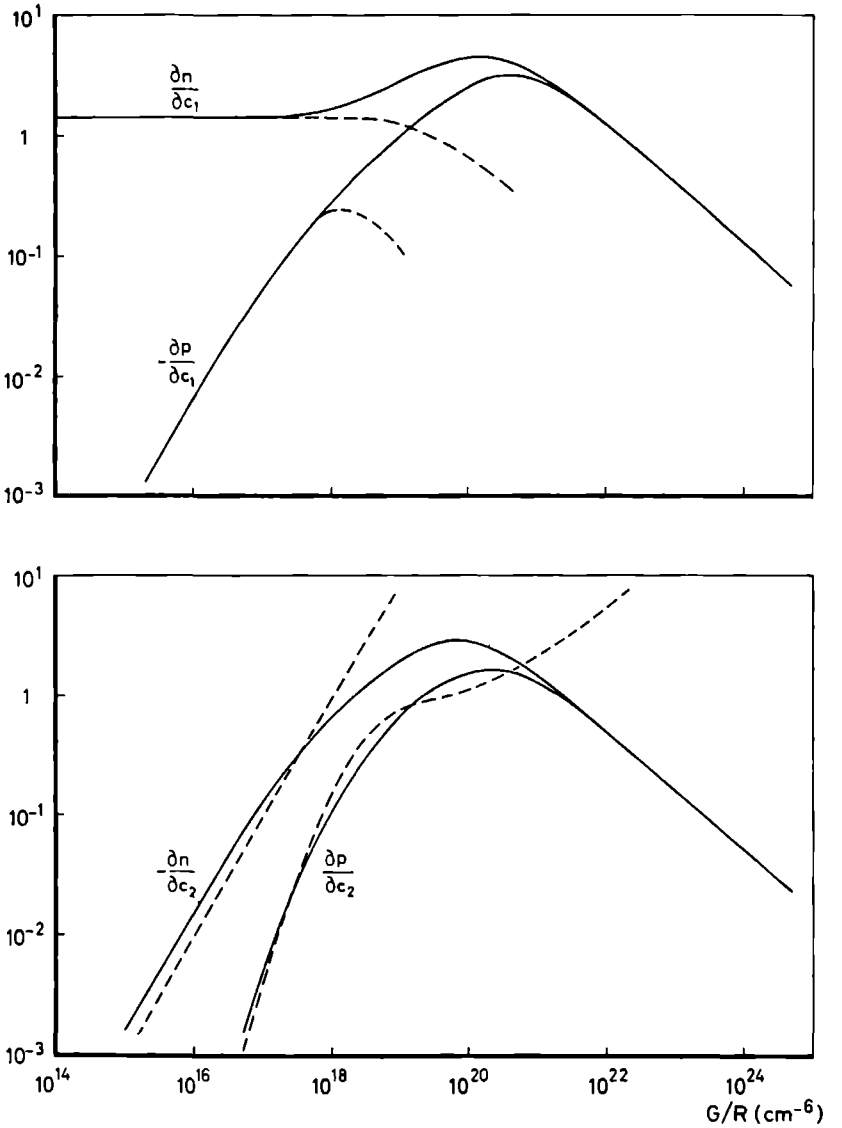

Fig. 5: Response of the free charge carrier concentration n and p to small changes in β_1/α_1 ($=c_1$) and β_2/α_2 ($=c_2$), as a function of G/R from an exact numerical calculation (solid curves) and from approximate formulas (dashed curves) for $\beta_1/\alpha_1 = \beta_2/\alpha_2 = 1\text{x}10^9$ cm^{-3}, $N = 2.5\text{x}10^{11}$ cm^{-3} and $P = 1\text{x}10^{11}$ cm^{-3}.

the majority impurity and the associated energy band. At high values of G/R the curves for n and p approach and reach the limiting dependence $(G/R)^{1/2}$ for intrinsic material.

The PTIS spectra are usually recorded with a far-infrared Fourier spectrometer. The additional chopped extrinsic light, coming from this spectrometer and reaching the sample, is only a fraction of the extrinsic (room temperature) background radiation. Therefore the influence of the additional extrinsic light can be described by replacing β_i/α_i by $(\beta_i+d\beta_i)/\alpha_i$, $i=1,2$.
The influence of far-infrared radiation on n and p and hence on the measured photoconductivity will be studied by considering the dimensionless quantities $\partial n/\partial c_i$ and $\partial p/\partial c_i$, where we defined $c_i=\beta_i/\alpha_i$. Just as before, in the case of low intensities of extrinsic and intrinsic radiation and low temperature the latter quantities can be determined analytically by using equations (7)-(9), yielding

$$\frac{\partial n}{\partial c_1} = \frac{N - P}{W} \tag{11}$$

$$\frac{\partial p}{\partial c_1} = - \frac{G}{4R} \cdot (N - P) \cdot \frac{(P + W)^2}{V^2 . W} \tag{12}$$

$$\frac{\partial n}{\partial c_2} = - \frac{G}{R} \cdot \frac{P}{c_2^2} \cdot \frac{1}{W} \tag{13}$$

$$\frac{\partial p}{\partial c_2} = \frac{G^2}{4R^2} \cdot \frac{P}{c_2^2} \cdot \frac{(P + W)^2}{V^2 . W} \quad . \tag{14}$$

In Fig. 5 $\partial n/\partial c_1$, $-\partial p/\partial c_1$, $-\partial n/\partial c_2$ and $\partial p/\partial c_2$ are shown as a function of G/R. The solid curves represent the results of an exact numerical calculation and the dashed curves the results using equations (11)-(14), for the same values of N, P, β_1/α_1 and β_2/α_2 as already used in Fig. 4. For low values of G/R formulas (11) and (12) are perfect approximations to the exact solution of the model. Formulas (13) and (14), however, fit less well for low values of G/R, because $\partial n/\partial c_2$ and $\partial p/\partial c_2$ depend strongly on P^o, which changes over many orders of magnitude from 0 towards P for increasing G/R (see Fig. 4).

A small increase in intensity of extrinsic light - e.g. by extra far-infrared radiation from a spectrometer - causes additional ionization of impurities. Figure 5 shows that $\partial n/\partial c_1$ is positive, and $\partial n/\partial c_2$ is negative, and that $|\partial n/\partial c_i| > |\partial p/\partial c_i|$ for $i=1,2$. Hence for low values of G/R the model predicts

that ionization of majority impurities by additional extrinsic light gives rise to an increase in total carrier concentration (n+p), whereas the corresponding ionization of minority impurities causes a decrease in (n+p). This is essentially the cause of the positive photoresponse from majority impurities and of the negative response from minority impurities, usually observed in PTIS spectra. For high values of G/R $|\partial n/\partial c_i|$ approaches $|\partial p/\partial c_i|$ for i=1,2 and $|\partial(n+p)/\partial c_i|$ decreases for increasing G/R. The decrease of $|\partial n/\partial c_i|$ and $|\partial p/\partial c_i|$ at high values of G/R is caused by the reduction of the lifetime of additional non-equilibrium carriers, which at high free carrier concentrations decreases with increasing concentrations.

When different types of majority impurities are present, one can infer their relative concentrations from the corresponding signal strengths in PTIS spectra, recorded in the absence of intrinsic light[2,8,13]. It could be interesting to check if - for our model with one type of majority and one type of minority impurity - the relative concentration of minority and majority impurities could be deduced from the PTIS spectra in a similar way. Therefore we consider the ratio of the magnitudes of the change in (n+p), caused by additional ionization of minority and majority impurities respectively. For a change of c_i to c_i+dc_i, i=1,2 and for the experimental regime where equations (11) to (14) hold, this ratio is given by

$$\frac{\frac{\partial}{\partial c_2}(n+p).\,dc_2}{\frac{\partial}{\partial c_1}(n+p).\,dc_1} = -\frac{1}{c_2^2}\cdot\frac{dc_2}{dc_1}\cdot\frac{P}{N-P}\cdot\frac{G}{R} \quad . \tag{15}$$

Equation (15) shows that this ratio is not a constant, but is proportional to to G/R, hence proportional to the intensity G_{rel} of the intrinsic light.

4.III. Experiment

In the preceding section we analyzed the distribution of electrons and holes over impurity states and energy bands in a semiconductor under continuous illumination with intrinsic light, and the response of this distribution to additional injection of majority or minority charge carriers into the energy bands. This section will deal with the experimentally determined time response of this distribution to additional injection by separate photothermal

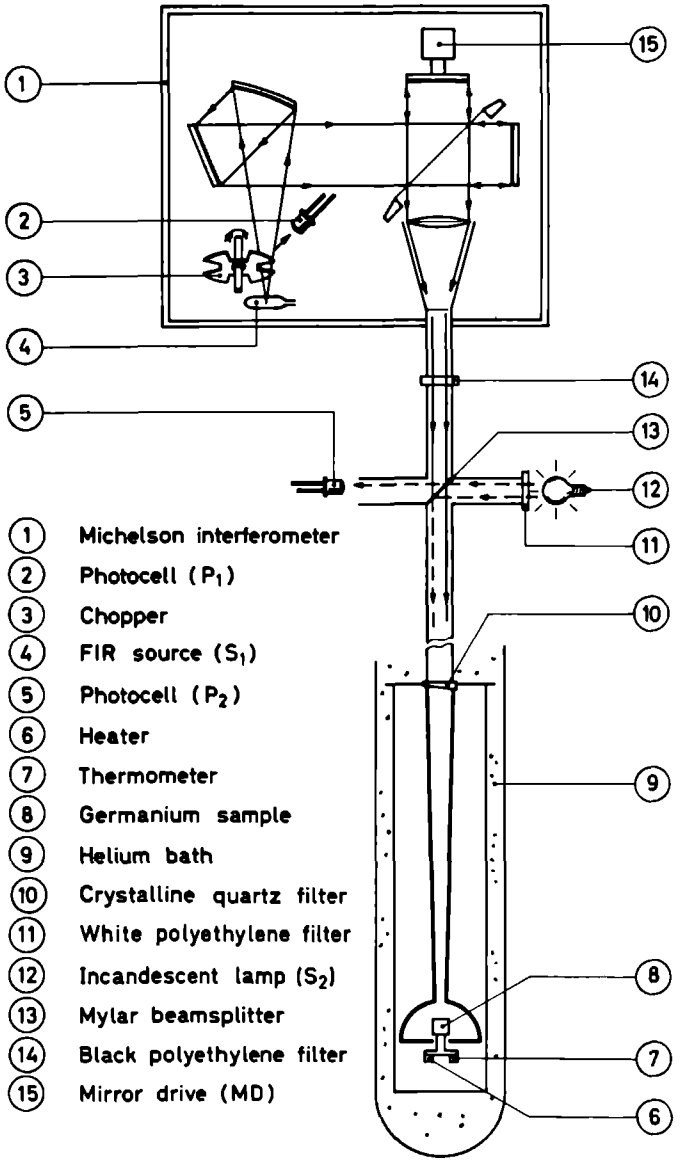

Fig. 6: Schematic diagram of the optical arrangement of the experiment.

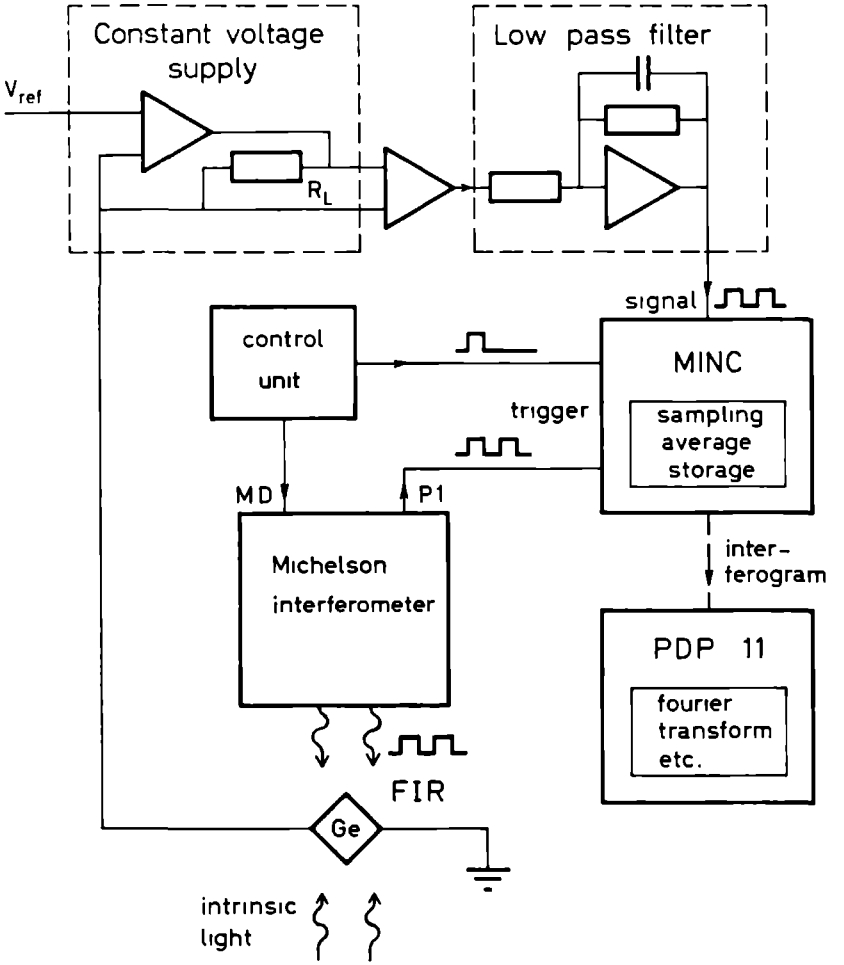

Fig. 7: Schematic diagram of the electronic set-up of the experimental arrangement.

ionization of majority and minority impurities in ultra-pure germanium. A general survey of the hardware of the experimental arrangement, suitable for the recording of time-resolved PTIS spectra under continuous intrinsic illumination is shown in Fig. 6. A far-infrared Grubb Parsons Michelson interferometer (1) provides the additional extrinsic light, while the intrinsic light is delivered by an incandescent lamp S_2 (12). The radiation, coming from the Michelson interferometer and the incandescent lamp, is combined by means of the mylar beamsplitter (13) and subsequently passes through a cooled crystalline quartz filter (10) into a semispherical, integrating cavity. The sample is clamped onto the base of the cavity and its temperature can be raised above the temperature of the surrounding helium bath (9) by means of a heater (6) and sensed with a thermometer (7). In the Michelson interferometer the radiation from source S_1 is modulated at 16 2/3 Hz by a mechanical chopper (3). A black polyethylene filter is used to make sure that no intrinsic light from the Michelson interferometer reaches the sample. Photocell P_1 is used to monitor the periodic intensity of the chopped far-infrared light. The continuous intensity G_{rel} of the intrinsic light is sensed by photocell P_2 and will henceforth be expressed in arbitrary units.

A general lay-out of the electronic system is shown in Fig. 7. The voltage drop across the Ge sample is fixed at a constant value V_{ref} via an electronic feedback system. The changes in conductance of the Ge sample, caused by the chopped far-infrared light, are determined by measuring the resulting changes in current through a load resistor in series with the sample. This signal is led via a differential amplifier and a low-pass filter to a MINC computer. A Control Unit provides the power pulses for the mirror drive MD (see Fig. 6), which translates the movable mirror in the Michelson interferometer. After each step of the MD, the Control Unit sends a trigger pulse to the MINC computer, which then starts a measuring cycle. In this cycle the signal is sampled during a number of chopping periods of the far-infrared light in equal time intervals of 0.75 msec, triggered by photocell P_1 (see Fig. 6). The datapoints sampled at corresponding times in each period are averaged and finally stored on diskettes. After a complete measuring run, lasting several hours, the interferograms obtained for the separate points of time are sent to a PDP-11 computer, which has many facilities for the manipulation of interferograms and spectra. Spectra are obtained, first by subtracting from the interferogram recorded at time t an interferogram sampled in the off-period of the far-infrared light just before the start of the next on-period. Subsequently the

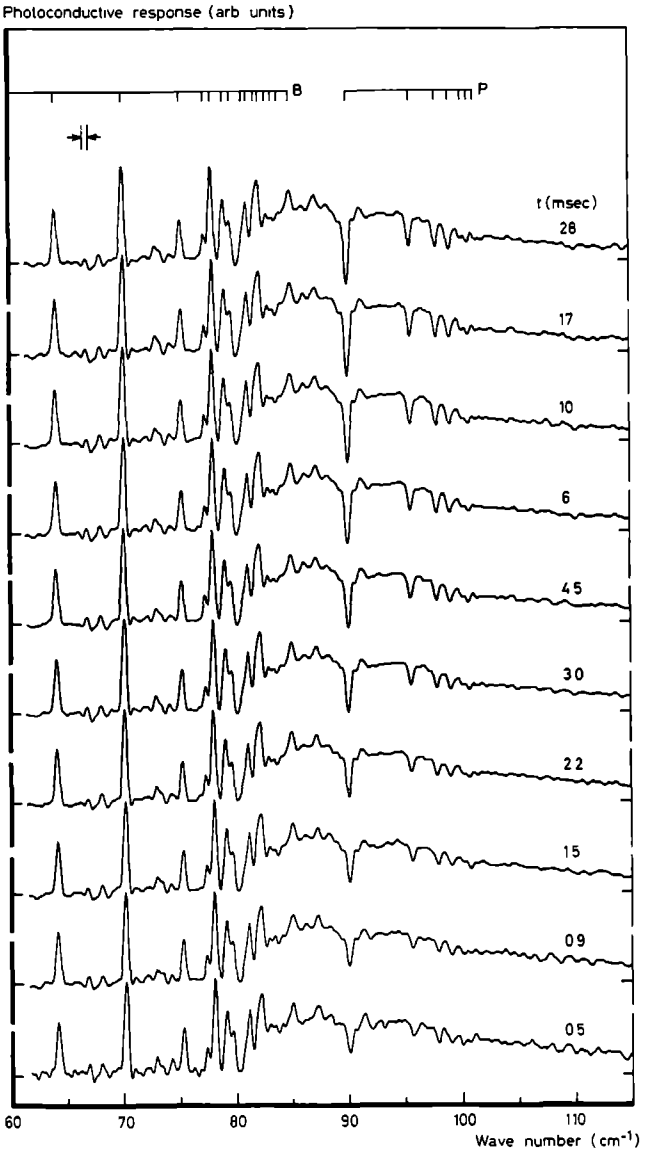

Fig. 8: Set of measured photoconductivity spectra, showing the time-evolution of the PTIS signal after switching on the far-infrared radiation under continuous illumination with intrinsic light. The sample was p-type Ge with $N_A - N_D = 2 \times 10^{11}$ *cm*$^{-3}$ *and a degree of compensation of about 0.4. The spectral resolution is indicated by arrows and the line positions of the majority boron and the minority phosphorus impurity are taken from reference 13 and 12 respectively.*

resulting interferogram was symmetrized by phase-correction, using the convolution method of Sakai, Vanasse and Forman[17], and finally a spectrum was calculated by applying a cosine Fourier transform.

The investigated sample was p-type material with $N_A-N_D=2x10^{11}$ cm^{-3} and with a degree of compensation of about 0.4, containing boron and phosphorus as dominating majority and minority impurities respectively. Electric contacts were made by pressing flat copper disks against two opposite faces of the sample, wetted with a Ga-In eutectic. A typical set of PTIS spectra, recorded under continuous illumination with intrinsic light with intensity $G_{rel}=7$ at discrete times t after the far-infrared light was switched on, is shown in Fig. 8. The magnitude of the photoresponse and the time scale have been corrected for the finite rise and decay times of the far-infrared light pulse, as monitored by photocell P_1. No noticeable time dependence in the photoresponse, originating from the boron majority impurities was ever observed. The PTIS signal originating from the phosphorus minority impurities exhibits a negative contribution to the photoresponse, at first increasing and finally saturating at high values of t. The time-evolution of the PTIS signal after switching off the FIR light was always observed to be the reverse of the corresponding time-evolution in the on-period. Several sets of spectra were recorded at different temperatures, bias voltages and intensities of intrinsic light. The individual photoresponse from the majority and minority impurities is very sensitive to a change in equilibrium concentration of free charge carriers[2]. This sensitivity is minimized by normalizing the negative photoresponse and therefore, when comparing different sets of spectra, we will consider the normalized negative photoresponse only. The normalized photoresponse is obtained from the spectra by taking the ratio of the height of the continuum belonging to the negative photoresponse from the minority impurities and the height of the corresponding continuum of the majority impurities. We consider the heights of the continua rather than the heights of the photoconductivity peaks, since the latter exhibit an additional temperature dependence due to the second step in the photothermal process[8,9]. The temperature was varied from 5 K to about 7 K. Below 5 K the noise increased considerably at otherwise equal signal strength. Above 7 K the signal itself decreased very fast with increasing temperature, due to emptying the ground states of the impurities because of thermal ionization. The bias voltage across the Ge sample with length 1 cm was varied from 0.5 V to 2.3 V, and also a set of spectra was recorded at 2 V with reverse polarity. It was observed that only variation of the intensity of the intrinsic light caused a

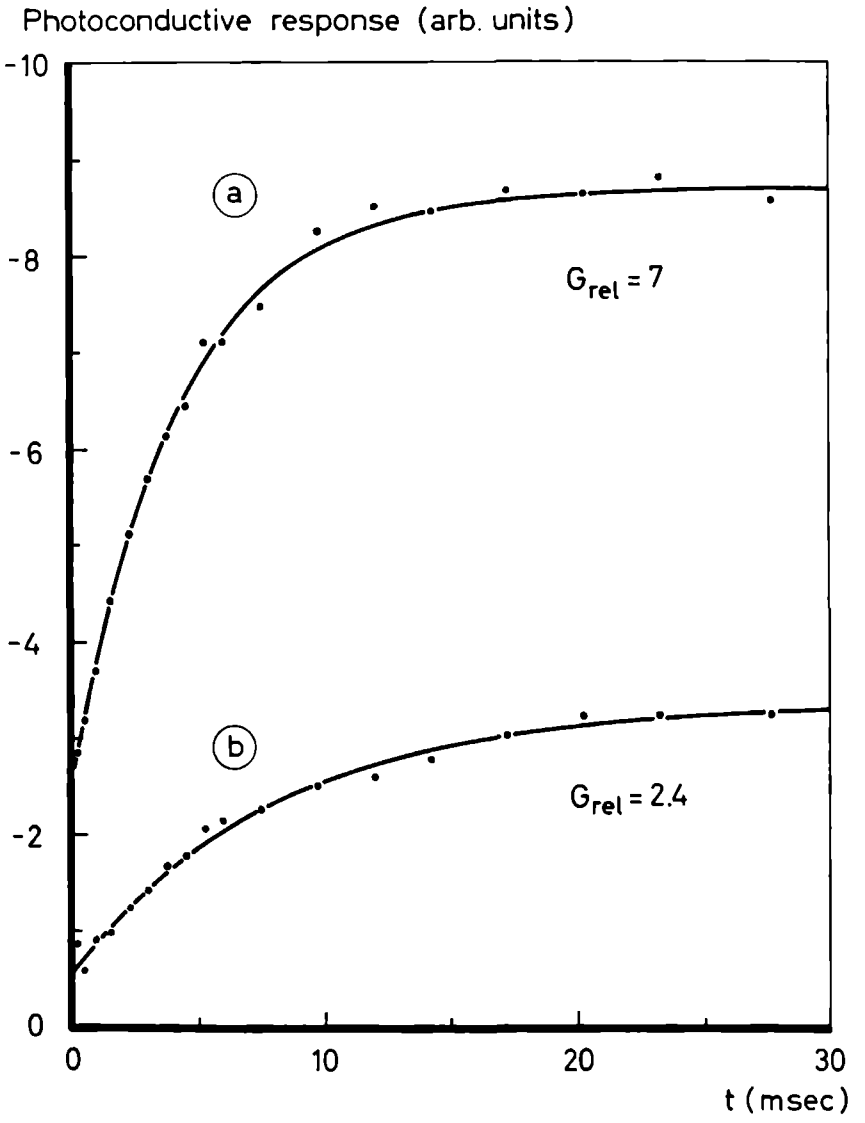

Fig. 9: Time-evolution of the measured normalized photoresponse from the minority phosphorus impurities for two values of intensity G_{rel} of the intrinsic light at 7 K. The solid curves represent the best fits to formula (16).

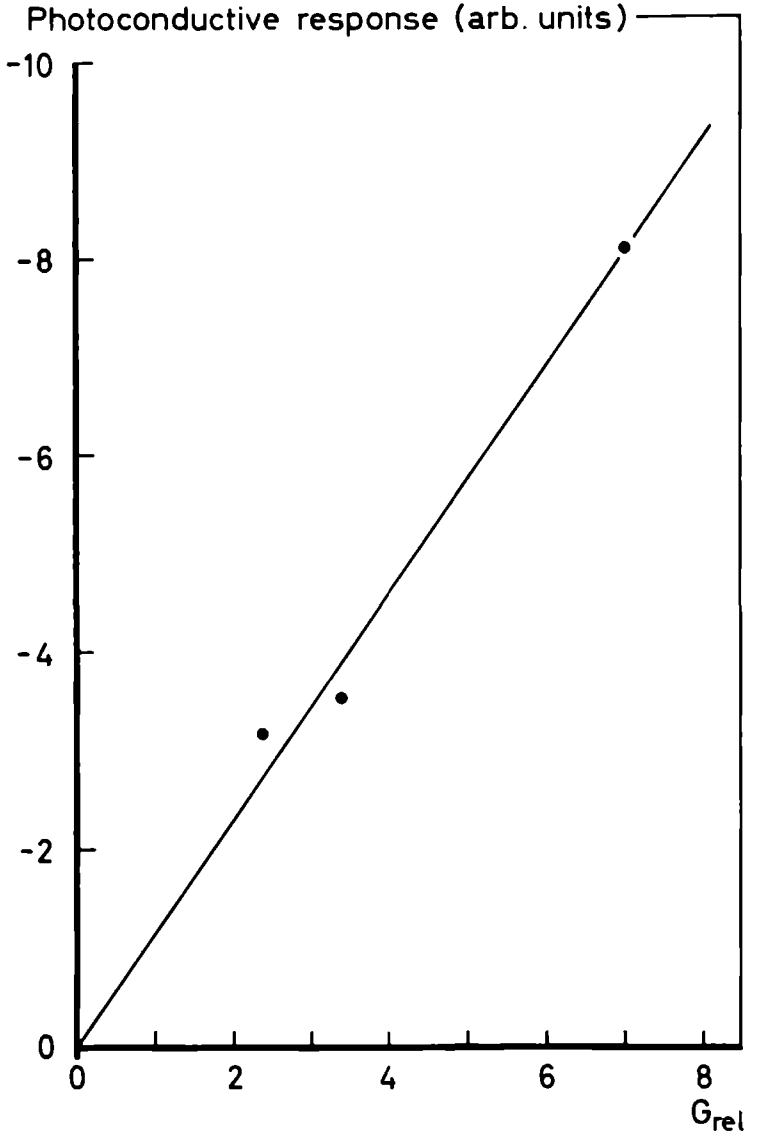

Fig. 10: Measured normalized negative photoresponse for different values of intensity G_{rel} of intrinsic light, determined at a time when the negative photoresponse was saturated. The solid line shows the best fit to a dependence where the photoresponse is proportional to G/R.

significant change in the magnitude of the normalized negative photoresponse or in its time dependence.

The intensity of the intrinsic light could be varied only within a small range. For too low intensities the negative photoresponse from the phosphorus impurity did not exceed the noise level. At too high intensities the temperature of the sample rose above 7 K, and the signal decreased below the noise level because of thermal ionization of the impurities. As an example the time-evolution of the normalized negative photoresponse is shown in Fig. 9, obtained from two sets of spectra which are recorded at 7 K for two values of the intensity G_{rel} of the intrinsic light. The normalized negative photoresponse exhibits an immediate change after the additional extrinsic far-infrared light is switched on, followed by a more gradual increase towards a saturation value. The curves represent fits to the datapoints, using the formula

$$S_o + S_1 . (1 - e^{-t/\tau}) \quad . \tag{16}$$

The value of τ represents the response time of the slow re-establishment of a new equilibrium distribution of electrons and holes over impurity states and energy bands. The curves fit quite well, indicating that the slow response can be described with a linear relaxation-time approximation. The parameters of these fits, together with those from a set of spectra recorded at G_{rel}=3.4, are given in Table 1. Fig. 10 shows the normalized negative photoresponse in the saturation region as a function of the intensity of the intrinsic light. Here we used the values S_o+S_1 from Table 1. As indicated by the solid line, the normalized negative photoresponse in the saturation region is proportional to the intensity of the intrinsic light.

Curves (a) and (b) in Fig. 11 represent the rise and decay curves of the photocurrent respectively, after switching on and off intrinsic light with intensity G_{rel}=1.0. The photocurrent was monitored with a Biomation 8100 transient recorder, by sensing the current through load resistor R_L while keeping the voltage drop across the Ge sample fixed at 2.3 V. The rise curve, starting at the value I_o of the dark current (i.e. the current in the absence of intrinsic light), already reaches 1/3 of its final value below 1 msec. Subsequently the photocurrent goes to a preliminary equilibrium value with a time constant of about 10 msec. This time constant is about the same as the one found from the set of far-infrared spectra and it is only dependent on G_{rel}, decreasing with increasing values of G_{rel}. After 1 sec the current increases

Table 1: Values for the parameters (defined by formula (16)) for the time-dependence of the measured normalized photoresponse from the minority phosphorus impurities, taken from the PTIS spectra recorded at 7 K under continuous illumination with intrinsic light.

G_{rel} (a.u.)	S_o (a.u.)	S_1 (a.u.)	τ (msec)
2.4	0.7 ± 0.3	3.3 ± 0.3	8 ± 2
3.4	0.8 ± 0.6	3.6 ± 0.6	6 ± 2
7.0	3.0 ± 0.6	3.7 ± 0.6	4.25 ± 0.75

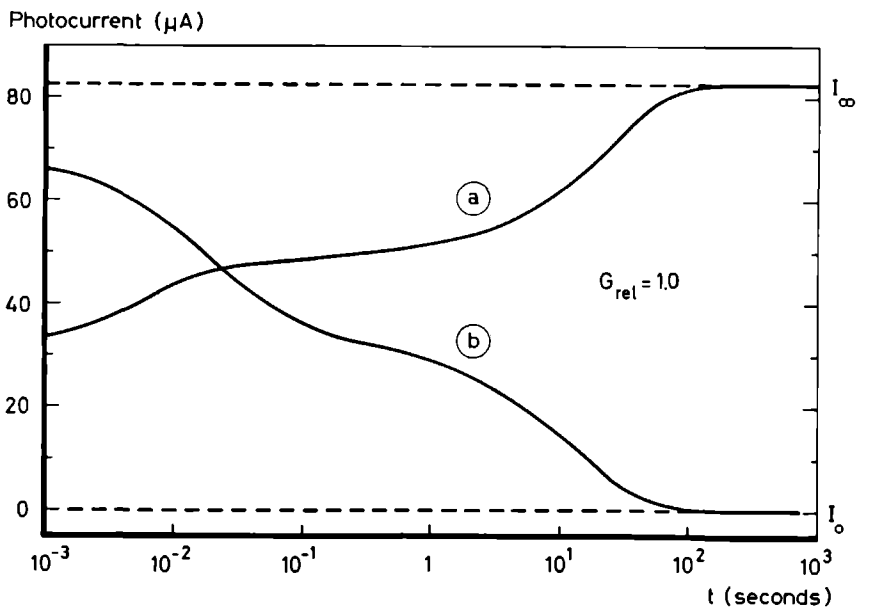

Fig. 11: Experimental rise (a) and decay (b) curves of the photocurrent after switching on and off the intrinsic light under continuous illumination with far-infrared radiation.

again with a time constant of the order of magnitude of 10 sec, caused by an additional release of charge carriers from the ground state of impurities to the energy bands after a temperature rise, due to absorption of intrinsic light. This rise in temperature is about 0.1 K, as monitored by the thermometer connected to the Ge sample. For the range of values of G_{rel} used, the final value $I_\infty - I_o$ was always between one and two times the value I_o of the current in the absence of intrinsic light.

4.IV. Discussion and conclusions

The results of the theory, explicitly developed before for an n-type semiconductor, can also be applied to p-type material, by interchanging the roles of electrons and holes as well as donors and acceptors. To avoid notational confusion throughout the discussion in this section, we will still associate n, N and subscript 1 to the majority free carriers and majority impurities, which for our p-type sample has to be associated with free holes and acceptors. The measurements discussed in this section are carried out on a p-type ultra-pure germanium sample with net impurity concentration $N_A - N_D = 2 \times 10^{11}$ cm^{-3} and with a degree of compensation of about 0.4. The typical values for β_1/α_1, β_2/α_2, N and P, used in the preceding theoretical analysis, were chosen in view of this sample and the experimental arrangement used. Therefore Figures 4 and 5 can be used to discuss the experimental results.

When recording PTIS spectra one does not directly measure the net change $\Delta n + \Delta p$ in total free carrier concentration, but rather the net change in conductance ΔS, given by

$$\Delta S = F \,.\, e \,.\, (\mu_1 . \Delta n + \mu_2 . \Delta p) \quad . \tag{17}$$

Here μ_1 and μ_2 denote the mobilities associated with the majority and minority charge carriers respectively and F is a geometrical factor. The mobilities μ_1 and μ_2 have about the same value in ultra-pure germanium at 4.2 K[15,18] and are temperature dependent. We assume that μ_1 and μ_2 also have about the same value at 7 K, since in ultra-pure germanium the temperature dependence for both μ_1 and μ_2 is caused by collisions of the free charge carriers with acoustic phonons. Therefore ΔS should represent a change in total free carrier concentration quite well. Analogous with the discussion before the total conductance - and hence the current - can also be considered to be proportional

to the total free carrier concentration. For the experimentally used range of intensities of the intrinsic light, the magnitude of the negative photoresponse from the minority impurities was almost as large as the magnitude of the positive photoresponse from the majority impurities. The increase in current $I_\infty - I_o$ was observed to be between one and two times the value I_o of the current in the absence of intrinsic light. Regarding Figures 4 and 5 these experimental facts are consistent with each other for G/R values of about 10^{18} cm^{-6}. Therefore we conclude that the range of applied intensities of the intrinsic light corresponds to G/R values of 10^{18} cm^{-6}.

In the preceding section we saw that, after the additional far-infrared light was switched on, the negative photoresponse from the minority impurities exhibits a fast (< 0.5 msec) jump, followed by a slow increase towards a saturation value with a characteristic time of the order of magnitude of 5 msec. About the same characteristic time was observed after switching on and off the intrinsic light. No dependence on polarity or magnitude of the applied bias-voltage across the Ge sample, nor on temperature was observed. Therefore we exclude possible effects due to rectifying properties in the contact region. Switching on far-infrared light first adds an additional number of free majority and minority carriers to the total system of free carriers, which is small with respect to (n+p). This is followed by a redistribution of electrons and holes over the energy bands and the impurity states.

The initial additional injection of majority carriers from the majority impurities finally leads to a net increase in (n+p), mainly determined by an increase in n (see Fig. 5). Hence in this process the dominating process is the exchange of majority carriers between the energy band and shallow majority impurities. For ultra-pure germanium the characteristic times for the exchange of electrons between donor levels and conduction band and of holes between acceptor levels and valence band are of the order of magnitude of microseconds [19]. In view of the high mobilities involved (~10^5 $cm^2V^{-1}sec^{-1}$ [17,18]) and the electric fields applied (~2 V/cm), the electrons and holes drift to the positive and negative electrodes within 10 μsec. This explains the fast (< 0.5 msec) photoresponse from the majority impurities. The initial additional injection of minority carriers from the minority impurities finally causes the total concentration of free charge carriers to decrease, mainly determined by a decrease in concentration of majority charge carriers (see also Fig. 5). Hence in the latter situation the electron-hole recombination process is important. We therefore associate the slow response time of 5 msec to be

associated with electron-hole recombination in the Ge-bulk material. The fast component of the negative photoresponse can be caused by the electron-hole recombination process near the surface which has a relative high concentration of surface states due to mechanical treatment of the sample. For an intrinsic semiconductor the electron-hole recombination time is given by $\sqrt{GR}$ [20]. Assuming that this relation also holds in ultra-pure germanium, separate values for G and R can be obtained. This yields $G=5x10^{6}$ $cm^{-3}sec^{-1}$ and for R, associated with the slow component, a value $5x10^{-12}$ $cm^{3}sec^{-1}$.

In a preceding section we put forward the possibility to obtain the degree of compensation - i.e. the ratio of the concentration of majority impurities and that of minority impurities - from the relative magnitude of the photoresponse from the minority and majority impurities, hence from the normalized negative photoresponse. It was predicted by means of equation (15) that the corresponding relative magnitude of the change in (n+p) should be proportional to G/R, hence to the intensity of the intrinsic light. This prediction has been confirmed by experiment, visible in Fig. 10, which shows the measured normalized photoresponse to be proportional to G_{rel}. Due to the dependence on G_{rel}, on the intensity of extrinsic light and on temperature, we conclude that one cannot simply deduce the degree of compensation from the normalized negative photoresponse from spectra, recorded under continuous illumination with intrinsic light. Very recently Darken[13] described a method to obtain the degree of compensation indirectly from the temperature dependence of the relative strength of the photoresponse from two different types of majority impurities in spectra recorded in the absence of intrinsic light.

For the range of intensities of intrinsic light applied the PTIS signal contained a slow (~5 msec) component, associated with the negative photoresponse of minority impurities, and a fast (< 0.5 msec) component, associated with the photoresponse of both minority and majority impurities. PTIS spectra are commonly recorded using phase-sensitive detection techniques by means of a lock-in amplifier. Because of the occurrence of both a fast and a slow component in the PTIS signal, there is no unique phase setting for which the quadrature signal is zero during the total duration of the recording of the interferogram. Such unique phase setting does not exist because for every point in the interferogram the relative contribution of the fast and slow component to the total PTIS signal is different. Therefore one cannot use a lock-in amplifier, if one wants to measure the magnitude of the photoresponse rather than to identify impurities. We strongly believe that the strange behaviour, shown in Figures 1 and 2,

is an artefact caused by the improper use of a lock-in amplifier. For a proper determination of the equilibrium value of the negative photoresponse one should record the difference in response in the on- and off-period of the additional extrinsic light long enough after the light is switched on and off respectively. For this purpose a two-channel Boxcar integrator can be used or, of course, an electronic sampling arrangement as described in this article.

In conclusion we can say that photothermal ionization spectroscopy is a very suited tool to investigate the equilibrium distribution of electrons and holes over impurity states and energy bands in ultra-pure semiconductors under continuous illumination with intrinsic light. By applying time-resolved spectroscopy the slow time response after the start of the photothermal process of one of the relevant processes involved, i.e. the electron-hole recombination process, can be measured. The simultaneous occurrence of the slow response time and of the fast response time of the other processes involved prohibits the use of phase-sensitive detection techniques by means of a lock-in amplifier at ordinary chopping frequencies.

References:

1. E.E. Haller, W.L. Hansen and F.S. Goulding, Adv. Phys. 30, 93 (1981) (Review).
2. Sh.M. Kogan and T.M. Lifshits, Phys. Status Solidi (a) 39, 11 (1977) (Review).
3. E.E. Haller and L.M. Falicov, Phys. Rev. Lett. 41, 1192 (1978).
4. E.E. Haller, B. Joós and L.M. Falicov, Phys. Rev. B 21, 4729 (1980).
5. B. Joós, E.E. Haller and L.M. Falicov, Phys. Rev. B 22, 832 (1980).
6. J. Broeckx, P. Clauws, K. van den Steen and J. Vennik, J. Phys. C: Solid St. Phys. 12, 4061 (1979).
7. H.W.H.M. Jongbloets, M.J.H. van de Steeg, J.H.M. Stoelinga and P. Wyder, J. Phys. C: Solid St. Phys. 13, 4769 (1980).
8. H.W.H.M. Jongbloets, J.H.M. Stoelinga, M.J.H. van de Steeg and P. Wyder, Phys. Rev. B 20, 3328 (1979).
9. H.W.H.M. Jongbloets, M.J.H. van de Steeg, J.H.M. Stoelinga and P. Wyder, J. Phys. C: Solid St. Phys. 13, 2139 (1980).
10. E.M. Bykova, T.M. Lifshits and V.I. Sidorov, Fiz. Tekh. Poluprov. 7, 986 (1973) [Sov. Phys. Semicond. 7, 671 (1973)].
11. E.E. Haller, W.L. Hansen, G.S. Hubbard and F.S. Goulding, IEEE Trans. Nucl. Sci. 23, 81 (1976).
12. M.S. Skolnick, L. Eaves, R.A. Stradling, J.C. Portal and S. Askenazy, Solid State Commun. 15, 1403 (1974).
13. L.S. Darken, J. Appl. Phys. 53, 3754 (1982).
14. V.N. Abakumov, V.I. Perel' and I.N. Yassievich, Fiz. Tekh. Poluprov. 12, 3 (1978) [Sov. Phys. Semicond. 12, 1 (1978)] (Review).
15. N.I. Golosai and V.I. Sidorov, Fiz. Tekh. Poluprov. 6, 2354 (1972) [Sov. Phys. Semicond. 6, 1976 (1973)].
16. See e.g. E.H. Putley, Proc. Phys. Soc. 72, 917 (1958).
17. H. Sakai, G.A. Vanasse and M.L. Forman, J. Opt. Soc. Am. 58, 84 (1968).
18. E.A. Kurkova and V.I. Sidorov, Fiz. Tekh. Poluprov. 9, 1286 (1975) [Sov. Phys. Semicond. 9, 850 (1975)].
19. E.M. Gershenzon, G.N. Gol'tsman , V.V. Multanovskiĭ and N.G. Ptitsyna, Zh. Eksp. Teor. Fiz. 77, 1450 (1979) [Sov. Phys. JETP 50, 728 (1979)].
20. S.M. Ryvkin, "Photoelectric Effects in Semiconductors", Consultants Bureau, New York, 1964; chapter 1.

Description

In the practice of Fourier spectroscopy not only the optical hardware and the associated electronics are important, but also a computer and operating programs are indispensable. The principles of Fourier transform spectroscopy and the hardware of a Michelson interferometer - a special type of Fourier spectrometer - have been dealt with already in the first part of chapter 2. In this appendix we will give a short survey of the computer system and a short description of the application software.

A diagram of the computer system is shown in Fig. 1. The configuration consists of a PDP-11/10 central processor with 32 K (words) memory and a KE11-B hardware integer multiply/divide unit (DEC), two VT55 display terminals, two RK05 hard disk units, a FACIT papertape reader, a Tektronix 4661 plotter and a control unit for the spectrometer. The interfaces between the computer and the plotter and control unit of the spectrometer ("scanner") have been developed and constructed by the electronics department of the Faculteit der Wis- en Natuurwetenschappen.

The software consists of separate sets of programs. Some of these programs are written in assembler language, others in FORTRAN. The first entry of the user into these sets of programs occurs via a call for program "FIR", according to the conventions of the RT-11 operating system. The user can interactively determine the course of the program by a suitable choice of option numbers. The program itself calls the required new program into memory by using the "CHAIN"-option of the FB-monitor. A general survey of the options which are available in program "FIR" and the structure of the program are shown in the second part of this appendix.

Program "FIR" constitutes of two main sections, the "MANIPULATE INTERFEROGRAMS" (MI)-section and the "MANIPULATE SPECTRA" (MS)-section. In MI the maximum number of datapoints of an interferogram is 4096. The datapoints of the interferograms can be read into memory either from papertape - produced by a Talley-punch in conjunction with an early type of control unit ("old scanner") or by a FACIT-punch connected to a new type of control unit ("new scanner") - or directly on-line by means of an interface between the PDP-11/10 and the new scanner. In the latter case the interferogram is also automatically stored on disk. Before applying a Fourier transform, the interferogram can be displayed

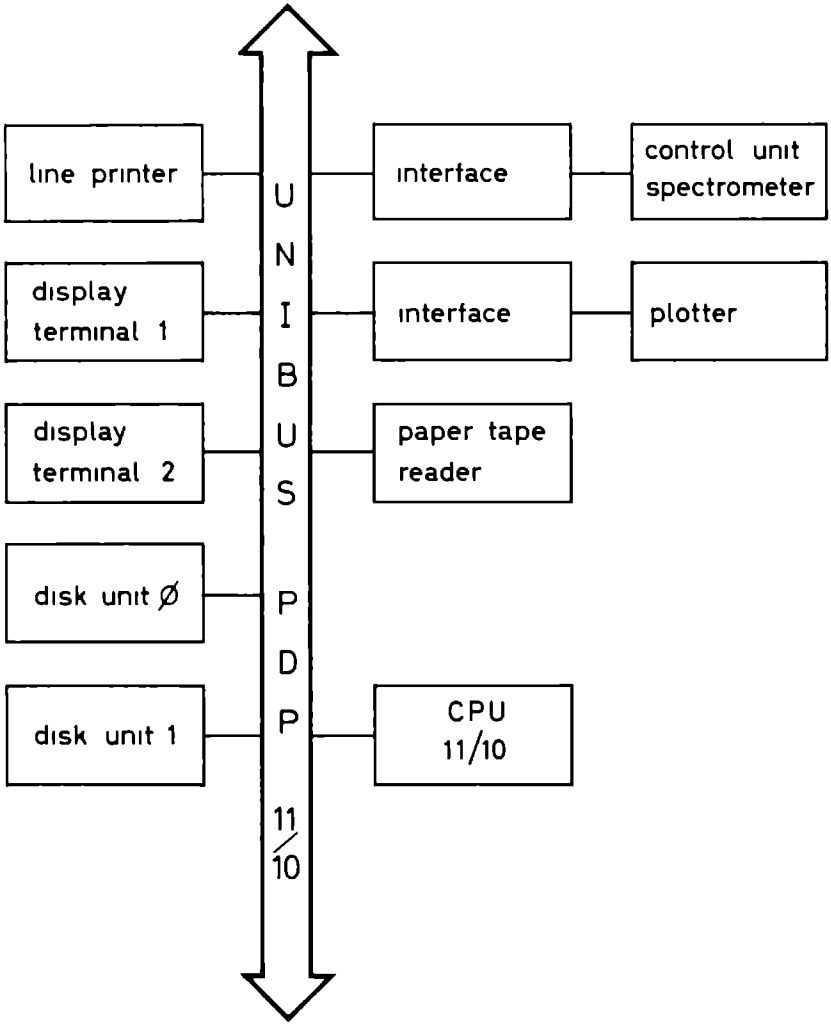

Fig. 1: Diagram of the computer system used in conjunction with the Fourier spectrometer.

on the display terminal or plotted, or the contents of the interferogram can be printed. The user can also change the data of an interferogram, e.g. when the interferogram contains erroneous datapoints caused by transient peaks.

In subsection "FT" of section MI spectra can be obtained from two- or one-sided interferograms. The interferograms can be multiplied, if desired, with a "cos"-apodization function ("light apodization") or a "$\cos^2$"-apodization function ("strong apodization"). From the two-sided interferogram a modulus spectrum can be calculated after the application of a complex Fourier transform. A real spectrum can be obtained by first calculating the symmetrized interferogram, associated with the measured two-sided or one-sided interferogram, by phase correction and subsequently applying a cosine Fourier transform. For the phase correction we used the convolution method of Sakai, Vanasse and Forman[1].

An additional set of special options is also available in "FT". The possibility to give the position of the centre of the interferogram is e.g. useful when dealing with monochromatic-line spectra. The user can also symmetrize an - e.g. asymmetrically recorded - two-sided interferogram. Moreover the phase-correction program can be warned that a sudden reverse of sign in the spectrum is a genuine spectral feature. After the choice of the "standard Fourier transform"-option - meaning the calculation of the modulus spectrum from a two-sided interferogram using a strong apodization - the spectrum is calculated immediately. The actual Fourier transform is obtained using the fast Fourier transform algorithm of Cooley and Tukey[2]. The required values of the cosines are obtained from a look-up table with 4096 entries. If desired, the resulting spectra can be stored on disk. If the interferogram belonged to a multichannel recording - up to 4 channels can be sampled simultaneously - , the computer program automatically takes care of handling the individual interferograms in turn.

In the MS-section the user can plot or display a spectrum, print the contents of the spectrum or integrate a part of the spectrum. He can also add, subtract, multiply, divide or average spectra and store the resulting datapoints on disk. For this purpose a set of scratch files are available on disk unit 0.

References:

1. H. Sakai, G.A. Vanasse and M.L. Forman, J. Opt. Soc. Am. 58, 84 (1968).
2. J.W. Cooley and J.W. Tukey, Math. Comput. 19, 297 (1965).

General flowchart of the interactive program "FIR"

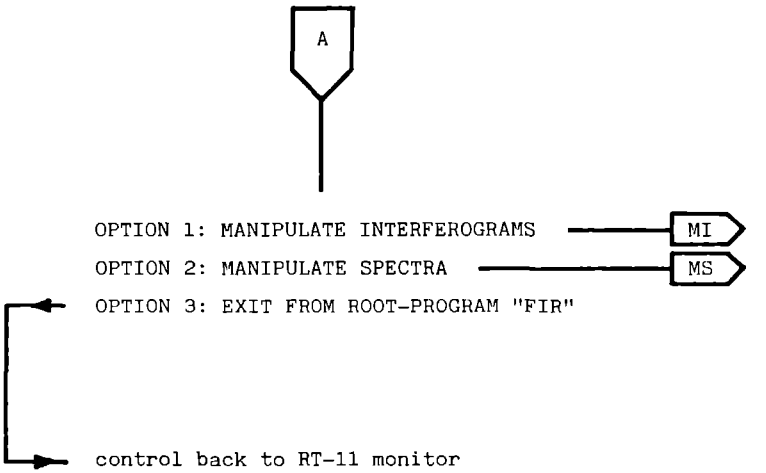

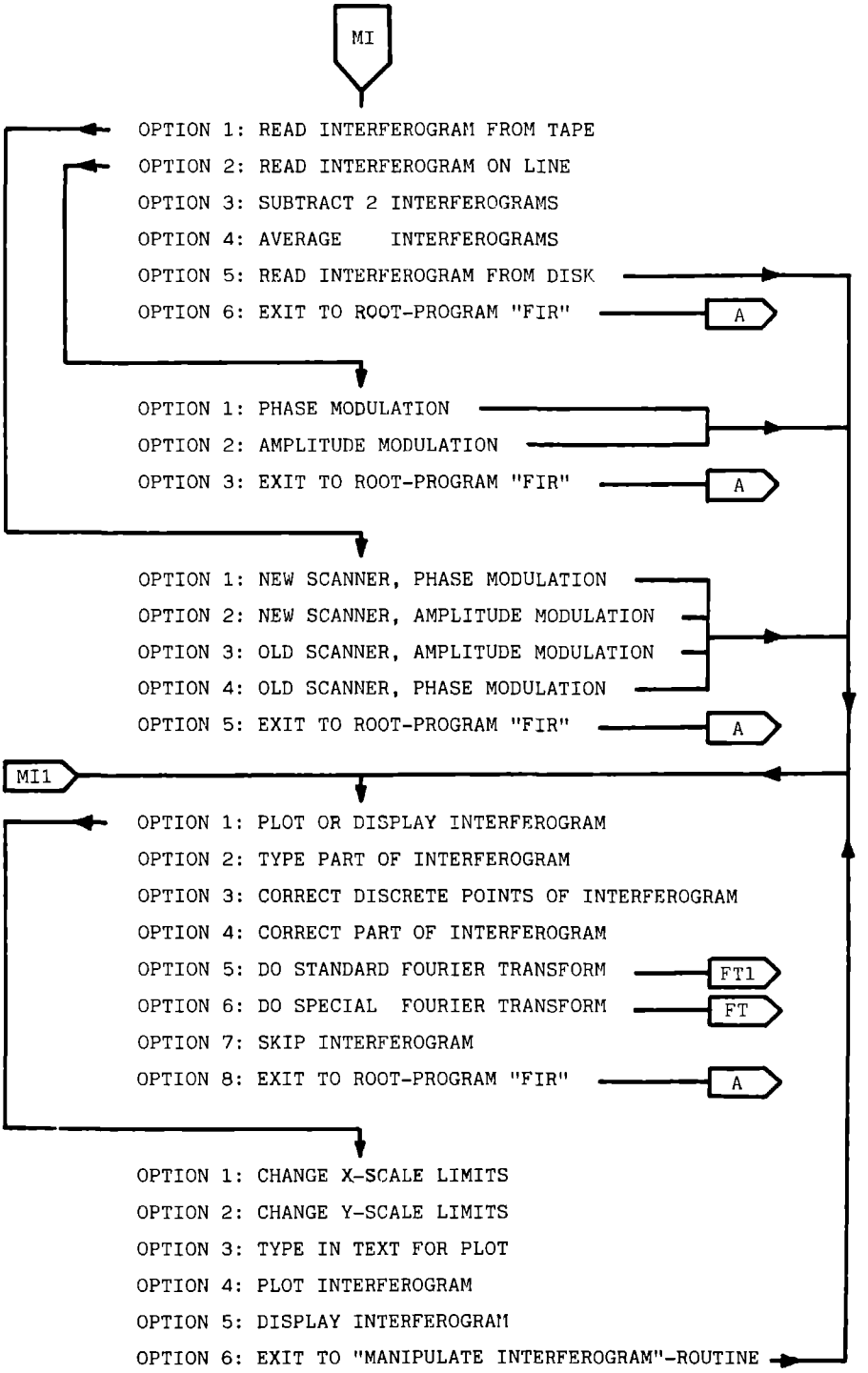
MI
OPTION 1: READ INTERFEROGRAM FROM TAPE
OPTION 2: READ INTERFEROGRAM ON LINE
OPTION 3: SUBTRACT 2 INTERFEROGRAMS
OPTION 4: AVERAGE INTERFEROGRAMS
OPTION 5: READ INTERFEROGRAM FROM DISK
OPTION 6: EXIT TO ROOT-PROGRAM "FIR"
A
OPTION 1: PHASE MODULATION
OPTION 2: AMPLITUDE MODULATION
OPTION 3: EXIT TO ROOT-PROGRAM "FIR"
A
OPTION 1: NEW SCANNER, PHASE MODULATION
OPTION 2: NEW SCANNER, AMPLITUDE MODULATION
OPTION 3: OLD SCANNER, AMPLITUDE MODULATION
OPTION 4: OLD SCANNER, PHASE MODULATION
OPTION 5: EXIT TO ROOT-PROGRAM "FIR"
A
MI1
OPTION 1: PLOT OR DISPLAY INTERFEROGRAM
OPTION 2: TYPE PART OF INTERFEROGRAM
OPTION 3: CORRECT DISCRETE POINTS OF INTERFEROGRAM
OPTION 4: CORRECT PART OF INTERFEROGRAM
OPTION 5: DO STANDARD FOURIER TRANSFORM
FT1
OPTION 6: DO SPECIAL FOURIER TRANSFORM
FT
OPTION 7: SKIP INTERFEROGRAM
OPTION 8: EXIT TO ROOT-PROGRAM "FIR"
A
OPTION 1: CHANGE X-SCALE LIMITS
OPTION 2: CHANGE Y-SCALE LIMITS
OPTION 3: TYPE IN TEXT FOR PLOT
OPTION 4: PLOT INTERFEROGRAM
OPTION 5: DISPLAY INTERFEROGRAM
OPTION 6: EXIT TO "MANIPULATE INTERFEROGRAM"-ROUTINE

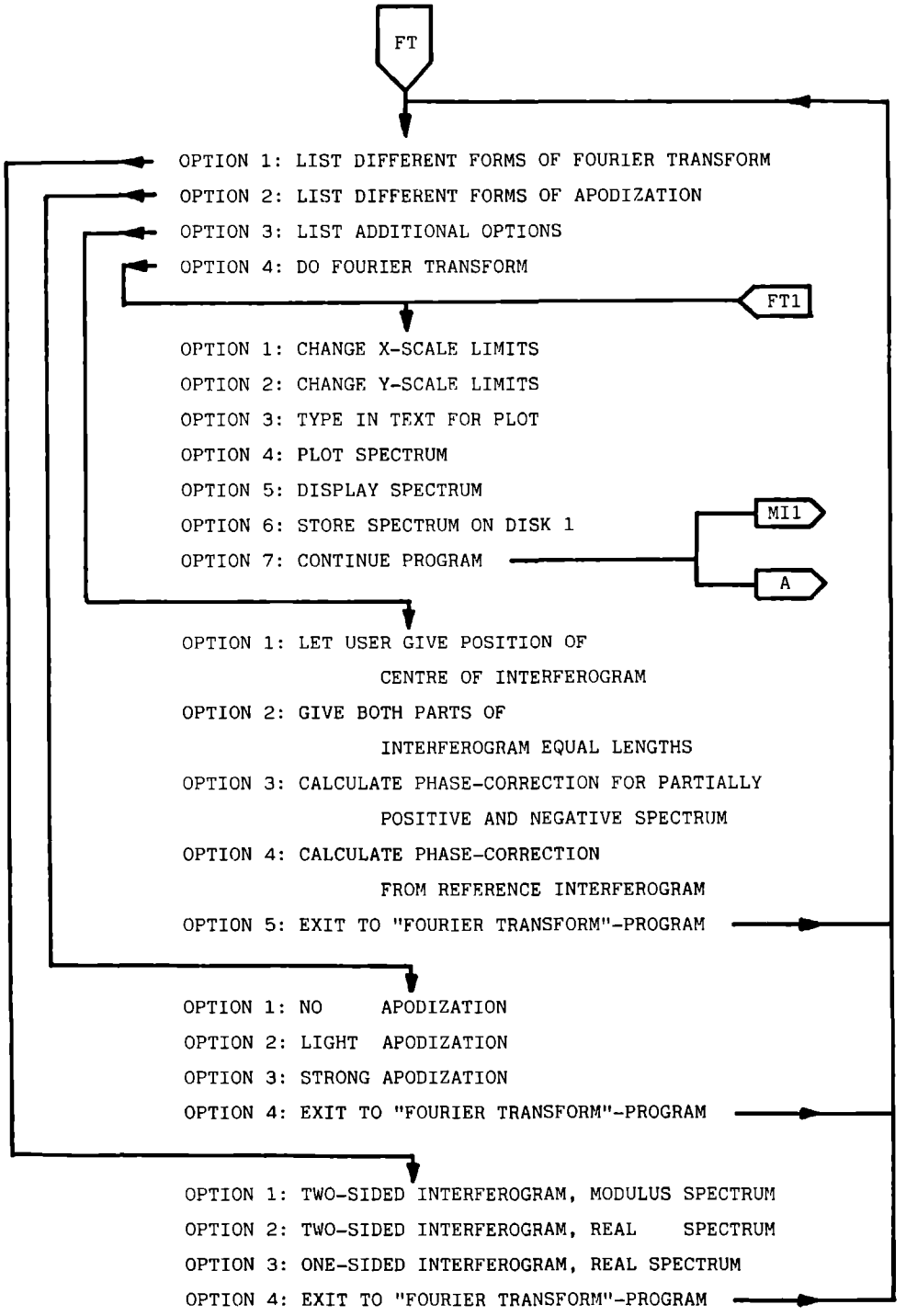
FT
OPTION 1: LIST DIFFERENT FORMS OF FOURIER TRANSFORM
OPTION 2: LIST DIFFERENT FORMS OF APODIZATION
OPTION 3: LIST ADDITIONAL OPTIONS
OPTION 4: DO FOURIER TRANSFORM
FT1
OPTION 1: CHANGE X-SCALE LIMITS
OPTION 2: CHANGE Y-SCALE LIMITS
OPTION 3: TYPE IN TEXT FOR PLOT
OPTION 4: PLOT SPECTRUM
OPTION 5: DISPLAY SPECTRUM
OPTION 6: STORE SPECTRUM ON DISK 1
OPTION 7: CONTINUE PROGRAM
MI1
A
OPTION 1: LET USER GIVE POSITION OF
CENTRE OF INTERFEROGRAM
OPTION 2: GIVE BOTH PARTS OF
INTERFEROGRAM EQUAL LENGTHS
OPTION 3: CALCULATE PHASE-CORRECTION FOR PARTIALLY
POSITIVE AND NEGATIVE SPECTRUM
OPTION 4: CALCULATE PHASE-CORRECTION
FROM REFERENCE INTERFEROGRAM
OPTION 5: EXIT TO "FOURIER TRANSFORM"-PROGRAM
OPTION 1: NO APODIZATION
OPTION 2: LIGHT APODIZATION
OPTION 3: STRONG APODIZATION
OPTION 4: EXIT TO "FOURIER TRANSFORM"-PROGRAM
OPTION 1: TWO-SIDED INTERFEROGRAM, MODULUS SPECTRUM
OPTION 2: TWO-SIDED INTERFEROGRAM, REAL SPECTRUM
OPTION 3: ONE-SIDED INTERFEROGRAM, REAL SPECTRUM
OPTION 4: EXIT TO "FOURIER TRANSFORM"-PROGRAM

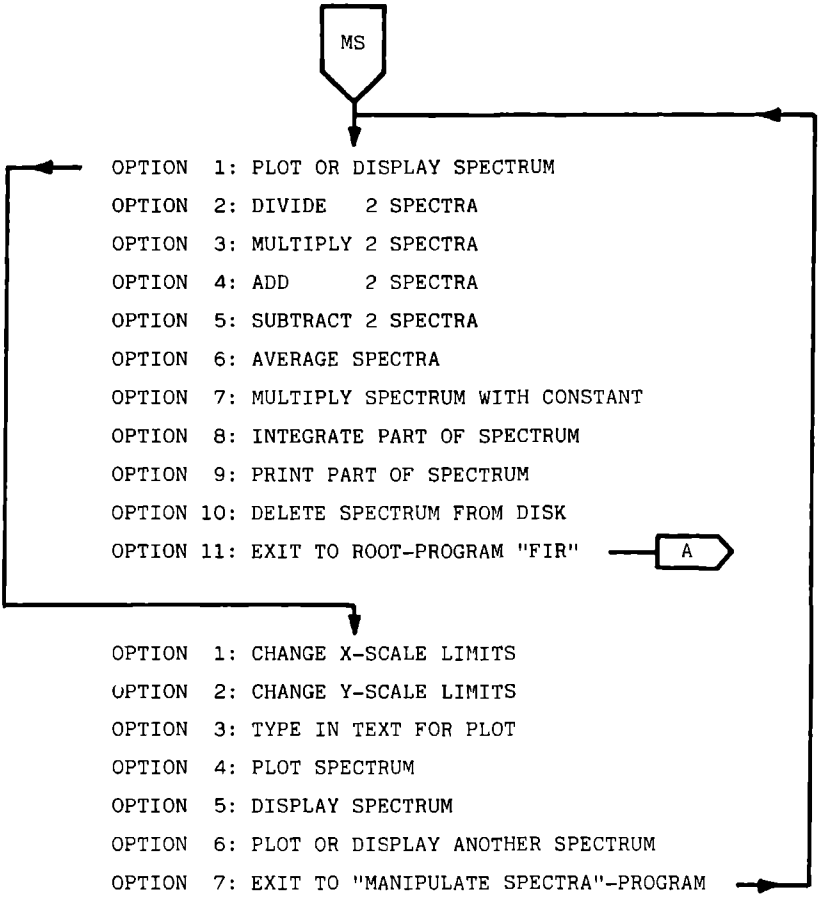
MS
OPTION 1: PLOT OR DISPLAY SPECTRUM
OPTION 2: DIVIDE 2 SPECTRA
OPTION 3: MULTIPLY 2 SPECTRA
OPTION 4: ADD 2 SPECTRA
OPTION 5: SUBTRACT 2 SPECTRA
OPTION 6: AVERAGE SPECTRA
OPTION 7: MULTIPLY SPECTRUM WITH CONSTANT
OPTION 8: INTEGRATE PART OF SPECTRUM
OPTION 9: PRINT PART OF SPECTRUM
OPTION 10: DELETE SPECTRUM FROM DISK
OPTION 11: EXIT TO ROOT-PROGRAM "FIR"
A
OPTION 1: CHANGE X-SCALE LIMITS
OPTION 2: CHANGE Y-SCALE LIMITS
OPTION 3: TYPE IN TEXT FOR PLOT
OPTION 4: PLOT SPECTRUM
OPTION 5: DISPLAY SPECTRUM
OPTION 6: PLOT OR DISPLAY ANOTHER SPECTRUM
OPTION 7: EXIT TO "MANIPULATE SPECTRA"-PROGRAM

This thesis deals with two main topics. The first is the possibility to detect fractional charge impurities - formed by quark-nucleon complexes - in semiconductors by means of photothermal ionization spectroscopy. The second is an investigation of the equilibrium system of electrons and holes, distributed over shallow impurity states and energy bands of ultra-pure semiconductors under continuous illumination with intrinsic light, by applying the same spectroscopic technique.

A Michelson interferometer has been constructed by the author, covering the wave number range 5 - 350 cm^{-1} in the far infrared. This special type of Fourier spectrometer and the principles of Fourier transform spectroscopy are described in the first part of chapter 2. During the build-up of the interferometer it was discovered that the travel of the movable mirror was subject to a periodic non-linearity, due to a pitch-error of the leading micrometer. In a Fourier spectrometer used in the step-and-integrate mode, such a non-linearity gives rise to ghostline structures in the spectra, if the increments in optical path difference between the two divided beams are not monitored by an accurate control system as a fringe-reference system. The ghostline structure resulting from a periodic non-linearity has been theoretically and experimentally studied and is described in the second part of chapter 2. A method of reducing the intensity of ghostlines for a given magnitude of non-linearity without the necessity to use a fringe-reference system is proposed and its practical applicability is demonstrated.

Chapter 3 deals with the detection of fractional charge impurities in semiconductors by applying photothermal ionization spectroscopy. First a phenomenological analysis is given for the expected signal strengths at a certain concentration of fractional charge impurities. From the absence of a signal, originating from fractional charge impurities, in spectra of an ultra-pure germanium sample recorded with the Michelson interferometer we could deduce that this sample contained less than 1.5×10^{11} acceptor-like fractional charge impurities per cm^3. In addition a value for the lowest detectable concentration of fractional charge impurities by application of photothermal ionization spectroscopy is determined for a typical experimental arrangement, yielding $\sim 1 \times 10^7$ detectable fractional charge impurities per cm^3. Modifications to the experiment are proposed which can lower this limit with at least a factor of 100.

In chapter 4 we describe a study of the equilibrium system of electrons and holes, distributed over shallow impurity states and energy bands of ultra-pure semiconductors, when the semiconducting sample is continuously illuminated with intrinsic light. This investigation was also carried out by applying photothermal ionization spectroscopy. First a set of rate of change equations is given, describing this system and its response to small additional injections of majority or minority free carriers into the energy bands by photothermal ionization of majority or minority impurities respectively. This model explains the usually observed increase of electrical conductivity of ultra-pure germanium, associated with the additional ionization of majority impurities, and the decrease because of the corresponding ionization of minority impurities. The measured time-evolution of the conductivity after the start of the photo-thermal process revealed a fast (< 0.5 msec) component in the signal, originating from both majority and minority impurities, as well as a slow (~5 msec) component from the minority impurities only, the latter response time having approximately the same magnitude as the chopping times usually applied. This slow response time has been attributed to a slow electron-hole recombination process in the bulk material. It has been demonstrated that the presence of both a fast and a slow component in the signal can cause artefacts in the spectra, when using phase-sensitive detection techniques by means of a lock-in amplifier.

The computer programs, suited for use on a PDP-11 and developed to manipulate interferograms and spectra, are described in an Appendix.

Dit proefschrift behandelt een tweetal hoofdonderwerpen. Het eerste gaat over de mogelijkheid om fractionele lading onzuiverheden - gevormd door quark-nucleon complexen - in halfgeleiders op te sporen met behulp van fotothermische ionisatie spectroscopie. Het tweede behelst een onderzoek aan het evenwichts-systeem van elektronen en gaten, die over de toestanden van ondiepe onzuiver-heden en over de energiebanden in ultrazuivere halfgeleiders verdeeld zijn onder continue belichting met intrinsiek licht, door het toepassen van dezelfde spectroscopische techniek.

Door de auteur is een Michelson interferometer gebouwd, die het golfgetal gebied 5 tot 350 cm^{-1} in het verre infrarood bestrijkt. Dit speciale type Fourier spectrometer en de principes van Fourier transformatie spectroscopie worden beschreven in het eerste deel van hoofdstuk 2. Tijdens het opbouwen van de interferometer werd ontdekt dat de verplaatsing van de bewegende spiegel een periodieke niet-lineariteit vertoonde, ten gevolge van een fout in de spoed van de aandrijvende micrometer. In een Fourier spectrometer, gebruikt op de stap-en-integreer wijze, geeft zo'n niet-lineariteit aanleiding tot spooklijnstruc-turen in de spectra, als de toenames in optisch weglengteverschil tussen de twee gesplitste bundels niet in de gaten gehouden worden door een nauwkeurig controle systeem zoals een referentiesysteem dat verplaatsingen meet m.b.v. interferentie patronen. De spooklijnstructuur, die het gevolg is van een periodieke niet-lineariteit, is theoretisch en experimenteel bestudeerd en wordt beschreven in het tweede gedeelte van hoofdstuk 2. Een methode wordt voorgesteld om de intensiteit van spooklijnen voor een gegeven grootte van een niet-lineariteit te reduceren zonder de noodzaak om een op het meten van interferentie patronen gebaseerd referentiesysteem te gebruiken, en de prak-tische toepasbaarheid ervan wordt aangetoond.

Hoofdstuk 3 gaat over de detectie van fractionele lading onzuiverheden in halfgeleiders door fotothermische ionisatie spectroscopie toe te passen. Eerst wordt een fenomenologische analyse gegeven voor de verwachte signaal sterktes bij een zekere concentratie van fractionele lading onzuiverheden. Uit de afwezigheid van signaal, afkomstig van fractionele lading onzuiverheden, in spectra van een ultrazuiver germanium preparaat, die verkregen zijn met de Michelson interferometer, konden wij afleiden dat dit preparaat minder dan 1.5×10^{11} acceptor-achtige fractionele lading onzuiverheden bevatte per cm^3. Bovendien wordt voor een typische experimentele opstelling een waarde voor de

met fotothermische ionisatie spectroscopie minimaal detecteerbare concentratie fractionele lading onzuiverheden bepaald, wat een minimale concentratie van $1x10^{7}$ cm^{-3} oplevert. Experimentele wijzigingen worden voorgesteld die deze limietwaarde minstens een factor 100 kunnen verlagen.

In hoofdstuk 4 beschrijven we een studie van het evenwichtssysteem van elektronen en gaten, die over de toestanden van ondiepe onzuiverheden en over de energie banden in ultrazuivere halfgeleiders verdeeld zijn, als het halfgeleider preparaat continue met intrinsiek licht belicht wordt. Ook dit onderzoek werd uitgevoerd door fotothermische ionisatie spectroscopie toe te passen. Eerst wordt een stelsel vergelijkingen gegeven, die het tempo van verandering van dit systeem beschrijven en de reactie van het systeem op kleine extra injecties van vrije meerderheids- of minderheidsladingdragers in de energie banden door fotothermische ionisatie van respectievelijk meerderheids- en minderheidsonzuiverheden. Dit model verklaart de gewoonlijk waargenomen toename in elektrische geleiding van ultrazuiver germanium, verbonden met extra ionisatie van meerderheidsonzuiverheden, en de afname door de corresponderende ionisatie van minderheidsonzuiverheden.

De gemeten evolutie in de tijd van de geleiding na de start van het fotothermische proces gaf zowel een snelle (< 0.5 msec) component in het signaal, afkomstig van meerderheids- én minderheidsonzuiverheden, te zien, als ook een langzame (~5 msec) component, afkomstig van alleen de minderheidsonzuiverheden. De respons tijd van deze laatste component heeft dezelfde orde van grootte als de gewoonlijk gebruikte choppertijden. Deze langzame respons tijd is toegeschreven aan een langzaam elektron-gat recombinatie proces in het bulk materiaal. Het is aangetoond dat het voorkomen van zowel een snelle als een langzame component in het signaal kan leiden tot artefacten in de spectra, wanneer bij het toepassen van fasegevoelige detectie technieken een lock-in versterker gebruikt wordt.

De computer programma's, geschikt voor gebruik op een PDP-11 en ontwikkeld om interferogrammen en spectra te manipuleren, worden in een appendix beschreven.

De schrijver van dit proefschrift werd op 27 december 1952 geboren in Wanroij. In 1971 behaalde hij het diploma gymnasium β aan het Boschveldcollege te Venraij.

In hetzelfde jaar begon hij met de studie natuurkunde aan de Katholieke Universiteit te Nijmegen. Na het kandidaatsexamen (maart 1974) koos hij vaste stof fysica als specialisatie.

Na zijn doctoraalexamen (december 1976) cum laude afgelegd te hebben, startte hij een promotieonderzoek in de groep experimentele natuurkunde IV aan de Katholieke Universiteit te Nijmegen, onder leiding van professor Dr. P. Wyder. Het eerste jaar van zijn promotieonderzoek had hij een promotiebeurs van het rijk, de rest van zijn promotietijd was hij F.O.M. medewerker.

Vanaf 1 augustus 1982 is hij werkzaam op het Philips Natuurkundig Laboratorium te Eindhoven.

STELLINGEN

I

De bijdrage van de electron-electron interactie tot de electrische weerstand van metalen met een bolvormig Fermi-oppervlak bij lage temperaturen wordt zeer sterk bepaald door de verhouding van de strooikansen van electronen aan enerzijds anisotrope en anderzijds isotrope strooikernen.

M. Kaveh en N. Wiser, J. Phys. F: Met. Phys. 12, 935 (1982)

II

Door de recente ontwikkelingen op het gebied van geautomatiseerde röntgen-diffractometers wordt de oude methode van Walker om fonon-spectra te bepalen m.b.v. diffuse verstrooiing van röntgenstraling opnieuw aantrekkelijk.

C.B. Walker, Phys. Rev. 103, 547 (1956)

III

Bij het bepalen van de compensatiegraad uit de temperatuurafhankelijkheid van de relatieve sterkte van twee verschillende soorten meerderheids-onzuiverheden in halfgeleiders, verwaarloost Darken ten onrechte de invloed van achtergrondstraling.

L.S. Darken, J. Appl. Phys. 53, 3754 (1982)

IV

De bewering van Broeckx, Kamiura, Clauws en Vennik dat de door hen waargenomen afname van fotogeleiding, verbonden met minder ondiepe onzuiverheden in germanium, versterkt wordt door het thermisch legen van het grondniveau van meer ondiepe onzuiverheden, is onjuist.

J. Broeckx, Y. Kamiura, P. Clauws en J. Vennik, Solid State Commun. 40, 149 (1981)

V

De Coulomb potentiaal tussen twee protonen moet gecorrigeerd worden voor de eindige afmetingen van het proton. De numerieke waardes voor deze gecorrigeerde potentiaal, gegeven door Sher, Signell en Heller, kunnen niet juist zijn.

M.S. Sher, P. Signell en L. Heller, Ann. Phys. (NY) 58, 1 (1970)

VI

De impliciete aanname van Morris, Palmer en Zuckerman dat de inelastische botsingsdoorsneden voor het systeem NH_3-H_2 onafhankelijk zijn van de kinetische temperatuur, is in strijd met experimentele resultaten.

M. Morris, P. Palmer en B. Zuckerman, Astrophys. J. 237, 1 (1980)
D.B.M. Klaassen, J.J. ter Meulen en A. Dymanus, geaccepteerd voor publicatie in J. Chem. Phys.

VII

De gastronomische eisen van menig Nederlander zijn samen te vatten met "veel is lekker".

VIII

Het veelvuldig te laat komen van Zuid-Nederlanders bij afspraken illustreert dat ook het begrip "op tijd" relatief is.

IX

De diversiteit in soorten veiligheidsgordels in auto's is niet bevorderlijk voor de veiligheid van lifters.

X

Het is een merkwaardig feit dat bij het grafisch weergeven van de meest uiteenlopende fysische verschijnselen steeds dezelfde set curvenmallen gebruikt kan worden.

De lengte van de beschrijving van computer-programma's geeft geen indicatie voor het aantal mensuren dat in de ontwikkeling van die programma's gestoken is.

M.J.H. van de Steeg

Nijmegen, 8 oktober 1982